

Exploring the redshift-space peculiar velocity field and its power spectrum

Lawrence Dam,^{1,*} Krzysztof Bolejko,² and Geraint F. Lewis¹

¹*Sydney Institute for Astronomy, School of Physics,
A28, The University of Sydney, NSW 2006, Australia*

²*School of Natural Sciences, College of Sciences and Engineering,
University of Tasmania, Private Bag 37, Hobart TAS 7001, Australia*

(Dated: February 18, 2022)

Redshift-space distortions (RSD) generically affect any spatially-dependent observable that is mapped using redshift information. The effect on the observed clustering of galaxies is the primary example of this. This paper is devoted to another example: the effect of RSD on the apparent peculiar motions of tracers as inferred from their positions in redshift space (i.e. the observed distance). Our theoretical study is motivated by practical considerations, mainly, the direct estimation of the velocity power spectrum, which is preferably carried out using the tracer’s redshift-space position (so as to avoid uncertainties in distance measurements). We formulate the redshift-space velocity field and show that RSD enters as a higher-order effect. Physically, this effect may be interpreted as a dissipative correction to the usual perfect-fluid description of dark matter. We show that the effect on the power spectrum is a damping on relatively large, quasilinear scales ($k \gtrsim 0.01 h \text{ Mpc}^{-1}$), as was observed, though unexplained, in N -body simulations elsewhere. This paper presents two power spectrum models for the peculiar velocity field in redshift space, both of which can be considered velocity analogues of existing clustering models. In particular, we show that the “Finger-of-God” effect, while also present in the velocity field, cannot be entirely blamed for the observed damping in simulations. Our work provides some of the missing modelling ingredients required for a density–velocity multi-tracer analysis, which has been proposed for upcoming redshift surveys.

arXiv:2105.12933v2 [astro-ph.CO] 29 Nov 2021

* Corresponding author
ldam4036@uni.sydney.edu.au

CONTENTS

I. Introduction	3
A. Motivation	3
II. Background	5
III. Distribution-function approach to RSD	6
A. Moments in real space	6
B. Moments in redshift space	7
1. Relation to velocity-moment expansion	8
IV. Redshift-space velocity field	9
A. Position space	9
1. A Green's function formula	10
B. Fourier space	11
V. Power spectrum model I: moment-expansion approach	13
A. Real-space velocity divergence power spectrum	13
B. Redshift-space velocity divergence power spectrum	16
1. Multipole moments	17
C. Redshift-space velocity	20
D. Further damping from velocity dispersion	21
VI. Power spectrum model II: cumulant-expansion approach	21
A. Analytic model	22
VII. Configuration space	25
A. Real space	26
B. Redshift space	27
VIII. Discussion and conclusions	28
A. RSD and the gradient expansion	28
B. Power spectrum	29
C. Comparison with previous work	29
IX. Summary and outlook	30
Acknowledgements	31
A. Power-law FFTLog numerical method	32
1. Integrals of type 22	33
Kernel expansion	33
2. Integrals of type 13	34
Asymptotic limits in the IR and UV	34
3. Configuration-space multipoles	35
B. Consistency check of derivative expansion	37
C. Explicit expressions for redshift-space kernels	38
D. Redshift-space correlation tensor	39
References	40

I. INTRODUCTION

Galaxy redshift surveys provide a useful way to probe cosmology through the large-scale structure of the Universe. The process begins with the basic task of mapping the distribution of galaxies (or other mass tracers). In principle, this is quite simple: place each galaxy in three-dimensional space by measuring both their angular position and radial distance. In practice, distances are rarely available, and one resorts to the redshift (and a model prior) to infer the galaxy’s distance. Redshifts, however, are imperfect indicators; they incur a Doppler shift from the galaxy’s own peculiar velocity, which translates to a shift—from the “real-space” position \mathbf{x} to the observed “redshift-space” position \mathbf{s} —according to

$$\mathbf{x} \rightarrow \mathbf{s} = \mathbf{x} + \frac{\mathbf{v}(\mathbf{x}) \cdot \hat{\mathbf{n}}}{aH} \hat{\mathbf{n}}, \quad (1)$$

where a is the scale factor, H is the Hubble parameter, $\hat{\mathbf{n}}$ is the direction of observation, and $\mathbf{v}(\mathbf{x}) \cdot \hat{\mathbf{n}}$ is the galaxy’s peculiar velocity along the line of sight (LOS). This mapping modifies only the radial positions of galaxies, leading to *redshift-space distortions* (RSD) in the galaxy clustering [1–4].

Far from being a nuisance, though, the measurement of RSD now forms a key science goal of redshift surveys, having been observed in numerous surveys, among various tracers [5–13]. The interest in RSD is that it can be used to probe f , the growth rate of cosmic structure [1, 4, 14]. This is through the fact that the distortions induce a systematic anisotropic signal on the clustering pattern, the size of which being determined by the growth rate through the amplitude of the displacement in eq. (1). The growth rate is of particular interest as different values are predicted by different dark-energy scenarios and modified-gravity theories [15–19]. Constraining it thereby provides a convenient way to distinguish the Λ CDM model from other alternatives. The RSD measurements to date are largely consistent with that predicted by Λ CDM (and so general relativity). A more demanding test of Λ CDM [20] will come with the next generation of redshift surveys, such as DESI [21], Euclid [22], and SPHEREx [23].

As this paper illustrates, RSD is not only limited to the galaxy clustering: any tracer sampled in three-dimensional redshift space will present a distorted view of the large-scale structure. This includes the velocity field underlying the large-scale streaming motions of galaxies—the focus of this paper. Just as galaxies *cluster* differently in redshift space, so too they *move* differently. In the former case the galaxy overdensity field becomes intertwined with the velocity field; in the latter case the velocity field becomes intertwined with itself. In both cases, there is additional cosmological information not present when galaxies are viewed at their true, real-space positions. Usefully, since the particular dependence on the growth rate changes, this can allow parameter degeneracies to be broken and tighter constraints to be obtained. Extracting this information, though, is more challenging given the difficulties of modelling in redshift space.

Besides the well-known cosmological value, there is a practical reason as to why a redshift-space-based analysis is preferable over a real-space one. As can be seen from eq. (1), when a tracer’s peculiar velocity is known (when distances are available) it becomes possible to shift the tracer back to its actual position. The shift, however, introduces a sizeable uncertainty through the peculiar velocity, which propagates to the inferred real-space position. A typical 20% uncertainty in the peculiar velocity (which largely derives from the distance estimate) then implies a position uncertainty of at least the same size. In order to estimate the velocity power it thus becomes necessary to take into account the uncertainty in the discrete sampling of the velocity field. This complication can be avoided if the positions are instead taken to be that determined by the spectroscopic redshifts. (Though note that the large velocity uncertainties still affect the power spectrum estimates through the shot noise term, which is weighted by these errors, unlike the density power spectrum.) So though the velocity field can in principle be analyzed in either real space or redshift space, the positions are simply better determined in the latter, being more closely connected to what is observed, rather than inferred.

A. Motivation

This paper is motivated by the present need for a theoretical model of the *redshift-space peculiar velocity field* and particularly its two-point statistics. This need first arose in the work of Koda *et al.* [24], who showed using a Fisher forecast the ability to substantially improve growth rate constraints with the “multi-tracer” method [25] applied to the galaxy density and peculiar velocities; i.e. with a joint analysis of the auto- and cross-power spectra of the redshift-space galaxy density and velocity fields (see also refs. [26, 27]). Without a physical model for the redshift-space velocity power spectrum, a simple empirical model calibrated on N -body simulations [28] was adopted. The simulations showed that the monopole moment of the measured power spectrum was damped, much as the “Fingers-of-God” (FoG) effect damps the galaxy power spectrum. This behaviour was found to be well described by a simple fitting function in the form of a FoG-like damping factor, which was parametrized by an empirical velocity

dispersion parameter. Unfortunately, this nuisance parameter was shown to degrade growth rate constraints by 30–50%, depending on the set of parameters chosen (as well as likely introducing a systematic bias). A number of other works have also relied on this model (e.g. [29–32]).

To minimize the loss of statistical power a physical model is required which can explain the damping ideally from first principles. The aim of this paper is to provide such a model. It is also timely, coming ahead of the imminent peculiar velocity surveys (e.g. [33, 34]), which are set to probe a larger volume with a denser sampling (and so improve the shot-noise properties of power spectrum measurements). Another opportunity [30, 32, 35–37] will be provided by the large sample of up to 10^6 type Ia supernovae from LSST [38].

To our knowledge a detailed treatment on the redshift-space velocity field has not previously been carried out. However, a couple of works have considered some related aspects.

Kaiser and Hudson [39] described two effects arising from random motion on the measurement of a galaxy’s peculiar velocity from its redshift-space position. The first effect is a consequence of the radial number density of galaxies increasing with distance: Given that a galaxy will be displaced from its actual location due to random motion, a galaxy with observed distance r is thus more likely to have “scattered” down from a larger distance (say, $r + dr$), than up from a shorter one ($r - dr$). This selection bias affects the observed sample, but it is a separate consideration that does not bear on our theory-based study.

More closely related to our work is the second effect. This is of a similar nature to the first effect, but arises specifically for an inhomogeneous mass distribution (whereas the first exists even if the galaxies were to be homogeneously distributed). In a spatial region centered, for example, on the nearside of a galaxy cluster (where the number density of galaxies is increasing as a function of distance) the number of galaxies scattered into the region from the farside will be larger than on the nearside, where there are fewer galaxies. When conditioned on the cluster—modelled simply as a plane-wave density perturbation δ_g —the mean displacement is no longer zero-centered. The measured LOS peculiar velocities $v_{\parallel} \equiv \mathbf{v} \cdot \hat{\mathbf{n}}$ in this region then changes by an amount $\Delta v_{\parallel} \simeq -(\partial\delta_g/\partial r)\sigma_v^2/H_0$, with σ_v the velocity dispersion, and H_0 the Hubble constant. A linear-theory calculation then showed that the peculiar velocity is biased low by $\Delta v_{\parallel}/v_{\parallel} \simeq -k^2\sigma_v^2/(\beta H_0^2)$, with $\beta \equiv f/b$ the distortion parameter, b the linear galaxy bias, and k the wavenumber. As a result, the velocity power spectrum is damped (isotropically) by a factor $D^2(k) = (1 - k^2\sigma_v^2/(\beta H_0^2))^2$. (In fact, this damping factor holds more generally than the plane-wave mass distribution considered by Kaiser and Hudson.¹)

Though this simple analytic model can provide the right amount damping observed in the simulations of Koda *et al.* [24], it also predicts problematically that (i) for a given wavenumber, damping affects all Fourier modes equally, not just the LOS modes; and that (ii) the amount of damping depends on galaxy bias. Both (i) and (ii) do not follow from the mapping (1), for if the transverse modes were damped it would imply that the angular positions also shift under the mapping. Moreover, because only the velocity field participates in the mapping, galaxy bias is not expected to appear. As we will show in this work, any field prescribed over redshift space can be formulated in terms of its real-space version convolved with eq. (1), independent of the dynamical relation between the galaxy (or matter) density and velocity fields.

The linear analysis by Kaiser and Hudson was not aimed at producing a fully-working model, but it does nevertheless identify a mechanism that can explain the damping. Here we will go further. With the systematic approach taken in this work, we will show (among other things) that there is also a long-range FoG-like effect, and because of which the random motions cannot be solely blamed for the damping observed in simulations.

In another work, Okumura *et al.* [40] performed a study similar to our own but for the *density-weighted* redshift-space velocity field (i.e. the “momentum” field). Such a field is closely related [41] to the kinetic Sunyaev–Zel’dovich effect [42]; and, in the context of a direct measurement of the velocity power, it is perhaps a more practical summary statistic (in terms of having a mass weighting; see refs. [43, 44]). However, in this work we specifically have in mind the aforementioned multi-tracer analysis of which the scientific return from upcoming surveys has been well studied [24, 29, 30]. (Though, note that our results also have relevance to a redshift-space-based analysis of velocity two-point correlations [45–50].)

Like this earlier work [40], we will also make use of the “distribution-function approach” [51–55] of phase space. This approach allows us to systematically compute from a derivative expansion the effects of RSD on density-weighted fields; the velocity field, however, is not density weighted but we will show how it still admits a similar formulation. We will go beyond this approach, though, by showing that another treatment is possible which does not make any approximations related to the mapping (1). (We will show in passing that the same treatment applies equally well to the momentum field.)

This paper is organized as follows. In Section II we briefly review the theory of RSD as it applies to the matter density field, and fix some of our notation. In Section III we introduce a more general formalism for RSD in terms of

¹ We find that the same damping factor $D(k)$ applies even for an arbitrary mass distribution $\delta = \delta_g/b$. This follows from recalling that \mathbf{v} is a potential flow, and adopting the plane-parallel limit (in which the LOS is fixed). Given these considerations we can write $\partial(\nabla \cdot \mathbf{v})/\partial r = \nabla^2 v_{\parallel}$. Then by the linearized continuity equation $\partial\delta_g/\partial r = -\nabla^2 v_{\parallel}/(\beta H_0)$, and so $\Delta v_{\parallel} \simeq \sigma_v^2 \nabla^2 v_{\parallel}/(\beta H_0^2)$. The result is obtained upon taking the Fourier transform of $v_{\parallel} + \Delta v_{\parallel}$.

the phase-space distribution function [51]; we will give a different derivation of the so-called velocity-moment expansion, and show in particular how density-weighted fields in redshift space follow from simple convolution integrals. In Section IV we derive the redshift-space velocity field using the results of the previous section; we show that the (exact) velocity field, not being density weighted, follows from a modified integral formula in terms of a Green’s function. Section V presents the first model of the redshift-space velocity power spectrum using the velocity-moment expansion and shows how the effect of RSD modifies a set of mode-coupling kernels. Section VI presents the second model, which is obtained using the integral formulae; in this model we show that the power spectrum can alternatively be written in terms of the statistics of pairwise velocities. To complete the study of the two-point statistics, in Section VII we derive the redshift-space correlation function of the LOS velocities. Conclusions and discussion follow in Section VIII. Our main results are summarized in Section IX. Several appendices collect supplementary material; of note is Appendix A describing our fast numerical implementation of the power spectrum models which exploits the Fast Fourier Transform (the “FFTLLog” method [56]).²

Notation and conventions. Our Fourier convention is

$$f(\mathbf{x}) = \int_{\mathbf{k}} \tilde{f}(\mathbf{k}) e^{-i\mathbf{k}\cdot\mathbf{x}}, \quad \tilde{f}(\mathbf{k}) = \int d^3\mathbf{x} f(\mathbf{x}) e^{i\mathbf{k}\cdot\mathbf{x}}, \quad (2)$$

where $\int_{\mathbf{k}}$ is a shorthand for $\int d^3\mathbf{k}/(2\pi)^3$, which we will often use throughout this paper. We work with the dimensionless velocity divergence defined as $\theta \equiv -\nabla \cdot \mathbf{v}/(aHf)$, where \mathbf{v} is the peculiar velocity field (or “velocity”), a is the scale factor, H is the Hubble parameter, and f is the linear growth rate. We will largely use the conformal Hubble parameter $\mathcal{H} \equiv (da/d\tau)/a = aH$, with τ the conformal time. For numerical work we adopt a spatially-flat Λ CDM cosmology with $\Omega_{m0} = 0.315$, $\Omega_{b0} = 0.04904$, $\sigma_8 = 0.829$, $n_s = 0.966$; the growth rate is parametrized in the usual way, i.e. $f(z) = \Omega_m(z)^{0.55}$ [57].

II. BACKGROUND

This paper is about the peculiar velocity field in redshift space. It will however be useful to recall some well-known results relating to RSD in the context of clustering (see ref. [58] for a review), as it will help us to understand some generic features in a simpler setting.

The starting point to study clustering in redshift space is to use the fact that the number of galaxies does not change in going from real space to redshift space; that is, the mapping (1) is number conserving. Formally, for an infinitesimal volume element $d^3\mathbf{s}$ in redshift space centered at \mathbf{s} , and $d^3\mathbf{x}$ in real space centered at \mathbf{x} , we have the relation

$$[1 + \delta^s(\mathbf{s})] d^3\mathbf{s} = [1 + \delta(\mathbf{x})] d^3\mathbf{x} \quad (3)$$

between the galaxy overdensity $\delta^s(\mathbf{s})$ in redshift space and $\delta(\mathbf{x})$ in real space. (Here we are assuming no galaxy bias for simplicity.) From this relation we have that

$$\delta^s(\mathbf{s}) = \frac{1}{J(\mathbf{x})} [1 + \delta(\mathbf{x})] - 1, \quad J(\mathbf{x}) \equiv \left| \frac{d^3\mathbf{s}}{d^3\mathbf{x}} \right| = 1 + \frac{1}{\mathcal{H}} \hat{\mathbf{n}} \cdot \nabla(\mathbf{v} \cdot \hat{\mathbf{n}}), \quad (4)$$

where J is the Jacobian of the mapping (1). By linearizing eq. (4) we obtain Kaiser’s formula [1], which reads in Fourier space

$$\tilde{\delta}^s(\mathbf{k}) = (1 + f\mu^2) \tilde{\delta}(\mathbf{k}), \quad (5)$$

where f is the linear growth rate, and μ is the cosine of the angle of separation between the wavevector \mathbf{k} and the LOS. According to this relation, structures viewed in redshift space will appear squashed along the LOS as the coherent infall of galaxies causes a LOS-directed displacement towards higher-density regions. Kaiser’s formula is valid in the “plane-parallel limit” in which the LOS is fixed (at $\hat{\mathbf{n}} = \hat{\mathbf{z}}$, say). In practice, this is a good approximation when the pairwise separations of the galaxy sample are small compared to their distances. Note that this formula assumes no velocity bias between galaxy velocity \mathbf{v}_g and the underlying matter flow, i.e. $\mathbf{v}_g = \mathbf{v}$.³ At least on perturbative scales this appears to be a quite valid assumption [60], and so we will assume no velocity bias throughout this work.

² Our code is publicly available and can be found at <https://github.com/lhd23/RSDPT-FFTLLog/>.

³ It can be argued [59] based on the equivalence principle that galaxies and matter must respond identically to the gravitational field (on suitably large scales); any deviations from $\mathbf{v}_g = \mathbf{v}$ enter as terms that are higher-order derivatives in \mathbf{v} , which are suppressed on large scales. Quantitatively, this is also supported by N -body simulations that show negligible halo velocity bias on scales $k \lesssim 0.2 h \text{ Mpc}^{-1}$ [60, 61].

From the Kaiser formula (5) we have the power spectrum

$$P^s(k, \mu) = (1 + f\mu^2)^2 P_L(k), \quad (6)$$

where $P_L(k)$ is the (real-space) linear power spectrum. This shows that the power in redshift space is enhanced along the LOS. It also shows that it contains information not present in real space: Distortions induce an anisotropy in the clustering statistics, and the degree of anisotropy observed can be used to constrain the growth rate f .

Equation (6) does not account for the fact that galaxies (typically residing in clusters) also possess virial motion, in addition to their large-scale streaming motions. In redshift space, virial motion gives rise to an elongation of structures along the LOS. This is the FoG effect and, in contrast to the Kaiser effect, arises from the nonlinear regime. As such, in the past a phenomenological approach was common [62], whereby eq. (6) is simply multiplied by a damping function, which preserves the Kaiser effect on large scales but suppresses the power on small scales.

Recent modelling efforts are largely based on a framework developed by Scoccimarro [63] which is able to provide a consistent treatment of clustering on a wide range of scales. In particular, it was shown that (in the plane-parallel limit) an exact formula for the redshift-space power spectrum can be obtained:

$$P^s(\mathbf{k}) = \int d^3\mathbf{r} e^{i\mathbf{k}\cdot\mathbf{r}} \left\langle e^{-ifk_z \Delta u_z} [1 + \delta(\mathbf{x})] [1 + \delta(\mathbf{x}')] \right\rangle, \quad (7)$$

where $\mathbf{r} = \mathbf{x} - \mathbf{x}'$ is the separation, $k_z \equiv \hat{\mathbf{k}} \cdot \hat{\mathbf{z}}$ is the LOS component of the wavevector, $\Delta u_z \equiv u_z(\mathbf{x}) - u_z(\mathbf{x}')$ is the pairwise LOS velocity, and $u_z \equiv \mathbf{v} \cdot \hat{\mathbf{z}} / (-\mathcal{H}f)$. Here the power spectrum is described in terms of moments of the pairwise LOS velocities; in particular, we have that $\langle \dots \rangle$ is the pairwise LOS velocity generating function. This general relation is the starting point for a number of power spectrum models (e.g. [64, 65]). In configuration space, eq. (7) implies the anisotropic two-point correlation function,

$$1 + \xi^s(s_\perp, s_\parallel) = \int_{-\infty}^{\infty} dr_\parallel [1 + \xi(r)] p(s_\parallel - r_\parallel | \mathbf{r}), \quad (8)$$

where $s_\parallel = s\mu$ and $r_\parallel = r\mu$ are real- and redshift-space separations along the LOS, respectively; $s_\perp = r_\perp$ is the transverse separation; $r = (r_\parallel^2 + r_\perp^2)^{1/2}$; $\xi(r)$ is the (real-space) two-point function; and p is the probability distribution function of the pairwise LOS velocities at separation \mathbf{r} . We see again that the distortions are characterized by the statistics of the pairwise velocities, but this time recalling earlier “streaming models” [2, 66]. In the case of a (scale-dependent) Gaussian distribution, we obtain the aptly named “Gaussian streaming model” [67, 68], which is widely-used today [69, 70]. Skew corrections to the Gaussian assumption have also been considered [71].

It is important to note that eqs. (7) and (8) are derived by appealing to number conservation (3), which is specific to tracers of the density field. Nevertheless, we will show, beginning with the distribution-function approach, that expressions similar to eqs. (7) and (8) also exist for the velocity field.

III. DISTRIBUTION-FUNCTION APPROACH TO RSD

A general procedure for prescribing fields in redshift space can be realized with the phase-space distribution function of dark matter particles [51–55]. While this will require introducing a certain amount of formalism, the advantage gained is a systematic way to treat RSD, extending the notion of “density field in redshift space” to any other bulk quantity, such as the velocity field. Indeed, by taking moments of the distribution function we can obtain the fluid description of dark matter, given either in real space or redshift space. This section briefly reviews the distribution-function approach to RSD, focussing on the “velocity-moment expansion” first given in [51]. We will further show that the velocity-moment expansion follows from more intuitive convolution formulae which permits another treatment of RSD with its own advantages.

A. Moments in real space

We begin with the one-particle phase-space distribution function, $f_1(\mathbf{x}, \mathbf{p}, \tau)$, which gives the probability $f_1(\mathbf{x}, \mathbf{p}, \tau) d^3\mathbf{x} d^3\mathbf{p}$ of finding one particle in an infinitesimal phase-space volume $d^3\mathbf{x} d^3\mathbf{p}$ centered on comoving position \mathbf{x} and momentum \mathbf{p} , at conformal time τ .⁴ The number-conservation argument may then be understood as a

⁴ We retain the subscript in f_1 that is often omitted so as to distinguish it from the growth rate (denoted f).

consequence of conservation of phase-space volume. In the following, as we do not yet need to consider dynamics, we will suppress the time dependence in $f_1(\mathbf{x}, \mathbf{p}, \tau)$ for brevity, and simply write $f_1(\mathbf{x}, \mathbf{p})$ (much as for any quantities derived from it).

The zeroth and first moments of the distribution function are of primary interest. The zeroth moment corresponds to the mass density and the first moment corresponds to the momentum density; the first cumulant is the bulk velocity and is given by the first moment divided by the zeroth moment. That is, we have

$$1 + \delta(\mathbf{x}) = \int d^3\mathbf{p} f_1(\mathbf{x}, \mathbf{p}), \quad (9)$$

$$\mathbf{v}(\mathbf{x}) = \int d^3\mathbf{p} \left(\frac{\mathbf{p}}{ma} \right) f_1(\mathbf{x}, \mathbf{p}) / \int d^3\mathbf{p} f_1(\mathbf{x}, \mathbf{p}), \quad (10)$$

where m is the particle mass and a is the scale factor. (The bulk velocity of particles in the cosmological context is the peculiar velocity.) The second moment is the stress tensor, $T_{ij}(\mathbf{x}) = [1 + \delta(\mathbf{x})]\sigma_{ij}(\mathbf{x})$, where σ_{ij} is the velocity dispersion given by

$$\sigma_{ij}(\mathbf{x}) = \left[\int d^3\mathbf{p} f_1(\mathbf{x}, \mathbf{p}) \left(\frac{p_i}{ma} \right) \left(\frac{p_j}{ma} \right) / \int d^3\mathbf{p} f_1(\mathbf{x}, \mathbf{p}) \right] - v_i(\mathbf{x})v_j(\mathbf{x}). \quad (11)$$

We also have the mass density $\rho(\mathbf{x}) = ma^{-3}[1 + \delta(\mathbf{x})]$, and the momentum density $\boldsymbol{\pi}(\mathbf{x}) = [1 + \delta(\mathbf{x})]\mathbf{v}(\mathbf{x})$.

On cosmological scales the action of gravity is dominant and it is customary to treat the matter particles as a pressureless perfect fluid (PPF), i.e. with vanishing stress tensor $T_{ij} = 0$ and pressure $p = 0$. This simplifies the dynamics considerably: all higher moments vanish and the ‘‘Boltzmann hierarchy’’ is closed for the zeroth and first moments. This yields a system of equations in the density and velocity which can be consistently solved. In this case the particle velocities are single-valued at each \mathbf{x} (‘‘single-streaming’’), and implies the distribution function takes the form

$$f_1(\mathbf{x}, \mathbf{p}) = f_1^{\text{PPF}}[\delta, \mathbf{v}] = [1 + \delta(\mathbf{x})] \delta_{\text{D}}(\mathbf{p} - am\mathbf{v}(\mathbf{x})), \quad (12)$$

i.e. in terms of the zeroth and first moments only.

B. Moments in redshift space

Redshift-space distortions cause a radial shift in the positions of tracers, with the apparent position depending on the tracer’s own state of motion. At the level of phase space the apparent positions—the positions in redshift space—of point particles become functions of their momenta. The observed configuration space then results from a LOS ‘‘projection’’ of phase-space dynamics onto the actual configuration space. This may be realized by convolving the real-space distribution function with the real-to-redshift-space mapping (1) to obtain the *redshift-space distribution function*,

$$f_1^s(\mathbf{s}, \mathbf{p}) \equiv \int d^3\mathbf{x} f_1(\mathbf{x}, \mathbf{p}) \delta_{\text{D}}\left(\mathbf{s} - \mathbf{x} - \mathcal{H}^{-1} \frac{\hat{\mathbf{n}} \cdot \mathbf{p}}{ma} \hat{\mathbf{n}}\right) = f_1\left(\mathbf{s} - \mathcal{H}^{-1} \frac{\hat{\mathbf{n}} \cdot \mathbf{p}}{ma} \hat{\mathbf{n}}, \mathbf{p}\right) \quad (13)$$

where $\hat{\mathbf{n}} = \mathbf{x}/|\mathbf{x}| = \mathbf{s}/|\mathbf{s}|$ is the LOS unit vector, and $\mathcal{H} \equiv aH$. (Throughout this paper a superscript s will be used to indicate a quantity defined over redshift space.) Progress can be made if we expand f_1^s in powers of $\hat{\mathbf{n}} \cdot \mathbf{p}/(ma)$, then integrate out momenta \mathbf{p} to, e.g. obtain the redshift-space density field, as done in ref. [51]. As we will show, there is another approach that can be taken with its own advantages.

First, we note that the usual number-conservation argument provides a useful relation (3) between real- and redshift-space density fields, but that it cannot be applied more generally to the wanted velocity field. We can however see that eq. (13) is consistent with number conservation (as it should be). For if the phase-space volume is conserved, $\int d^3\mathbf{x} \int d^3\mathbf{p} f_1(\mathbf{x}, \mathbf{p}) = \int d^3\mathbf{s} \int d^3\mathbf{p} f_1^s(\mathbf{s}, \mathbf{p})$, we have locally that $[1 + \delta^s(\mathbf{s})]d^3\mathbf{s} = [1 + \delta(\mathbf{x})]d^3\mathbf{x}$.

Next, making use of the specific PPF form given by eq. (12), we can derive a convolution formula from which the velocity-moment expansion is obtained. To demonstrate, observe for the density field [cf. eq. (9)]

$$\begin{aligned} 1 + \delta^s(\mathbf{s}) &= \int d^3\mathbf{p} f_1^s(\mathbf{s}, \mathbf{p}) \\ &= \int d^3\mathbf{x} \int d^3\mathbf{p} \delta_{\text{D}}\left(\mathbf{s} - \mathbf{x} - \mathcal{H}^{-1} \frac{\hat{\mathbf{n}} \cdot \mathbf{p}}{ma} \hat{\mathbf{n}}\right) [1 + \delta(\mathbf{x})] \delta_{\text{D}}(\mathbf{p} - am\mathbf{v}(\mathbf{x})), \end{aligned} \quad (14)$$

where in the second line we substituted f_1^s for eq. (13), in which f_1 is given by its PPF form (12). Upon integrating out momenta we have

$$1 + \delta^s(\mathbf{s}) = \int d^3\mathbf{x} [1 + \delta(\mathbf{x})] \delta_D(\mathbf{s} - \mathbf{x} - \mathcal{H}^{-1}v_{\parallel}(\mathbf{x})\hat{\mathbf{n}}). \quad (15)$$

This simple formula makes intuitive sense: to construct the redshift-space version of $1 + \delta$, take all real-space mass elements $1 + \delta$ at \mathbf{x} and reassign them to \mathbf{s} , according to the real-to-redshift-space mapping (realized through the delta function). Of course different \mathbf{x} may give rise to the same \mathbf{s} , so naturally we are to integrate over real space. (Specifically, since the transverse components are unaffected by the mapping, we only need to integrate over the LOS component $x_{\parallel} \equiv \mathbf{x} \cdot \hat{\mathbf{n}}$.)

It is not hard to see that the formula (15) generalizes straightforwardly to any other moment we care to compute (in the PPF approximation), since we have that the n th moment is just $M_{i_1 \dots i_n} \equiv (1 + \delta)v_{i_1} \dots v_{i_n}$. For example, the first moment is the momentum field and reads

$$[1 + \delta^s(\mathbf{s})] \mathbf{v}^s(\mathbf{s}) = \int d^3\mathbf{x} [1 + \delta(\mathbf{x})] \mathbf{v}(\mathbf{x}) \delta_D(\mathbf{s} - \mathbf{x} - \mathcal{H}^{-1}v_{\parallel}(\mathbf{x})\hat{\mathbf{n}}), \quad (16)$$

with \mathbf{v}^s the redshift-space velocity field. Here we see that, unlike the momentum field, the velocity field \mathbf{v}^s is not density weighted so cannot apparently be expressed purely in terms of \mathbf{v} ; rather it is the first *cumulant* of the distribution function. However, as we will soon see, we can still write \mathbf{v}^s in a way that resembles the intuitive convolution form given by eqs. (15) and (16) but with slight modification.

1. Relation to velocity-moment expansion

We now show that the velocity-moment expansion of the distribution-function approach follows from the integral representation (15). We will go through the steps in some detail as they will turn out to be instructive for a subsequent calculation on the velocity field.

Beginning with eq. (15), we replace the Dirac delta function with its plane-wave expansion to obtain

$$1 + \delta^s(\mathbf{s}) = \int d^3\mathbf{x} [1 + \delta(\mathbf{x})] \int \frac{d^3\mathbf{k}}{(2\pi)^3} e^{-i\mathbf{k} \cdot (\mathbf{s} - \mathbf{x})} e^{i\mathcal{H}^{-1}v_{\parallel}(\mathbf{x})\mathbf{k} \cdot \hat{\mathbf{n}}}. \quad (17)$$

This form gives another way to view eq. (15), namely, as the convolution of its real-space density field with plane waves of different velocity-induced phases. Next, we define $k_{\parallel} \equiv \mathbf{k} \cdot \hat{\mathbf{n}}$ and Taylor expand the second exponential to get

$$e^{i\mathcal{H}^{-1}v_{\parallel}k_{\parallel}} = \sum_{n=0}^{\infty} \frac{1}{n!} (i\mathcal{H}^{-1}v_{\parallel}k_{\parallel})^n = 1 + \frac{1}{\mathcal{H}} i v_{\parallel} k_{\parallel} - \frac{1}{2\mathcal{H}^2} (v_{\parallel} k_{\parallel})^2 + \dots \quad (18)$$

Since $(\nabla_{\parallel})^n e^{-i\mathbf{k} \cdot (\mathbf{s} - \mathbf{x})} = (-ik_{\parallel})^n e^{-i\mathbf{k} \cdot (\mathbf{s} - \mathbf{x})}$, each term in the foregoing expansion can be generated by the action of a basis of differential operators acting on plane waves. We can thus exchange powers of k_{\parallel} for powers of $\nabla_{\parallel} = \hat{\mathbf{n}} \cdot \partial/\partial\mathbf{s}$ (acting on the inner integral), and write eq. (17) as

$$\begin{aligned} 1 + \delta^s(\mathbf{s}) &= \int d^3\mathbf{x} [1 + \delta(\mathbf{x})] \sum_{n=0}^{\infty} \frac{1}{n!} \left(-\frac{1}{\mathcal{H}} v_{\parallel}(\mathbf{x}) \nabla_{\parallel} \right)^n \int \frac{d^3\mathbf{k}}{(2\pi)^3} e^{i\mathbf{k} \cdot (\mathbf{s} - \mathbf{x})} \\ &= \int d^3\mathbf{x} [1 + \delta(\mathbf{x})] \delta_D(\mathbf{s} - \mathbf{x}) - \frac{1}{\mathcal{H}} \nabla_{\parallel} \int d^3\mathbf{x} [1 + \delta(\mathbf{x})] v_{\parallel}(\mathbf{x}) \delta_D(\mathbf{s} - \mathbf{x}) + \dots \end{aligned}$$

Owing to the delta functions the integrals are easily done, and altogether yield the *velocity-moment expansion* in position space,

$$1 + \delta^s(\mathbf{s}) = \sum_{n=0}^{\infty} \frac{1}{n!} \left(\frac{-1}{\mathcal{H}} \right)^n \nabla_{\parallel}^n T_{\parallel}^{(n)}(\mathbf{s}), \quad (19)$$

where the density-weighted LOS velocity moments are defined as

$$T_{\parallel}^{(n)}(\mathbf{s}) \equiv [1 + \delta(\mathbf{s})] v_{\parallel}(\mathbf{s})^n. \quad (20)$$

Taking the Fourier transform of eq. (19) we then recover [see equation (2.6) in ref. [51]]

$$\tilde{\delta}^s(\mathbf{k}) = \sum_{n=0}^{\infty} \frac{1}{n!} \left(\frac{ik_{\parallel}}{\mathcal{H}} \right)^n \tilde{T}_{\parallel}^{(n)}(\mathbf{k}), \quad (21)$$

with $\tilde{T}_{\parallel}^{(n)}$ the Fourier transform of $T_{\parallel}^{(n)}$, and the background ($k = 0$) mode omitted. Note that in ref. [51] $T_{\parallel}^{(n)}$ is defined in terms of a general distribution function, whereas here we have adopted its PPF form (12). In the end this makes no difference; we are invoking the simplifying PPF approximation at the level of phase space, which will be assumed anyway for predictions using perturbation theory.

The above calculation can be repeated for any other moment of f^s , always resulting in the same form (19). More precisely, we also have expressions for the n th moment $M_{i_1 \dots i_n}^s$ by simply replacing $1 + \delta^s$ with $M_{i_1 \dots i_n}^s$, and $1 + \delta$ with $M_{i_1 \dots i_n}$. For example, the momentum field $\boldsymbol{\pi}^s \equiv (1 + \delta^s) \mathbf{v}^s$ is

$$\boldsymbol{\pi}^s(\mathbf{s}) = \sum_{n=0}^{\infty} \frac{1}{n!} \left(\frac{-1}{\mathcal{H}} \right)^n \nabla_{\parallel}^n \left[(1 + \delta(\mathbf{s})) v_{\parallel}(\mathbf{s})^n \mathbf{v}(\mathbf{s}) \right], \quad (22)$$

and the LOS component $\pi_{\parallel}^s \equiv \boldsymbol{\pi}^s \cdot \hat{\mathbf{n}}$ can be written in terms of the LOS velocity moments $T_{\parallel}^{(n)}$ as [cf. eq. (19)]

$$\pi_{\parallel}^s(\mathbf{s}) = \sum_{n=0}^{\infty} \frac{1}{n!} \left(\frac{-1}{\mathcal{H}} \right)^n \nabla_{\parallel}^n T_{\parallel}^{(n+1)}(\mathbf{s}). \quad (23)$$

We note that the Fourier transform of this expression was given in ref. [40].

It is easy to check that Kaiser's formula (5) is recovered by truncating eq. (19) at $n = 1$ and using linear theory. It can also be shown that the two-point function $\langle (1 + \delta^s)(1 + \delta^s) \rangle$ implied by eq. (15) recovers Scoccimarro's streaming model (8). (In contrast to our previous calculations one instead leaves unexpanded the second exponential in eq. (17). Such an approach will be preferable to the velocity-moment expansion for reasons we will discuss later in Section VD.)

IV. REDSHIFT-SPACE VELOCITY FIELD

A. Position space

The velocity field in redshift space is defined in terms of the phase-space distribution function by [cf. eq. (10)]

$$\mathbf{v}^s(\mathbf{s}) \equiv \int d^3\mathbf{p} \left(\frac{\mathbf{p}}{ma} \right) f_1^s(\mathbf{s}, \mathbf{p}) / \int d^3\mathbf{p} f_1^s(\mathbf{s}, \mathbf{p}), \quad (24)$$

i.e. the first cumulant of f_1^s (first moment divided by the zeroth moment). Specializing to the case of a pressureless perfect fluid (appropriate for dark matter), the moments are thus given by eqs. (15) and (16), and we have the following exact expression in terms of spatial integrals over real-space δ and \mathbf{v} :

$$\mathbf{v}^s(\mathbf{s}) = \frac{\int d^3\mathbf{x} [1 + \delta(\mathbf{x})] \mathbf{v}(\mathbf{x}) \delta_{\text{D}}(\mathbf{s} - \mathbf{x} - \mathcal{H}^{-1} v_{\parallel}(\mathbf{x}) \hat{\mathbf{n}})}{\int d^3\mathbf{x} [1 + \delta(\mathbf{x})] \delta_{\text{D}}(\mathbf{s} - \mathbf{x} - \mathcal{H}^{-1} v_{\parallel}(\mathbf{x}) \hat{\mathbf{n}})}. \quad (25)$$

According to this expression, the velocity field in redshift space appears to be density weighted. Of course, in real space the velocity field is volume weighted, and we will show that upon formal expansion of the right-hand side of eq. (25), it remains volume weighted in redshift space, as well; i.e. the apparent density weighting vanishes through cancellation. To obtain the expansion we introduce the bookkeeping parameter ϵ , then Taylor expand about $\epsilon = 0$. Thus, starting with eq. (25), performing a plane-wave expansion of the Dirac delta functions contained therein, as in eq. (17); taking $\mathbf{v} \rightarrow \epsilon \mathbf{v}$; performing a formal expansion, $\mathbf{v}^s(\mathbf{s}) = \sum_n \epsilon^n \mathbf{v}_n^s(\mathbf{s})$; setting $\epsilon = 1$; we find

$$\mathbf{v}^s(\mathbf{s}) = \mathbf{v}(\mathbf{s}) + \sum_{n=1}^{\infty} \frac{1}{n!} \left(\frac{-1}{\mathcal{H}} \right)^n \nabla_{\parallel}^{n-1} \left[v_{\parallel}(\mathbf{s})^n \nabla_{\parallel} \mathbf{v}(\mathbf{s}) \right], \quad (26)$$

⁵ One can also expand in powers of δ , though this turns out to be unnecessary. The velocity is not a density-weighted field and the apparent dependence on δ in eq. (25) drops out in redshift space, as (trivially) occurs in real space. As eq. (32) shows, \mathbf{v}^s can be written in terms of \mathbf{v} only.

where $\nabla_{\parallel} = \hat{\mathbf{n}} \cdot \nabla$. Clearly we have that at leading order $\mathbf{v}^s \simeq \mathbf{v}$. (Contrast this with the overdensity δ^s where, working to the same precision, we have eq. (5), the Kaiser formula.) Equation (26) shows that RSD in the velocity field (given by the sum) enters at next-to-leading order in the real-to-redshift-space mapping. As mentioned, notice also that δ does not appear; this is to be expected as only \mathbf{v} appears in the mapping (1).

As a consistency check, we have verified that the product of the expansions, eqs. (26) and (19), recovers the expansion (23), i.e. that we have $\boldsymbol{\pi}^s = (1 + \delta^s)\mathbf{v}^s$. This is easy to check order-by-order; the general case requires more work, which we give details on in Appendix B.

The physical meaning of the higher-order terms in eq. (26) can be understood by observing that the series is organized as a derivative expansion,⁶

$$\mathbf{v}^s[\mathbf{v}] = \mathbf{v}_{(0)}^s + \mathbf{v}_{(1)}^s + \mathbf{v}_{(2)}^s + \dots, \quad (27)$$

in that the $(n+1)$ th term $\mathbf{v}_{(n)}^s = \mathbf{v}_{(n)}^s[\mathbf{v}]$ depends linearly on terms containing n th-order derivatives, which includes products of lower-order derivatives. We can thus view eq. (26) as a *hydrodynamic gradient expansion* [72], where derivative terms $\mathbf{v}_{(1)}^s, \mathbf{v}_{(2)}^s, \dots$ correspond to corrections to the perfect-fluid approximation (zeroth-order terms). In particular, first derivatives give rise to dissipative effects in the fluid when viewed in redshift space: it is no longer the perfect fluid of real space. (Recall the continuity equation and Euler's equation describe the motion of a perfect fluid. When there are dissipative effects Euler's equation is modified but the continuity equation is not [73].) Since we will compute the leading nontrivial-order effect of RSD on the power spectrum we will need to keep terms in the expansion to third order in \mathbf{v} :

$$\mathbf{v}_{(0)}^s = \mathbf{v}, \quad (28a)$$

$$\mathbf{v}_{(1)}^s = -\frac{1}{\mathcal{H}}v_{\parallel}\nabla_{\parallel}\mathbf{v}, \quad (28b)$$

$$\mathbf{v}_{(2)}^s = \frac{1}{\mathcal{H}^2}v_{\parallel}\nabla_{\parallel}v_{\parallel}\nabla_{\parallel}\mathbf{v} + \frac{1}{2\mathcal{H}^2}v_{\parallel}^2\nabla_{\parallel}^2\mathbf{v}. \quad (28c)$$

The derivative expansion in eq. (26) should of course be understood perturbatively so that—with the velocity field generated by a small matter density perturbation δ —the size of successive terms are of decreasing relevance. This is easy to see if we consider for concreteness a plane-wave perturbation with wavenumber k , for then derivative terms in eq. (26) are order $\nabla_{\parallel}v_{\parallel}/\mathcal{H} \sim v_{\parallel}k/\mathcal{H}$. The n th term in the series (26) then gives a correction to real-space \mathbf{v} of order

$$(v_{\parallel}k/\mathcal{H})^{n-1} \sim \theta^{n-1} \sim \delta^{n-1}, \quad (29)$$

where θ is the velocity divergence [defined below by eq. (37)]. We therefore see that higher-derivative terms correspond to higher powers of δ , and are accordingly suppressed.

1. A Green's function formula

We now show that the derivative expansion of \mathbf{v}^s results from a convolution integral of the form given by eq. (15) for $1 + \delta^s$. The formula is equivalent to the series expansion (28) when considered to all orders, but has certain other advantages when we come to compute the two-point statistics (Section VI).

We have mentioned that the velocity \mathbf{v}^s is the first cumulant of the distribution function and so cannot apparently be written as a simple convolution. This is partly true; it cannot be done for \mathbf{v}^s but can be done for the *gradient* of \mathbf{v}^s . The trick is in observing that if we act with ∇_{\parallel} on eq. (26) the resulting expansion is precisely of the same form as the moment expansion (19); that is, we have

$$\nabla_{\parallel}\mathbf{v}^s(\mathbf{s}) = \sum_{n=0}^{\infty} \frac{1}{n!} \left(\frac{-1}{\mathcal{H}}\right)^n \nabla_{\parallel}^n \left[v_{\parallel}(\mathbf{s})^n \nabla_{\parallel}\mathbf{v}(\mathbf{s}) \right]. \quad (30)$$

By comparing this series to that of eq. (19), we see that here $\nabla_{\parallel}\mathbf{v}^s$ takes the place of $1 + \delta^s$, while $\nabla_{\parallel}\mathbf{v}$ takes the place of $1 + \delta$ (in $T_{\parallel}^{(L)}$). Because eq. (19) is the series expansion of eq. (15) we deduce the relation

$$\nabla_{\parallel}\mathbf{v}^s(\mathbf{s}) = \int d^3\mathbf{x} \nabla_{\parallel}\mathbf{v}(\mathbf{x}) \delta_{\text{D}}(\mathbf{s} - \mathbf{x} - \mathcal{H}^{-1}v_{\parallel}(\mathbf{x})\hat{\mathbf{n}}), \quad (31)$$

⁶ Note that the density and momentum expansions, eqs. (19) and (23), can also be described as derivative expansions.

i.e. the formal expansion of this integral formula is eq. (30).

One can view eq. (31) as an equation of the form $\mathcal{L}\mathbf{v}^s = \mathbf{\Delta}$, with the linear differential operator $\mathcal{L} = \nabla_{\parallel}$ and $\mathbf{\Delta}(\mathbf{s})$ regarded as a source term. To solve this equation we will specialize to the LOS component and adopt the plane-parallel limit (treating the LOS $\hat{\mathbf{n}}$ as constant). Thus projecting the differential equation onto $\hat{\mathbf{n}}$ we have $\mathcal{L}v_{\parallel}^s = \Delta_{\parallel}(\mathbf{s})$, which can be solved by means of a Green's function G to give

$$\begin{aligned} v_{\parallel}^s(\mathbf{s}) &= \int d^3\mathbf{s}' G(\mathbf{s} - \mathbf{s}') \int d^3\mathbf{x} \nabla_{\parallel} v_{\parallel}(\mathbf{x}) \delta_{\text{D}}(\mathbf{s}' - \mathbf{x} - \mathcal{H}^{-1}v_{\parallel}(\mathbf{x})\hat{\mathbf{n}}) \\ &= \int d^3\mathbf{x} \nabla_{\parallel} v_{\parallel}(\mathbf{x}) G(\mathbf{s} - \mathbf{x} - \mathcal{H}^{-1}v_{\parallel}(\mathbf{x})\hat{\mathbf{n}}). \end{aligned} \quad (32)$$

Comparing the second line with eq. (15) shows that the Green's function takes the place of the delta function (as might be guessed from the nonlocal nature of v_{\parallel}^s). To construct the Green's function we recall that G is such that $\mathcal{L}G = \delta_{\text{D}}$. In Fourier space this equation is solved by $\tilde{G}(\mathbf{k}) = 1/(-i\mathbf{k} \cdot \hat{\mathbf{n}})$, so we have that⁷

$$G(\mathbf{s}) = \int \frac{d^3\mathbf{k}}{(2\pi)^3} \frac{e^{-i\mathbf{k} \cdot \mathbf{s}}}{-i\mathbf{k} \cdot \hat{\mathbf{n}}} \quad (34)$$

$$= \frac{1}{2} \int_0^{\infty} d\lambda \delta_{\text{D}}(\mathbf{s} - \lambda\hat{\mathbf{n}}) - \frac{1}{2} \int_0^{\infty} d\lambda \delta_{\text{D}}(\mathbf{s} + \lambda\hat{\mathbf{n}}). \quad (35)$$

Note that this reduces to one-dimensional integrals because the LOS in the mapping (1) only affects the radial coordinate. We can also recognize the first and second term in the second line as the advanced and retarded Green's function, respectively. We can then write v_{\parallel}^s as (after making the change of variable $\lambda = \mathcal{H}^{-1}w$)

$$\begin{aligned} v_{\parallel}^s(\mathbf{s}) &= \frac{1}{2} \int d^3\mathbf{x} \nabla_{\parallel} v_{\parallel}(\mathbf{x}) \int_0^{\infty} \mathcal{H}^{-1}dw \delta_{\text{D}}[\mathbf{s} - \mathbf{x} - \mathcal{H}^{-1}(v_{\parallel}(\mathbf{x}) + w)\hat{\mathbf{n}}] \\ &\quad - \frac{1}{2} \int d^3\mathbf{x} \nabla_{\parallel} v_{\parallel}(\mathbf{x}) \int_0^{\infty} \mathcal{H}^{-1}dw \delta_{\text{D}}[\mathbf{s} - \mathbf{x} - \mathcal{H}^{-1}(v_{\parallel}(\mathbf{x}) - w)\hat{\mathbf{n}}]. \end{aligned} \quad (36)$$

This position-space formula is exact, and can be understood as an integral representation of the expansion (26) (in that we recover the LOS component of eq. (26) if we expand the Green's function in plane waves).⁸ We will return to these expressions in Section VD.

B. Fourier space

The power spectrum of eq. (28) (and related two-point statistics) will be presented in the following sections. We will thus need expressions for eq. (28) in Fourier space, which we will present in the remainder of this section. It will be convenient, however, to work with the *scaled* velocity field $\mathbf{u} \equiv -\mathbf{v}/(\mathcal{H}f)$, for \mathbf{u} then has units of length, $\nabla \cdot \mathbf{u}$ is dimensionless, and (in linear theory) $\delta = \theta$, where

$$\theta(\mathbf{x}) \equiv \nabla \cdot \mathbf{u} = -\nabla \cdot \mathbf{v}/(\mathcal{H}f) \quad (37)$$

is the (scaled) velocity divergence. Analogous relations also hold for the redshift-space versions.

We will now turn attention to the velocity divergence. In Fourier space eq. (37) reads

$$\tilde{\theta}(\mathbf{k}) = -i\mathbf{k} \cdot \tilde{\mathbf{u}}(\mathbf{k}) = i\mathbf{k} \cdot \tilde{\mathbf{v}}(\mathbf{k})/(\mathcal{H}f), \quad (38)$$

where tildes denote Fourier-space fields. In general, the velocity field can be decomposed into a curl-free (irrotational) part and divergence-free (rotational) part. In our case the cosmic velocity field is to a good approximation a potential

⁷ In the second line we have used the spectral representation

$$\frac{1}{-i\mathbf{k} \cdot \hat{\mathbf{n}}} = \frac{1}{2} \int_{-\infty}^{\infty} d\lambda e^{i\lambda\mathbf{k} \cdot \hat{\mathbf{n}}} \text{sgn}(\lambda), \quad (33)$$

where $\text{sgn}(x)$ is the sign function. In other words, the Fourier transform of $\text{sgn}(\lambda)/2$ is $1/(-i\mathbf{k} \cdot \hat{\mathbf{n}})$, for λ dual to $\mathbf{k} \cdot \hat{\mathbf{n}}$.

⁸ It might be noticed that eq. (36) is not the most general solution, for if we return to $\mathcal{L}v_{\parallel}^s = \Delta_{\parallel}$ we see that we are free to add to eq. (36) a vector field \mathbf{v}_h that satisfies the homogeneous equation $\mathcal{L}\mathbf{v}_h = 0$. This means \mathbf{v}_h must have constant radial component. Furthermore, because \mathbf{v}_h is irrotational (because \mathbf{v}^s is) we conclude that it is a constant radial vector field (emanating from the observer). This homogeneous solution should be discarded if we are to recover the correct solution (26); by not doing so the LOS component (the observable part) can be specified arbitrarily, and therefore physically meaningless. Of course, choosing suitable boundary conditions, such as that $\int d^3\mathbf{x} \mathbf{v}(\mathbf{x}) = 0$ (no bulk flow), eliminates this freedom.

flow (being sourced by the gradient of the potential Φ) and is determined by a scalar, the velocity divergence.⁹ Thus, knowledge of θ is sufficient to fully recover the velocity field, and in Fourier space eq. (38) yields the simple relation

$$\tilde{\mathbf{v}}(\mathbf{k}) = -\mathcal{H}f \frac{i\mathbf{k}}{k^2} \tilde{\theta}(\mathbf{k}). \quad (39)$$

Passing to redshift space, the velocity field \mathbf{v}^s (or \mathbf{u}^s) remains irrotational so that it suffices to work with θ^s . In other words, no curl modes are induced by going into redshift space; the redshift mapping only modifies the *radial* positions. (It is easily checked that $\nabla \times \mathbf{u}^s = 0$, starting from eq. (26) and writing \mathbf{u} as the gradient of a potential.)

The remainder of this section is devoted to the evaluation of $\theta^s \simeq \theta_1^s + \theta_2^s + \theta_3^s$ [cf. eq. (28)] in terms of the Fourier transform of the real-space field θ (for which predictions of its n -point statistics are well known [74]). To ease notation we will drop the tildes on Fourier-space quantities and write, e.g. $\theta^s(\mathbf{k})$, instead of $\tilde{\theta}^s(\mathbf{k})$. We compute the Fourier transform of each term θ_n^s in turn, using eq. (38), and noting that θ_1^s is leading order, θ_2^s is next-to-leading order, and θ_3^s is next-to-next-to-leading order. For the first term, clearly $\theta_1^s = \theta$ since $\mathbf{v}_{(0)}^s = \mathbf{v}$. The second term is a composite of two fields so, using the convolution theorem and noting that the Fourier transform of $\nabla_{\parallel} \mathbf{v} \equiv (\hat{\mathbf{n}} \cdot \nabla) \mathbf{v}$ is $(-i\hat{\mathbf{n}} \cdot \mathbf{k})\mathbf{v}(\mathbf{k})$, we have

$$\mathbf{v}_{(1)}^s(\mathbf{k}) = \frac{i}{\mathcal{H}} \int_{\mathbf{q}} (\hat{\mathbf{n}} \cdot \mathbf{q}) \mathbf{v}(\mathbf{q}) v_{\parallel}(\mathbf{k} - \mathbf{q}) \quad (40)$$

with our Fourier shorthand. This implies

$$\begin{aligned} \theta_2^s(\mathbf{k}) &= f \int_{\mathbf{q}} \frac{(\hat{\mathbf{n}} \cdot \mathbf{q})(\mathbf{q} \cdot \mathbf{k}) [(\mathbf{k} - \mathbf{q}) \cdot \hat{\mathbf{n}}]}{q^2 |\mathbf{k} - \mathbf{q}|^2} \theta(\mathbf{q}) \theta(\mathbf{k} - \mathbf{q}) \\ &\equiv f \int_{\mathbf{q}} K^{(2)}(\mathbf{k} - \mathbf{q}, \mathbf{q}; \hat{\mathbf{n}}) \theta(\mathbf{q}) \theta(\mathbf{k} - \mathbf{q}). \end{aligned} \quad (41)$$

In the second line we have defined the (dimensionless) mode-coupling kernel $K^{(2)}$, but it will turn out to be more convenient to work with the symmetrized kernel defined as¹⁰

$$\begin{aligned} K_S^{(2)}(\mathbf{q}_1, \mathbf{q}_2; \hat{\mathbf{n}}) &\equiv \frac{1}{2} \left(K^{(2)}(\mathbf{q}_1, \mathbf{q}_2; \hat{\mathbf{n}}) + K^{(2)}(\mathbf{q}_2, \mathbf{q}_1; \hat{\mathbf{n}}) \right) \\ &= \frac{1}{2} |\mathbf{q}_1 + \mathbf{q}_2|^2 \frac{(\mathbf{q}_1 \cdot \hat{\mathbf{n}})(\mathbf{q}_2 \cdot \hat{\mathbf{n}})}{(q_1 q_2)^2}. \end{aligned} \quad (42)$$

(Note that there is no quantitative difference whether the integral (41) is evaluated using $K_S^{(2)}$ or $K^{(2)}$.)

Finally, the third-order term $\mathbf{v}_{(2)}^s$ corresponds to a scalar divergence

$$\theta_3^s(\mathbf{k}) = f^2 \int_{\mathbf{q}_1} \int_{\mathbf{q}_2} \int_{\mathbf{q}_3} K_S^{(3)}(\mathbf{q}_1, \mathbf{q}_2, \mathbf{q}_3) \theta(\mathbf{q}_1) \theta(\mathbf{q}_2) \theta(\mathbf{q}_3) (2\pi)^3 \delta_D(\mathbf{k} - \mathbf{q}_1 - \mathbf{q}_2 - \mathbf{q}_3), \quad (43)$$

where we find for the symmetrized kernel after a straightforward (if lengthy) calculation

$$\begin{aligned} K_S^{(3)}(\mathbf{q}_1, \mathbf{q}_2, \mathbf{q}_3; \hat{\mathbf{n}}) &\equiv \frac{1}{3!} \left(K^{(3)}(\mathbf{q}_1, \mathbf{q}_2, \mathbf{q}_3; \hat{\mathbf{n}}) + 5 \text{ perm.} \right) \\ &= \frac{1}{6} |\mathbf{q}_1 + \mathbf{q}_2 + \mathbf{q}_3|^2 [(\mathbf{q}_1 + \mathbf{q}_2 + \mathbf{q}_3) \cdot \hat{\mathbf{n}}] \frac{(\mathbf{q}_1 \cdot \hat{\mathbf{n}})(\mathbf{q}_2 \cdot \hat{\mathbf{n}})(\mathbf{q}_3 \cdot \hat{\mathbf{n}})}{(q_1 q_2 q_3)^2}. \end{aligned} \quad (44)$$

In particular, the only configuration we will need collapses this to the simple form

$$K_S^{(3)}(\mathbf{k}, \mathbf{q}, -\mathbf{q}; \hat{\mathbf{n}}) = -\frac{(\mathbf{k} \cdot \hat{\mathbf{n}})^2 (\mathbf{q} \cdot \hat{\mathbf{n}})^2}{6 q^4}. \quad (45)$$

⁹ Vorticity does not arise in standard gravitational instability theory. Although this does not preclude vorticity that was generated in the early Universe, any initial vorticity will decay by the Hubble expansion as $1/a$ in the absence of anisotropic forces.

¹⁰ Equation (41) can be equivalently written as $\int_{\mathbf{q}_1} \int_{\mathbf{q}_2} K^{(2)}(\mathbf{q}_1, \mathbf{q}_2) \theta(\mathbf{q}_1) \theta(\mathbf{q}_2) (2\pi)^3 \delta_D(\mathbf{k} - \mathbf{q}_1 - \mathbf{q}_2)$. Since all terms in eq. (26) are products purely of velocity, or derivatives thereof, they become convolutions in Fourier space (filtered by some kernel). We then use the standard trick that, because the product of the fields is symmetric in the variables \mathbf{q}_1 and \mathbf{q}_2 , the integral against the anti-symmetric part of K is zero. Thus, only the symmetric part of K needs to be considered.

Because all terms in eq. (26) are products of \mathbf{v} (and derivatives thereof) we find that the n th term in the series expansion of θ^s is given by the general formula

$$\theta_n^s(\mathbf{k}, z) = f^{n-1} \left[\prod_{i=1}^n \int \frac{d^3 \mathbf{q}_i}{(2\pi)^3} \theta(\mathbf{q}_i, z) \right] K_S^{(n)}(\mathbf{q}_1, \dots, \mathbf{q}_n) (2\pi)^3 \delta_D \left(\mathbf{k} - \sum_{j=1}^n \mathbf{q}_j \right). \quad (46)$$

This is similar to expressions found in perturbation theory (Section V A). One difference here is each term has an overall factor of a certain power of the growth rate f ; higher-order terms have greater sensitivity to the growth rate (though understood perturbatively, and being higher-derivative, these terms are of decreasing significance). Here we have $K_S^{(1)} = 1$ (no distortions at leading order since $\theta^s = \theta$), while higher-order kernels $K_S^{(n)}$ will depend on $\hat{\mathbf{n}}$ via the LOS momenta $\hat{\mathbf{q}}_1 \cdot \hat{\mathbf{n}}$, $\hat{\mathbf{q}}_2 \cdot \hat{\mathbf{n}}$, etc. We may also notice that θ^s , unlike δ^s , is determined only by its real-space equivalent θ . This can be traced to the real-to-redshift-space mapping being a function of the velocity field; the velocity field is volume weighted, not density weighted (as are all other cumulants of the distribution function).

To summarize, θ (and therefore θ^s) is here taken to be a fully-nonlinear field. The resulting formal expansion is of course to be treated perturbatively (for the series to be convergent), i.e. $\theta \sim vk/\mathcal{H} \sim \delta$ is a small fluctuation about zero, as is the working assumption in the distribution-function approach. We have hence exhibited in eq. (28) the expansion up to third order, and presented the associated (symmetrized) kernels in eqs. (42) and (44), which we will use in the following section.

V. POWER SPECTRUM MODEL I: MOMENT-EXPANSION APPROACH

Now that we have an expression (46) for the redshift-space velocity field we will compute its power spectrum. So far though we have only treated (rather formally) the mapping from real space to redshift space (1) without dynamical considerations; we did not make explicit use of the Boltzmann (or fluid) equations when considering the distribution function (or its moments). In order to obtain a model of the power spectrum we will thus need to specify the dynamical evolution. Since eq. (46) describes the redshift-space velocity divergence $\theta^s(\mathbf{k}, z)$ in terms of its real-space equivalent $\theta(\mathbf{k}, z)$, it will suffice to fix the dynamics in real space. The velocity power spectrum is easily recovered from the velocity divergence power spectrum using eq. (39).

We will require a nonlinear description of $\theta(\mathbf{k}, z)$. As we have mentioned, linear theory is inadequate to see the effect of RSD; there is no analogue to the well-known Kaiser effect in the large-scale limit, for there is no mean streaming velocity (in the way that there is a mean density). Nonlinearities must be considered and for this we will use Eulerian standard perturbation theory (SPT) at one-loop precision [74]. This will allow us to compute the leading-order contribution to the nonlinear power spectrum (the one-loop power spectrum). As we will see the RSD imprint on quasilinear and nonlinear scales, in contrast to the clustering picture, which is apparent on all scales.

A. Real-space velocity divergence power spectrum

The large-scale structure exhibited in the distribution of matter is the result of gravitational instability. Regions slightly overdense initially are further enhanced over time as more matter accumulates. The velocity field then arises from potential gradients set up by matter density fluctuations. In the regime where the fluctuations may be considered small the matter density field (or velocity field) is well described by linear dynamics, which has the property that (large-scale) Fourier modes grow at the same rate. However, over time linear theory breaks down as gravity drives initially small density fluctuations towards nonlinearity.

This subsection reviews how to systematically compute nonlinear corrections to linear theory using one-loop PT. We will keep the discussion brief by presenting only the results needed to specify our power spectrum model (given by eq. (61) below).

In SPT the dynamics are governed by the continuity, Euler, and Poisson equations, describing the time evolution of a self-gravitating, pressureless perfect fluid. Provided that the amplitude of the overdensity field δ and velocity divergence field θ is small these equations can be solved perturbatively with the power-series ansatz

$$\delta(\mathbf{k}, z) = \sum_{n=1}^{\infty} D(z)^n \delta^{(n)}(\mathbf{k}), \quad (47)$$

$$\theta(\mathbf{k}, z) = \sum_{n=1}^{\infty} D(z)^n \theta^{(n)}(\mathbf{k}), \quad (48)$$

where $D(z)$ is the linear growth factor (here normalized to unity at $z = 0$), and the velocity divergence is defined in eq. (37).¹¹ In the following we work at $z = 0$ to suppress unimportant factors of D^n in calculations; they are of course trivial to carry through and can be restored in the end result. (Note that peculiar velocity surveys probe low redshifts, $z \lesssim 0.01$, so setting $D = 1$ is appropriate.)

The first-order solution shows that $\delta^{(1)}(\mathbf{k}) = \theta^{(1)}(\mathbf{k})$ and recovers the usual linear theory predictions—namely, $\delta(\mathbf{k}, z) = D(z)\delta^{(1)}(\mathbf{k}) = \theta(\mathbf{k}, z)$ and $\mathbf{v}(\mathbf{k}, z) = -(\mathbf{i}\mathbf{k}/k^2)\mathcal{H}f\delta(\mathbf{k}, z)$. If we consider the second-order solution, we will also have a term quadratic in the linear field $\delta^{(1)}$; in general, the n th-order term (e.g. $\theta^{(n)}$) contains a product of n linear fields. Working at the same level of precision as before, nonlinearities in the divergence field need to be considered up to third order, $\theta \simeq \theta^{(1)} + \theta^{(2)} + \theta^{(3)}$. Solving the fluid equations with the ansatz (48) we have the standard mode-coupling formula,

$$\theta^{(n)}(\mathbf{k}) = \left[\prod_{i=1}^n \int \frac{d^3\mathbf{q}_i}{(2\pi)^3} \delta^{(1)}(\mathbf{q}_i) \right] G_S^{(n)}(\mathbf{q}_1, \dots, \mathbf{q}_n) (2\pi)^3 \delta_D\left(\mathbf{k} - \sum_{j=1}^n \mathbf{q}_j\right), \quad (49)$$

where the mode-coupling kernels $G_S^{(n)}$ are obtained from a set of recursion relations (that can be found in ref. [74]).¹² In general, the n th-order kernel $G_S^{(n)}$ depends on a combination of lower-order kernels, up to $F_S^{(n-1)}$ and $G_S^{(n-1)}$. At one loop we need only consider the second- and third-order kernels. The kernel $G_S^{(3)}$ is not widely used, so for convenience we present it here (together with $G_S^{(2)}$):

$$G_S^{(2)}(\mathbf{q}_1, \mathbf{q}_2) = \frac{3}{7} + \frac{4}{7} \frac{(\mathbf{q}_1 \cdot \mathbf{q}_2)^2}{q_1^2 q_2^2} + \frac{1}{2} \frac{\mathbf{q}_1 \cdot \mathbf{q}_2}{q_1 q_2} \left(\frac{q_1}{q_2} + \frac{q_2}{q_1} \right), \quad (50)$$

$$\begin{aligned} G_S^{(3)}(\mathbf{k}, \mathbf{q}, -\mathbf{q}) &= \frac{1}{|\mathbf{k} - \mathbf{q}|^2} \left[-\frac{2(\mathbf{k} \cdot \mathbf{q})^3}{63k^2q^2} + \frac{4(\mathbf{k} \cdot \mathbf{q})^3}{63q^4} + \frac{(\mathbf{k} \cdot \mathbf{q})^2}{36k^2} - \frac{5(\mathbf{k} \cdot \mathbf{q})^2}{84q^2} \right. \\ &\quad \left. - \frac{k^2(\mathbf{k} \cdot \mathbf{q})^2}{18q^4} + \frac{\mathbf{k} \cdot \mathbf{q}}{252} + \frac{19k^2\mathbf{k} \cdot \mathbf{q}}{252q^2} - \frac{k^2}{42} \right] \\ &+ \frac{1}{|\mathbf{k} + \mathbf{q}|^2} \left[-\frac{5(\mathbf{k} \cdot \mathbf{q})^3}{63k^2q^2} - \frac{11(\mathbf{k} \cdot \mathbf{q})^3}{63q^4} - \frac{(\mathbf{k} \cdot \mathbf{q})^2}{36k^2} - \frac{43(\mathbf{k} \cdot \mathbf{q})^2}{252q^2} \right. \\ &\quad \left. - \frac{k^2(\mathbf{k} \cdot \mathbf{q})^2}{9q^4} - \frac{\mathbf{k} \cdot \mathbf{q}}{252} - \frac{19k^2\mathbf{k} \cdot \mathbf{q}}{252q^2} - \frac{k^2}{42} \right]. \end{aligned} \quad (51)$$

Note that the general expression for $G_S^{(3)}(\mathbf{q}_1, \mathbf{q}_2, \mathbf{q}_3)$ is rather lengthy so we have written it in the only configuration needed for the power spectrum calculation. (In fact, the the only part of $G_S^{(3)}$ needed to calculate the one-loop spectrum is the angle-averaged part, which depends on $\mu' \equiv \hat{\mathbf{k}} \cdot \hat{\mathbf{q}}$. And while integrating out μ' is straightforward, the above form allows for fast numerical evaluation by exploiting the Fast Fourier Transform; see Appendix A.)

Turning to the power spectrum, the nonlinear contributions will come from a nonvanishing bispectrum, as well as the usual one-loop corrections to the real-space power spectrum:

$$P_{\theta\theta}^{1\text{-loop}}(k) = P_L(k) + P_{22}(k) + 2P_{13}(k), \quad (52)$$

where the power spectrum is defined by $\langle \theta(\mathbf{k})\theta(\mathbf{k}') \rangle = (2\pi)^3 \delta_D(\mathbf{k} + \mathbf{k}') P_{\theta\theta}(k)$; the linear power spectra is degenerate, $P_L \equiv P_{\delta\delta}^L = P_{\theta\theta}^L$; and the one-loop contributions reads

$$P_{22}(k) = 2 \int_{\mathbf{q}} [G_S^{(2)}(\mathbf{q}, \mathbf{k} - \mathbf{q})]^2 P_L(q) P_L(|\mathbf{k} - \mathbf{q}|), \quad (53a)$$

$$P_{13}(k) = 3P_L(k) \int_{\mathbf{q}} G_S^{(3)}(\mathbf{k}, \mathbf{q}, -\mathbf{q}) P_L(q). \quad (53b)$$

The subscripts of these terms indicates the number of fields evaluated at each of the two points; e.g. P_{13} corresponds to three linear fields at the first location and a single linear field at the second (the factor of two in eq. (52) accounts

¹¹ Our definition of θ absorbs an overall factor of $-\mathcal{H}f$ that often appears on the right-hand side of eq. (48).

¹² A similar expression exists for $\delta^{(n)}$ in terms of kernels $F_S^{(n)}$, but we will not need it.

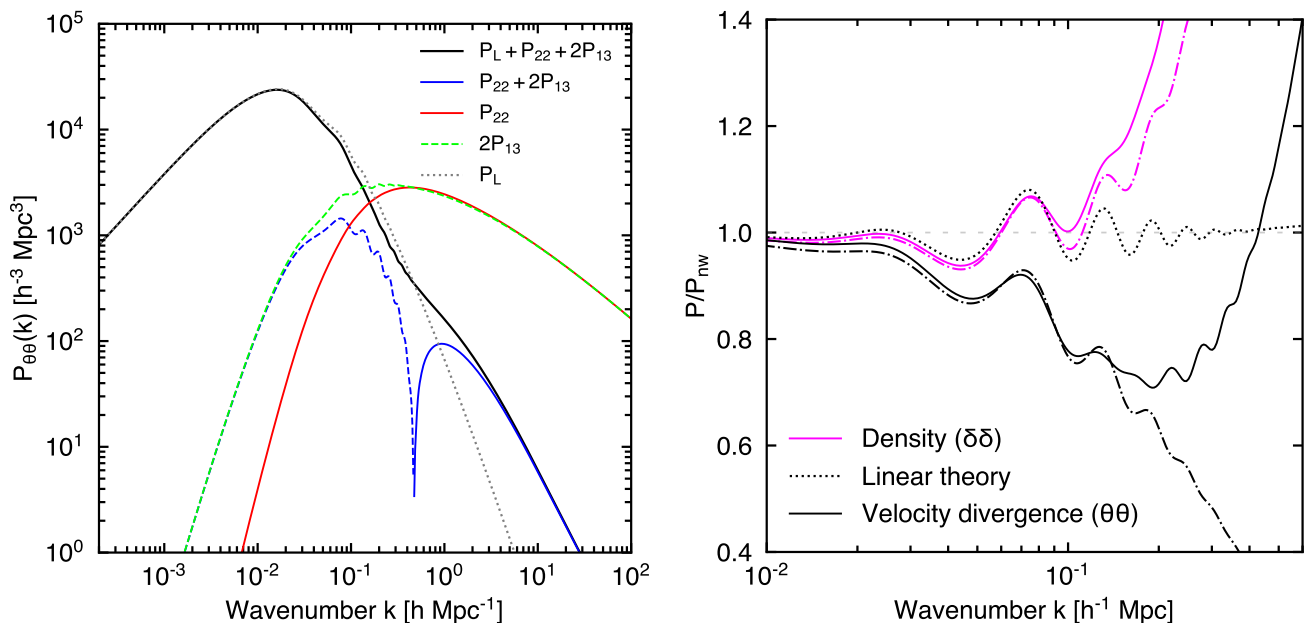


FIG. 1: Real-space power spectra at $z = 0$. *Left panel:* The one-loop velocity divergence power spectrum (solid black line) is comprised of the linear power spectrum P_L (dotted black line) and nonlinear corrections, P_{22} (solid red line) and P_{13} (dashed green line). Note that power spectrum contributions can be negative valued and in that case we show instead the absolute value (dashed lines). *Right panel:* Power spectra normalized to the linear “no-wiggle” power spectrum [75]. The inclusion of one-loop corrections (solid lines) is seen to break the degeneracy in linear theory (dotted black) between the density and velocity divergence power spectra. The scales on which the one-loop power spectra is able to match simulations can be seen through comparison with the nonlinear power spectra (dash-dotted lines) indicated by the empirically-calibrated fitting formulae for density [76, 77] (“Halofit”) and velocity divergence [78] auto-power spectra. Notice in particular that for the velocity divergence the departure from linear theory (dotted black line) is seen to begin sooner (i.e. at smaller k) than for the density; that is, on scales where linear theory is adequate for density, nonlinear corrections are needed for the velocity divergence.

for the reverse case). Note that the factors of two and three in eqs. (53a) and (53b) result from using the symmetrized forms of the kernels.

Finally, the last ingredient we will need is the tree-level bispectrum,

$$B_{\theta\theta\theta}(k_1, k_2, k_3) = 2G_S^{(2)}(\mathbf{k}_1, \mathbf{k}_2)P_L(k_1)P_L(k_2) + 2 \text{ cyc.}, \quad (54)$$

where we recall that the bispectrum is defined by $\langle \theta(\mathbf{k}_1)\theta(\mathbf{k}_2)\theta(\mathbf{k}_3) \rangle = (2\pi)^3 \delta_D(\mathbf{k}_1 + \mathbf{k}_2 + \mathbf{k}_3) B_{\theta\theta\theta}(k_1, k_2, k_3)$.¹³ Since translation invariance implies the triangle condition, $\mathbf{k}_1 + \mathbf{k}_2 + \mathbf{k}_3 = 0$, the bispectrum depends only on three numbers, either three lengths or two lengths and one angle.

In figure 1 we show the one-loop prediction of the (real-space) power spectrum. While in linear theory the (scaled) velocity divergence is equivalent to the matter density, in nonlinear theory there is a decrease in power on scales $k \lesssim 0.1 h \text{Mpc}^{-1}$. This has been observed in simulations [24, 63, 79, 80]. By contrast the linear density field remains valid up to $k \simeq 0.1 h \text{Mpc}^{-1}$. Taking into account nonlinear effects therefore shows that the velocity field grows more slowly than predicted by linear theory, leading to a decrease in power. This would be the case for the density field as well if not for an accidental cancellation that occurs over the same range of scales. The difference is that the velocity divergence field responds more readily to tidal forces, giving rise to non-radial motions that tends to counter gravitational collapse [74]. Unlike the density field the onset of the nonlinear regime of the velocity field begins at lower k (larger scales).

¹³ Note that depending on the definition of θ a factor of $(-Hf)^3$ may appear on the right-hand side of eq. (54). With our definition (37) this factor has been absorbed into the bispectrum.

B. Redshift-space velocity divergence power spectrum

So far we have presented the well-known real-space statistics by expanding $\theta(\mathbf{k})$ using third-order perturbation theory. We will now use these results to compute the one-loop redshift-space power spectrum. To see what terms are relevant consider again

$$\theta^s(\mathbf{k}) = \theta_1^s(\mathbf{k}) + \theta_2^s(\mathbf{k}) + \theta_3^s(\mathbf{k}) + \dots, \quad (55)$$

where the subscript denotes the number of (nonlinear) fields being coupled, so $\theta_1^s(\mathbf{k}) \equiv \theta(\mathbf{k})$ is just the real-space field given by eq. (48), $\theta_2^s(\mathbf{k})$ denotes the convolution of two $\theta(\mathbf{k})$ fields filtered by the kernel $K_S^{(2)}$, etc.

Again, we have suppressed the dependence of $\theta_2^s, \theta_3^s, \dots$ on the LOS $\hat{\mathbf{n}}$. [The subscripts in eq. (55) are not to be confused with the superscripts in eq. (49) that are instead used to indicate the number of *linearized* fields being coupled.] In this paper we will work under the plane-parallel limit, allowing us to treat the LOS $\hat{\mathbf{n}}$ as a constant across the imagined galaxy sample.¹⁴ Since we only have to consider a single LOS we will take this to be along the z -axis $\hat{\mathbf{n}} = \hat{\mathbf{z}}$ and denote the LOS velocity component by v_z , rather than v_{\parallel} .

With the mapping and field specified we can now calculate the redshift-space power spectrum. We have for the two-point function

$$\langle \theta^s(\mathbf{k}) \theta^s(\mathbf{k}') \rangle = \langle \theta_1^s(\mathbf{k}) \theta_1^s(\mathbf{k}') \rangle + 2 \langle \theta(\mathbf{k}) \theta_2^s(\mathbf{k}') \rangle + 2 \langle \theta_1^s(\mathbf{k}) \theta_3^s(\mathbf{k}') \rangle + \langle \theta_2^s(\mathbf{k}) \theta_2^s(\mathbf{k}') \rangle + \dots. \quad (56)$$

The power spectrum $P_{\theta\theta}^s(\mathbf{k})$ is defined by $\langle \theta^s(\mathbf{k}) \theta^s(\mathbf{k}') \rangle = (2\pi)^3 \delta_{\mathbf{D}}(\mathbf{k} + \mathbf{k}') P_{\theta\theta}^s(\mathbf{k})$. The first term on the right-hand side of eq. (56) is the usual two-point function in the absence of RSDs that we have already seen in Section V A. The remaining terms are then induced by RSD and will be calculated in this section. Since we model the redshift-space power spectrum at one loop we truncate θ^s at third order in $\delta^{(1)}$. Accordingly, eq. (56) reads

$$\langle \theta^s(\mathbf{k}) \theta^s(\mathbf{k}') \rangle \simeq \langle \theta(\mathbf{k}) \theta(\mathbf{k}') \rangle + 2 \langle \theta(\mathbf{k}) \theta_2^s(\mathbf{k}') \rangle + 2 \langle \theta^{(1)}(\mathbf{k}) \theta_3^s(\mathbf{k}') \rangle + \langle \theta_2^s(\mathbf{k}) \theta_2^s(\mathbf{k}') \rangle. \quad (57)$$

The first term on the right-hand side corresponds to the fact that the redshift-space velocity field is at leading order equal to its real-space equivalent, as already discussed. The other terms are therefore induced in redshift space and read, upon substituting in eq. (46) together with eq. (48),

$$\langle \theta(\mathbf{k}) \theta_2^s(\mathbf{k}') \rangle = f \int_{\mathbf{q}} K_S^{(2)}(\mathbf{q}, \mathbf{k}' - \mathbf{q}) \langle \theta(\mathbf{k}) \theta(\mathbf{q}) \theta(\mathbf{k}' - \mathbf{q}) \rangle_{\text{tree}}, \quad (58a)$$

$$\langle \theta^{(1)}(\mathbf{k}) \theta_3^s(\mathbf{k}') \rangle = f^2 \int_{\mathbf{q}} \int_{\mathbf{q}'} K_S^{(3)}(\mathbf{q}, \mathbf{q}', \mathbf{k}' - \mathbf{q} - \mathbf{q}') \langle \theta^{(1)}(\mathbf{k}) \theta^{(1)}(\mathbf{q}) \theta^{(1)}(\mathbf{q}') \theta^{(1)}(\mathbf{k}' - \mathbf{q} - \mathbf{q}') \rangle, \quad (58b)$$

$$\langle \theta_2^s(\mathbf{k}) \theta_2^s(\mathbf{k}') \rangle = f^2 \int_{\mathbf{q}} \int_{\mathbf{q}'} K_S^{(2)}(\mathbf{q}, \mathbf{k} - \mathbf{q}) K_S^{(2)}(\mathbf{q}', \mathbf{k}' - \mathbf{q}') \langle \theta^{(1)}(\mathbf{q}) \theta^{(1)}(\mathbf{k} - \mathbf{q}) \theta^{(1)}(\mathbf{q}') \theta^{(1)}(\mathbf{k}' - \mathbf{q}') \rangle. \quad (58c)$$

Equations (58b) and (58c) can be expressed in terms of two-point functions using Wick's theorem; alternatively, if we notice that the loop integrals are of the “13” and “22” forms (cf. eqs. (53a) and (53b)), we can write at once

$$\langle \theta^{(1)}(\mathbf{k}) \theta_3^s(\mathbf{k}') \rangle = (2\pi)^3 \delta_{\mathbf{D}}(\mathbf{k} + \mathbf{k}') f^2 P_L(k) \int_{\mathbf{q}} 3 K_S^{(3)}(\mathbf{k}, \mathbf{q}, -\mathbf{q}) P_L(q), \quad (59a)$$

$$\langle \theta_2^s(\mathbf{k}) \theta_2^s(\mathbf{k}') \rangle = (2\pi)^3 \delta_{\mathbf{D}}(\mathbf{k} + \mathbf{k}') f^2 \int_{\mathbf{q}} 2 [K_S^{(2)}(\mathbf{q}, \mathbf{k} - \mathbf{q})]^2 P_L(q) P_L(|\mathbf{k} - \mathbf{q}|). \quad (59b)$$

This leaves eq. (58a), which involves a three-point function; thus, substituting in the tree-level bispectrum (54) we have

$$\langle \theta(\mathbf{k}) \theta_2^s(\mathbf{k}') \rangle = (2\pi)^3 \delta_{\mathbf{D}}(\mathbf{k} + \mathbf{k}') f \int_{\mathbf{q}} K_S^{(2)}(\mathbf{q}, \mathbf{k} - \mathbf{q}) B_{\theta\theta\theta}(k, q, |\mathbf{k} - \mathbf{q}|) \quad (60a)$$

$$\begin{aligned} &= (2\pi)^3 \delta_{\mathbf{D}}(\mathbf{k} + \mathbf{k}') f \left[4 P_L(k) \int_{\mathbf{q}} K_S^{(2)}(\mathbf{q}, \mathbf{k} - \mathbf{q}) G_S^{(2)}(\mathbf{k}, -\mathbf{q}) P_L(q) \right. \\ &\quad \left. + 2 \int_{\mathbf{q}} K_S^{(2)}(\mathbf{q}, \mathbf{k} - \mathbf{q}) G_S^{(2)}(\mathbf{q}, \mathbf{k} - \mathbf{q}) P_L(q) P_L(|\mathbf{k} - \mathbf{q}|) \right]. \quad (60b) \end{aligned}$$

¹⁴ While we do not consider wide-angle effects in this work, given that realistic peculiar velocity surveys are statistics limited (with $\sim 20\%$ measurement uncertainties), it might be expected that their impact on analysis is modest or negligible.

In addition to substituting in the bispectrum, the first equality has been obtained by taking $\mathbf{q} \rightarrow -\mathbf{q}$ in the integrand (since the integration is over all space), followed by setting $\mathbf{k}' = -\mathbf{k}$ using the delta function; the second equality is obtained by taking $\mathbf{q} \rightarrow \mathbf{k} - \mathbf{q}$; in both equalities we have used that $K_S^{(n)}$ and $G_S^{(n)}$ are parity symmetric, e.g. $K_S^{(2)}(\mathbf{q}_1, \mathbf{q}_2) = K_S^{(2)}(-\mathbf{q}_1, -\mathbf{q}_2)$. The result of these simplifications shows that eq. (60a) yields additional “13” and “22” loop contributions.

Now, gathering the previous results we can write the redshift-space power spectrum succinctly as [cf. eq. (52)]

$$P_{\theta\theta}^s(\mathbf{k}) = P_L(k) + P_{22}^s(\mathbf{k}) + 2P_{13}^s(\mathbf{k}), \quad (61)$$

where the 13- and 22-loop integrals are brought into the forms [cf. eqs. (53a) and (53b)]

$$P_{22}^s(\mathbf{k}) \equiv 2 \int_{\mathbf{q}} [Z^{(2)}(\mathbf{q}, \mathbf{k} - \mathbf{q})]^2 P_L(q) P_L(|\mathbf{k} - \mathbf{q}|), \quad (62a)$$

$$P_{13}^s(\mathbf{k}) \equiv 3P_L(k) \int_{\mathbf{q}} Z^{(3)}(\mathbf{k}, \mathbf{q}, -\mathbf{q}) P_L(q), \quad (62b)$$

with the *redshift-space velocity divergence kernels*,

$$Z^{(1)}(\mathbf{q}) \equiv 1, \quad (63a)$$

$$Z^{(2)}(\mathbf{q}_1, \mathbf{q}_2) \equiv G_S^{(2)}(\mathbf{q}_1, \mathbf{q}_2) + fK_S^{(2)}(\mathbf{q}_1, \mathbf{q}_2), \quad (63b)$$

$$Z^{(3)}(\mathbf{q}_1, \mathbf{q}_2, \mathbf{q}_3) \equiv G_S^{(3)}(\mathbf{q}_1, \mathbf{q}_2, \mathbf{q}_3) + \frac{4}{3}fK_S^{(2)}(\mathbf{q}_2, \mathbf{q}_1 + \mathbf{q}_3)G_S^{(2)}(\mathbf{q}_1, \mathbf{q}_3) + f^2K_S^{(3)}(\mathbf{q}_1, \mathbf{q}_2, \mathbf{q}_3). \quad (63c)$$

[Although not needed here, $Z^{(1)}$ is defined in accordance with the lowest-order redshift map being the identity map.] These kernels are akin to the redshift-space density kernels given in ref. [81]. There is one obvious point of difference, however, which is that here linear theory is inadequate to reveal the RSD effect on the velocity field: the first-order kernel $Z^{(1)}$ is unity, whereas for the density field it is equal to the Kaiser factor, $1 + f\mu^2$ [$\mu = \hat{\mathbf{k}} \cdot \hat{\mathbf{z}}$]. We can notice that these kernels carry additional information about the growth rate (and potentially be used to break degeneracies with other parameters). And as with $K_S^{(n)}$, these kernels are functions that depend on $\hat{\mathbf{n}}$ through the scalars $\hat{\mathbf{n}} \cdot \mathbf{q}_i$ (though we have suppressed their dependence here). Finally, we remark that it is straightforward enough to calculate the bispectrum of θ^s using these kernels, though we point out that $Z^{(2)}$ is already in symmetrized form, but $Z^{(3)}$ is not (because of the cross-term).

With these expressions we can thus compute $P_{\theta\theta}^s(\mathbf{k})$ in an analogous way to the one-loop power spectrum (52), but instead with direction-dependent kernels. However, for now we will keep separate the RSD terms (terms that depend on K_S) as doing so will help to simplify the extraction of multipoles later on.

Like $G_S^{(3)}$, the redshift-space kernel $K_S^{(3)}$ also results in a k -dependent correction to P_L . The contribution of this term to $P_{\theta\theta}^s(\mathbf{k})$ is found to be

$$2f^2P_L(k) \int_{\mathbf{q}} 3K_S^{(3)}(\mathbf{k}, \mathbf{q}, -\mathbf{q})P_L(q) = -f^2\mu^2k^2P_L(k)\sigma_u^2, \quad (64)$$

where σ_u^2 is the one-dimensional (scaled) velocity dispersion,

$$\sigma_u^2 \equiv \frac{1}{3} \int_{\mathbf{q}} \frac{P_L(q)}{q^2} = \sigma_v^2/(\mathcal{H}f)^2 \quad (65)$$

(and can be interpreted as the one-dimensional displacement dispersion in the Lagrangian description of the fluid). As figure 2 shows, this contribution is subdominant to the other “13” term given by $K_S^{(2)}G_S^{(2)}$. The $K_S^{(2)}K_S^{(2)}$ contribution (as labelled in figure 2) is similarly small in magnitude. This term corresponds to a second-order redshift mapping which, at one loop, amounts to a mode-coupling of linearized fields only (i.e. the linear theory prediction is not sufficient to see a sizable redshift effect).

1. Multipole moments

The distortions that occur in redshift space are directed along the LOS and implies the loss of statistical isotropy; the power spectrum is no longer invariant under rotations and will in general depend on the wavevector \mathbf{k} . However,

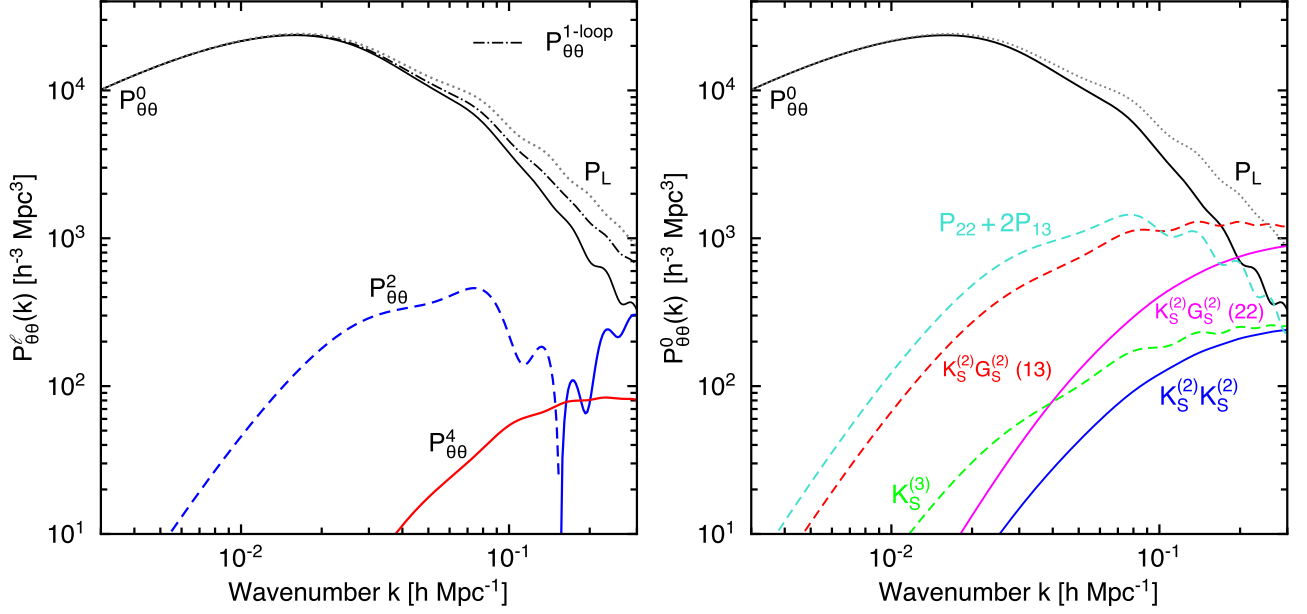


FIG. 2: Multipoles of the redshift-space velocity divergence power spectrum. *Left panel:* Comparison between multipoles in real and redshift space. In redshift space, there is in addition to the monopole (solid black) a quadrupole (solid blue) and hexadecapole (solid red). *Right panel:* Contributions to the redshift-space monopole from each (composite) kernel in eq. (61). As in figure 1 dashed lines indicate negative values. In this work, one-loop integrals are evaluated using the FFTLog parameters $\nu = -0.6$, $N = 256$, $k_{\min} = 10^{-4} h \text{ Mpc}^{-1}$ and $k_{\max} = 100 h \text{ Mpc}^{-1}$.

the power spectrum retains azimuthal symmetry about the LOS $\hat{\mathbf{n}}$, so depends not on \mathbf{k} but two components—the wavenumber k and $\mu \equiv \hat{\mathbf{k}} \cdot \hat{\mathbf{n}}$, the cosine of the angle formed between the LOS and the wavevector. These distortions are conveniently characterized in terms of multipole moments about $\hat{\mathbf{n}}$ by expanding $P_{\theta\theta}^s(\mathbf{k})$ in Legendre polynomials:

$$P_{\theta\theta}^s(k, \mu) = \sum_{\ell} P_{\theta\theta}^{\ell}(k) \mathcal{L}_{\ell}(\mu), \quad (66)$$

where the multipole moments are

$$P_{\theta\theta}^{\ell}(k) \equiv (2\ell + 1) \int_{-1}^1 \frac{d\mu}{2} \mathcal{L}_{\ell}(\mu) P_{\theta\theta}^s(k, \mu), \quad (67)$$

and $\mathcal{L}_{\ell}(\mu)$ is the Legendre polynomial of order ℓ . The anisotropic contributions to $P_{\theta\theta}^s(\mathbf{k})$ correspond to the $\ell > 0$ multipoles and arise from all terms in eq. (61), except the first three, which contribute to the $\ell = 0$ multipole moment.

The real-space loop integrals are typically performed by choosing spherical coordinates with the pole aligned with \mathbf{k} . In such coordinates the integral over ϕ is trivial and reduces the loop integral to an integral over q and $\mu' = \hat{\mathbf{k}} \cdot \hat{\mathbf{q}}$. Here the presence of $\hat{\mathbf{n}}$ in the kernels complicates this because there are now $\mathbf{q} \cdot \hat{\mathbf{n}}$ terms, and there is no longer rotational symmetry in ϕ . It can still, however, be carried out analytically by choosing coordinates such that the z -axis is aligned with \mathbf{k} (i.e. $\mathbf{k} = k\hat{\mathbf{z}}$). In components parallel and perpendicular to $\hat{\mathbf{z}}$, we have $\mathbf{q} = (q_{\perp} \cos \phi, q_{\perp} \sin \phi, q_z)$ and $\hat{\mathbf{n}} = (\hat{n}_{\perp} \cos \phi_o, \hat{n}_{\perp} \sin \phi_o, \hat{n}_z)$; defining the separation angles, $\mu \equiv \hat{\mathbf{k}} \cdot \hat{\mathbf{n}}$ and $\mu' \equiv \hat{\mathbf{k}} \cdot \hat{\mathbf{q}}$, so that $q_z = q\mu'$, $\hat{n}_z = \mu$, $q_{\perp} = q\sqrt{1 - \mu'^2}$, and $\hat{n}_{\perp} = \sqrt{1 - \mu^2}$, we have the parametrization

$$\mathbf{q} = q(\sqrt{1 - \mu'^2} \cos \phi, \sqrt{1 - \mu'^2} \sin \phi, \mu'), \quad (68a)$$

$$\hat{\mathbf{n}} = (\sqrt{1 - \mu^2}, 0, \mu). \quad (68b)$$

(Note that here we have chosen $\phi_o = 0$ as allowed by the rotational freedom to orient the xy -plane.) The multipole

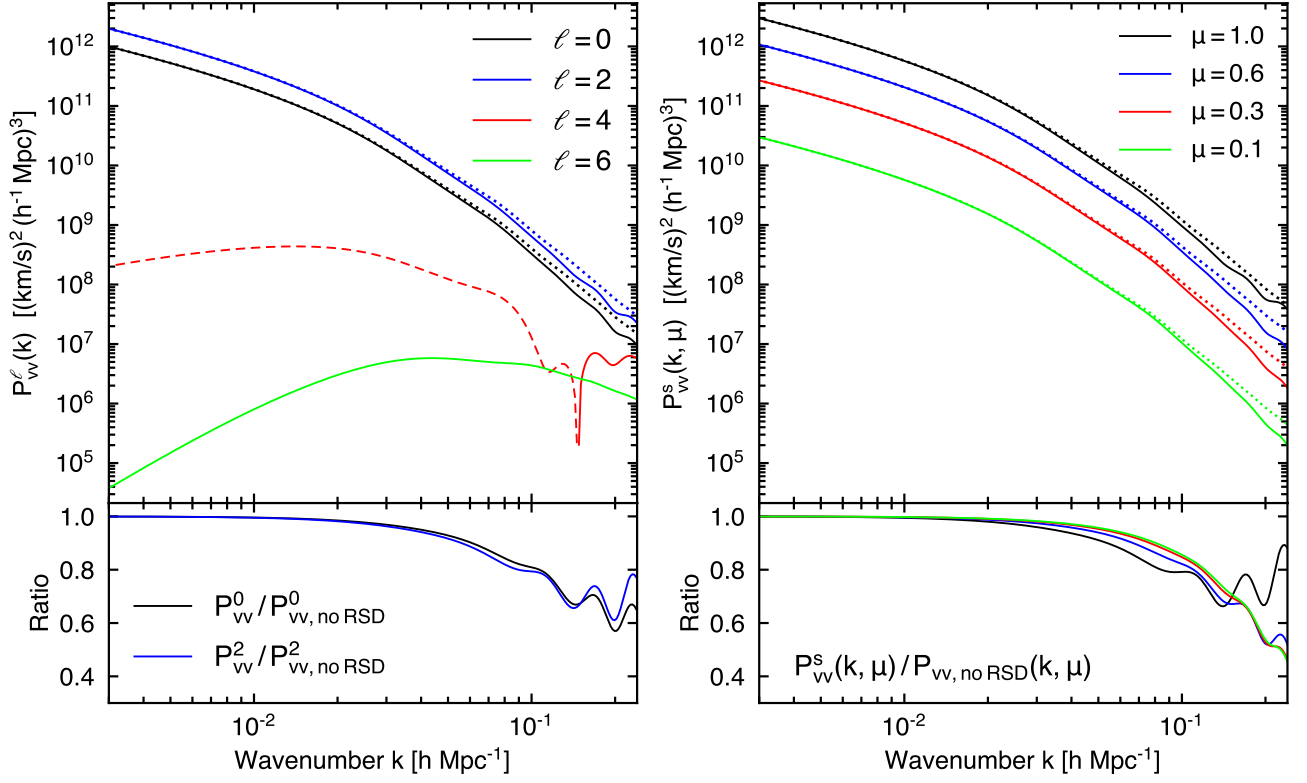


FIG. 3: Multipoles of the redshift-space velocity power spectrum (left panel) and the angular dependence of the total power spectrum (right panel). Note that in a typical survey the maximum separation between a pair of galaxies is $r_{\text{max}} \simeq 300 h^{-1} \text{Mpc}$, which roughly indicates the largest measurable mode is $k_{\text{min}} = 2\pi/r_{\text{max}} \approx 0.02 h \text{Mpc}^{-1}$. Notice that the dominant contribution comes in the form of a quadrupole moment, not the monopole moment as might be expected.

moments then read

$$P_{\theta\theta}^\ell(k) = P_L(k) \delta_{\ell 0}^K + \frac{k^3}{2\pi^2} \left[\int r^2 dr P_L(kr) \int \frac{d\mu'}{2} I_{22}^\ell(r, \mu') P_L(k\psi(r, \mu')) + 2P_L(k) \int r^2 dr P_L(kr) \int \frac{d\mu'}{2} I_{13}^\ell(r, \mu') \right], \quad (69)$$

where $\delta_{\ell 0}^K$ is the Kronecker delta, $r \equiv q/k$, $\psi(r, \mu') \equiv \sqrt{1 + r^2 - 2r\mu'}$, and

$$I_{22}^\ell(r, \mu') \equiv (2\ell + 1) \int \frac{d\mu}{2} \mathcal{L}_\ell(\mu) \int \frac{d\phi}{2\pi} 2[Z_2(r, \mu, \mu', \phi)]^2, \quad (70a)$$

$$I_{13}^\ell(r, \mu') \equiv (2\ell + 1) \int \frac{d\mu}{2} \mathcal{L}_\ell(\mu) \int \frac{d\phi}{2\pi} 3Z_3(r, \mu, \mu', \phi). \quad (70b)$$

Closed-form expressions of these kernels can be found in Appendix C. Note that the μ' integral in the last term of eq. (69) is over polynomials of μ' and is analytic. As with the redshift-space density power spectrum (in the plane-parallel limit), only the monopole ($\ell = 0$), quadrupole ($\ell = 2$), and hexadecapole ($\ell = 4$) are non-vanishing. While the above expression is presented in a form readily evaluated numerically by standard quadrature methods, these computations are intensive. In Appendix A we show how these can be efficiently evaluated using the FFTLog approach [82, 83].

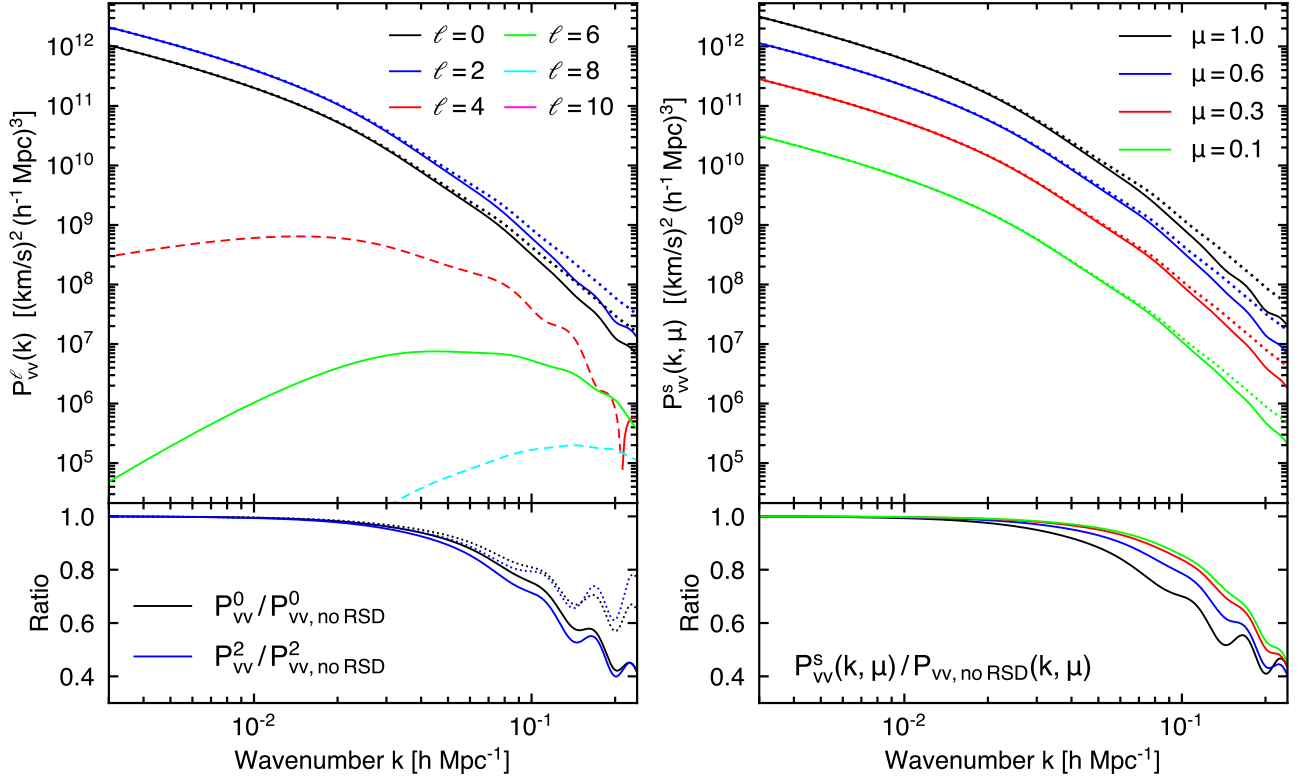


FIG. 4: Power spectrum damped by virial velocities with dispersion $\sigma_v = 350$ km/s, and using the Gaussian $\exp(-x^2)$ damping model. The multipole moments of the power spectrum are shown in the left panel, while in the right panel we show the two-dimensional power spectrum $P_{vv}^s(k, \mu)$.

C. Redshift-space velocity

We now return to v_z^s , the observable in a peculiar velocity survey. It is easy to write down its power spectrum since in Fourier space $v_z^s(\mathbf{k}) = \mathcal{H}f(ik_z/k^2)\theta^s(\mathbf{k})$; that is, we can write the power spectrum of v_z^s in terms of that for θ^s just presented,

$$P_{vv}^s(k, \mu) = \left(\frac{\mathcal{H}f\mu}{k}\right)^2 P_{\theta\theta}^s(k, \mu) \equiv \sum_{\ell} P_{vv}^{\ell}(k) \mathcal{L}_{\ell}(\mu), \quad (71)$$

where $\mu = k_z/k$. The multipole moments are defined in an analogous way to $P_{\theta\theta}^{\ell}$ (67), and are

$$P_{vv}^{\ell}(k) = \left(\frac{\mathcal{H}f}{k}\right)^2 \sum_{\ell'} A_{\ell\ell'} P_{\theta\theta}^{\ell'}(k), \quad (A_{\ell\ell'}) = \begin{pmatrix} \frac{1}{3} & \frac{2}{15} & 0 \\ \frac{2}{3} & \frac{11}{21} & \frac{4}{21} \\ 0 & \frac{12}{35} & \frac{39}{77} \\ 0 & 0 & \frac{10}{33} \end{pmatrix}. \quad (72)$$

The nonzero multipole moments are given by $\ell = 0, 2, 4, 6$ and are shown in figure 3. In particular, the multipole structure exhibits a $\ell = 6$ moment (“tetrahexacontapole”—or 64-pole), which we note is not present in the power spectrum of the velocity divergence. However, this merely arises from the geometric factor $\propto \mu^2$ in eq. (72); it also has the further effect of coupling different $P_{\theta\theta}^{\ell}$ to a given P_{vv}^{ℓ} with coefficients given through the matrix $(A_{\ell\ell'})$. In $(A_{\ell\ell'})$ we see that the first column represents the usual monopole–quadrupole split (1/3–2/3) of the real-space velocity power spectrum. (Notice also that columns add to unity.) Evidently, we also have additional contributions not found in real space as can be seen in eq. (69). Thus the second and third columns are new contributions to the anisotropy; specifically these are contributions arising from nonzero $P_{\theta\theta}^2$ and $P_{\theta\theta}^4$.

D. Further damping from velocity dispersion

The power spectrum we have so far presented describes the coherence of the galaxy motions on sufficiently large scales where the fluid description is valid. In this regime the dark matter is single-streaming and the velocity field is well defined. As such this model necessarily does not account for effects resulting from multi-streaming, i.e. the virial motions of galaxies associated with clusters. Such effects, arising from various baryonic processes, are important but beyond PT. Qualitatively though, in the context of galaxy clustering, the effect of virial motions is simply to cause a damping of the small-scale power due to the elongation of nonlinear structures along the LOS (the FoG effect). This is a smearing of the matter distribution, implying a shallower gravitational potential in redshift space, and thus a decrease in the velocity power.

To account for this effect and complete the model we will simply adopt a phenomenological damping (similar to that used to model the standard FoG effect). The complete model is given by augmenting the previous model by taking

$$P_{vv}^s(\mathbf{k}) \rightarrow D_v^2(k\mu)P_{vv}^s(\mathbf{k}), \quad (73)$$

where $P_{vv}^s(\mathbf{k})$ is given by eq. (71) and $D_v^2(x) \equiv \exp(-x^2)$ is the damping factor, with $x \equiv k\mu\sigma_u$.

For the purpose of keeping the phenomenological model separate from the PT predictions, we express the multipoles of the complete model in terms of the previous ones (71) as

$$P_{vv}^\ell(k) \rightarrow (2\ell + 1) \sum_{\ell', \ell''} \begin{pmatrix} \ell & \ell' & \ell'' \\ 0 & 0 & 0 \end{pmatrix}^2 A^{\ell'}(k) P_{vv}^{\ell''}(k), \quad (74)$$

where $A^\ell(k)$ is the ℓ th multipole moment of $D_v^2(k\mu)$, $P_{vv}^{\ell''}(k)$ is given by eq. (72), and the 2×3 array is the Wigner 3j-symbol [84] (which results from the integral over the product of three Legendre polynomials). For typical damping models, a low-order truncation of the multipole expansion (e.g. up to $\ell = 4$) is accurate enough for our needs. Figure 4 shows the power spectrum with the inclusion of nonlinear damping. As can be seen, the PT predictions on large scales are maintained but are increasingly modified on small scales. At $k \simeq 0.1 h \text{ Mpc}^{-1}$, the power is suppressed by 30%, about 10% of which coming from nonlinear damping described in this section. This is lower than the damping predicted by Kaiser and Hudson [39], as discussed in Section I, but is not surprising given that we have shown PT predicts an additional suppression of power. As such the damping observed in the simulations of ref. [24] is only partially explained by the virial motions.

VI. POWER SPECTRUM MODEL II: CUMULANT-EXPANSION APPROACH

Many of the techniques developed for redshift-space statistics of galaxy clustering (e.g. [63–65, 67, 85–87]) carry over to the related velocity statistics. This will allow us to motivate FoG-like effects that was missed in the straightforward moment expansion of the previous section. To do this we need to return to the exact Fourier for $v_z^s(\mathbf{s})$ given by eq. (32). In Fourier space, $v_z^s(\mathbf{k})$ is easily obtained from eq. (32) by inserting into it the Fourier representation of the Green's function (34); after changing the order of integration, we read off [$u_z^s \equiv -v_z^s/(\mathcal{H}f)$]

$$u_z^s(\mathbf{k}) = \frac{1}{-ik_z} \int d^3\mathbf{x} e^{i\mathbf{k}\cdot\mathbf{x}} e^{-ifk_z u_z(\mathbf{x})} \nabla_z u_z(\mathbf{x}), \quad (75)$$

with $k_z = \mathbf{k} \cdot \hat{\mathbf{z}} = k\mu$. In Fourier space we see that redshift-space distortions arise from a velocity-induced phase factor $e^{-ifk_z u_z(\mathbf{x})}$; in its absence we recover $u_z^s(\mathbf{k}) = u_z(\mathbf{k})$. Now, using that by translation invariance the two-point function can only depend on $\mathbf{r} = \mathbf{x} - \mathbf{x}'$, we have the power spectrum

$$P_{uu}^s(\mathbf{k}) = \frac{1}{k_z^2} \int d^3\mathbf{r} e^{i\mathbf{k}\cdot\mathbf{r}} \left\langle e^{-ifk_z \Delta u_z} \nabla_z u_z(\mathbf{x}) \nabla_z u_z(\mathbf{x}') \right\rangle, \quad (76)$$

in which $\Delta u_z \equiv u_z(\mathbf{x}) - u_z(\mathbf{x}')$ is the pairwise relative velocity along the LOS. Indeed, the perturbative model (61) can be recovered from the exact model (76); that is, by Taylor expanding the velocity-dependent exponential in eq. (75) to third order in u_z , then evaluating the resulting moments using one-loop PT. (Equivalently, the same result can be obtained if in the power spectrum (76) the second exponential is expanded to second order in Δu_z .)

Given the novelty of the redshift-space velocity power spectrum (76) it is instructive to compare it to the analogous density power spectrum given by eq. (7) (but derived assuming number conservation). It is not hard to see that

the basic form of the two power spectra are quite similar. The main difference is the weighting in the pairwise LOS *velocity-moment generating function* given by $\langle \dots \rangle$; that is, in eq. (7) the moments are density weighted, while in eq. (76) they are velocity-gradient weighted; in both cases they share the same phase factor. This phase factor can be brought out by rewriting eq. (7) in terms of connected n -point functions using that, by the cumulant expansion theorem, we have in general

$$\langle e^{j_1 A_1} A_2 A_3 \rangle = \exp \langle e^{j_1 A_1} \rangle_c \left[\langle e^{j_1 A_1} A_2 A_3 \rangle_c + \langle e^{j_1 A_1} A_2 \rangle_c \langle e^{j_1 A_1} A_3 \rangle_c \right], \quad (77)$$

where A_1, A_2, A_3 are random variables, and j_1 is a constant. In the case of the density power spectrum [eq. (7)] we set $A_2 = 1 + \delta(\mathbf{x})$, $A_3 = 1 + \delta(\mathbf{x}')$, whereas for the velocity power spectrum [eq. (76)] we set $A_2 = \nabla_z u_z(\mathbf{x})$, $A_3 = \nabla_z u_z(\mathbf{x}')$; in both cases $j_1 = -ifk_z$ and $A_1 = \Delta u_z$.¹⁵ (Note that eq. (77) follows from the relation between the moment and cumulant generating function, $\langle e^{\mathbf{j} \cdot \mathbf{A}} \rangle = \exp \langle e^{\mathbf{j} \cdot \mathbf{A}} \rangle_c$, with \mathbf{j} some constant vector.)

The factor $\exp \langle e^{j_1 A_1} \rangle_c$ is typically understood as the putative FoG damping prefactor, which has in the past been modelled phenomenologically in the “dispersion models” [62]. Clearly we can see that a FoG-like effect is generic to both power spectra. This suggests that we can treat “FoG” damping in the velocity power spectrum in much the same way (if not exactly the same way) as for its density counterpart.

A. Analytic model

To specify the model we will need to evaluate the connected n -point functions in eq. (76). As in eq. (61) we use one-loop PT, but only for terms within square brackets in eq. (76); the FoG factor $\exp \langle e^{j_1 A_1} \rangle_c$ will be treated separately using more empirical arguments.

First, we take the large-scale limit $j_1 \rightarrow 0$ (or $k \rightarrow 0$). Thus treating j_1 as an expansion parameter, and expanding the exponentials in eq. (77), we get

$$\langle e^{j_1 A_1} A_2 A_3 \rangle \simeq D_{1\text{pt}}^2 D_{2\text{pt}}^2 \left[\langle A_2 A_3 \rangle_c + j_1 \langle A_1 A_2 A_3 \rangle_c + \frac{1}{2} j_1^2 \langle A_1^2 A_2 A_3 \rangle_c + j_1^2 \langle A_1 A_2 \rangle_c \langle A_1 A_3 \rangle_c \right]. \quad (78)$$

Here we have expanded to second order in j_1 , as is sufficient for a one-loop calculation. In particular, we have only expanded the terms inside square brackets. Following ref. [87], the putative FoG damping factor $\exp \langle e^{j_1 A_1} \rangle_c$ has been decomposed into two kinds of FoG factors: $D_{1\text{pt}}^2 = D_{1\text{pt}}^2(k_z)$, which consists purely of one-point contributions and so can be taken out of the spatial integral; and $D_{2\text{pt}}^2 = D_{2\text{pt}}^2(k_z, \mathbf{r})$, which consists of both one- and two-point correlations.

A simple procedure to bring out an overall FoG damping term from the integral in eq. (76) is then to simply ignore spatial correlations—drop $D_{2\text{pt}}^2$ from eq. (78). This step might be justified by analogy with the density power spectrum, where it has been shown to produce a model—the widely-used “TNS model” [64]—that provides a good fit to simulations [88]. Thus, substituting eq. (78) into eq. (76), and hence dropping $D_{2\text{pt}}^2$, we have for the one-loop power spectrum model,

$$P_{uu}^s(\mathbf{k}) = D_{1\text{pt}}^2 \int d^3 \mathbf{r} e^{i\mathbf{k} \cdot \mathbf{r}} \frac{1}{k_z^2} \left[\langle A_2 A_3 \rangle + j_1 \langle A_1 A_2 A_3 \rangle + j_1^2 \langle A_1 A_2 \rangle \langle A_1 A_3 \rangle + \mathcal{O}(j_1^3) \right],$$

with $j_1 = -ifk_z$, $A_1 = u_z(\mathbf{x}) - u_z(\mathbf{x}')$, $A_2 = \nabla_z u_z(\mathbf{x})$, and $A_3 = \nabla_z u_z(\mathbf{x}')$. (79)

Note that $\langle A_2 A_3 \rangle_c = \langle A_2 A_3 \rangle$, $\langle A_1 A_2 A_3 \rangle_c = \langle A_1 A_2 A_3 \rangle$, but that in general $\langle A_1^2 A_2 A_3 \rangle_c \neq \langle A_1^2 A_2 A_3 \rangle$; in addition, we drop $\langle A_1^2 A_2 A_3 \rangle_c$ as it is a two-loop correction.¹⁶

The first term in eq. (79) corresponds to the leading-order real-to-redshift-space map, which as we have mentioned is the identity map (no distortions). The second term in eq. (79) contains a mixture of effects arising from the next-to-leading-order redshift mapping and nonlinear dynamics (the “ $K_S^{(2)} G_S^{(2)}$ ” contributions in figure 2).¹⁷ In the limit $j_1 \rightarrow 0$, eq. (79) reduces to

$$P_{uu}^s(\mathbf{k}) = D_{1\text{pt}}^2(k_z) P_{uu}(\mathbf{k}). \quad (80)$$

¹⁵ Another expression for $P_{\delta\delta}^s$, derived from eq. (7), has instead $A_2 = \delta(\mathbf{x}) + f \nabla_z u_z(\mathbf{x})$, $A_3 = \delta(\mathbf{x}') + f \nabla_z u_z(\mathbf{x}')$, with j_1 and A_1 the same as in eq. (7). This expression makes explicit use of the Jacobian of the redshift mapping (1). The related Taruya, Nishimichi and Saito (TNS) model [64] is obtained by using the cumulant expansion theorem on the resulting expression.

¹⁶ The connected moment $\langle A_1^2 A_2 A_3 \rangle_c$, in Fourier space, involves the trispectrum at the first nontrivial order. This term is therefore $\mathcal{O}(P_L^3)$, i.e. a two-loop correction.

¹⁷ The other terms—labelled “ $K_S^{(3)}$ ” and “ $K_S^{(2)} K_S^{(2)}$ ” in figure 2—originate from $\langle A_1^2 A_2 A_3 \rangle$ but do not appear in the cumulant expansion.

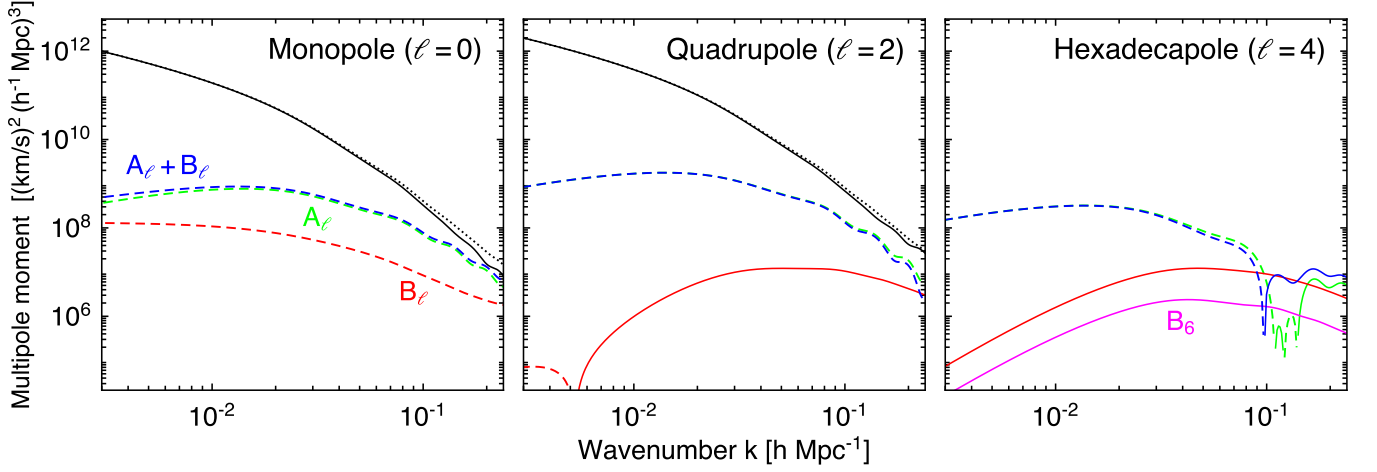


FIG. 5: Multipoles of distortion terms A and B in the cumulant expansion model. The effect on the total power spectrum $P_{uu}^\ell + A_\ell + B_\ell$ (solid black) is to be compared to the corresponding undistorted, real-space result (dotted black). Note that in real space there is no $\ell = 4$ multipole moment; all lines have been scaled by $(\mathcal{H}f)^2$; and as before we display the absolute value of the moments (dashed lines indicate negative values).

(Recall that taking the same limit but for the density field recovers the Scoccimarro model, $P_{\delta\delta}^s = D_{1\text{pt}}^2(P_{\delta\delta} + 2f\mu^2 P_{\delta\theta} + f^2\mu^4 P_{\theta\theta})$ [63].) Provided the velocity dispersion is nonzero, eq. (80) shows that there is an “FoG” effect, even for a velocity field described exactly by linear theory. This is to be contrasted with the moment expansion of Section V, where damping effects are entirely absent in linear theory (since real- and redshift-space velocity fields coincide).

Going beyond linear theory to next-to-leading order then shows there are two additional contributions to consider. Let us write the redshift-space power spectrum as

$$P_{uu}^s(\mathbf{k}) = D_{1\text{pt}}^2(k_z) \left[P_{uu}(\mathbf{k}) + A(\mathbf{k}) + B(\mathbf{k}) \right]. \quad (81)$$

This model can be compared with that of eq. (61). The obvious improvement is the appearance now of damping from velocity dispersion (through resumming the one-point contributions). Further, the A and B terms that we have treated perturbatively do not make the assumption that the amplitude of the fields are small (which was assumed in the velocity-moment expansion approach.) Rather, it is the correlations at large separations that are expected to be weak, even if the amplitude of the field at each point is large.

The term A involves a three-point function, whereas B amounts to a convolution; both are order $(P_L)^2$ (up to \mathbf{k} -dependent factors). After carrying out the necessary Fourier transforms, they read

$$A(\mathbf{k}) \equiv j_1 \int d^3\mathbf{r} e^{i\mathbf{k}\cdot\mathbf{r}} \frac{1}{k_z^2} \langle A_1 A_2 A_3 \rangle = 2f \int_{\mathbf{q}} \mathcal{K}^{(A)}(\mathbf{q}, \mathbf{k} - \mathbf{q}) B_{\theta\theta\theta}(q, |\mathbf{k} - \mathbf{q}|, k), \quad (82a)$$

$$B(\mathbf{k}) \equiv j_1^2 \int d^3\mathbf{r} e^{i\mathbf{k}\cdot\mathbf{r}} \frac{1}{k_z^2} \langle A_1 A_2 \rangle \langle A_1 A_3 \rangle = f^2 \int_{\mathbf{q}} \mathcal{K}^{(B)}(\mathbf{q}, \mathbf{k} - \mathbf{q}) P_L(q) P_L(|\mathbf{k} - \mathbf{q}|), \quad (82b)$$

Here the equalities have been obtained by evaluating the n -point functions using one-loop PT; $B_{\theta\theta\theta}$ is the tree-level bispectrum (54); and, in deriving eq. (82b), we have used that $\langle u_z(\mathbf{x}) \nabla_z u_z(\mathbf{x}') \rangle = -\langle u_z(\mathbf{x}') \nabla_z u_z(\mathbf{x}) \rangle$. The kernels are $\mathcal{K}^{(A)}(\mathbf{q}, \mathbf{q}') \equiv q_z^2 q'_z k_z / (qq'k)^2$ and $\mathcal{K}^{(B)}(\mathbf{q}, \mathbf{q}') \equiv (q_z q'_z)^3 / (qq')^4$. (Note that unlike $K_S^{(n)}$ they are not dimensionless, but have units inverse length-squared.) As before, since the kernels are multiplied by functions symmetric under permutations of their arguments, we may replace them with their symmetrized versions, which are (with the LOS here made explicit)

$$\mathcal{K}_S^{(A)}(\mathbf{q}, \mathbf{q}') = \frac{(\mathbf{q} \cdot \hat{\mathbf{z}})(\mathbf{q}' \cdot \hat{\mathbf{z}})[(\mathbf{q} + \mathbf{q}') \cdot \hat{\mathbf{z}}]^2}{2(qq')^2 |\mathbf{q} + \mathbf{q}'|^2}, \quad (83a)$$

$$\mathcal{K}_S^{(B)}(\mathbf{q}, \mathbf{q}') = \frac{[(\mathbf{q} \cdot \hat{\mathbf{z}})(\mathbf{q}' \cdot \hat{\mathbf{z}})]^3}{(qq')^4}. \quad (83b)$$

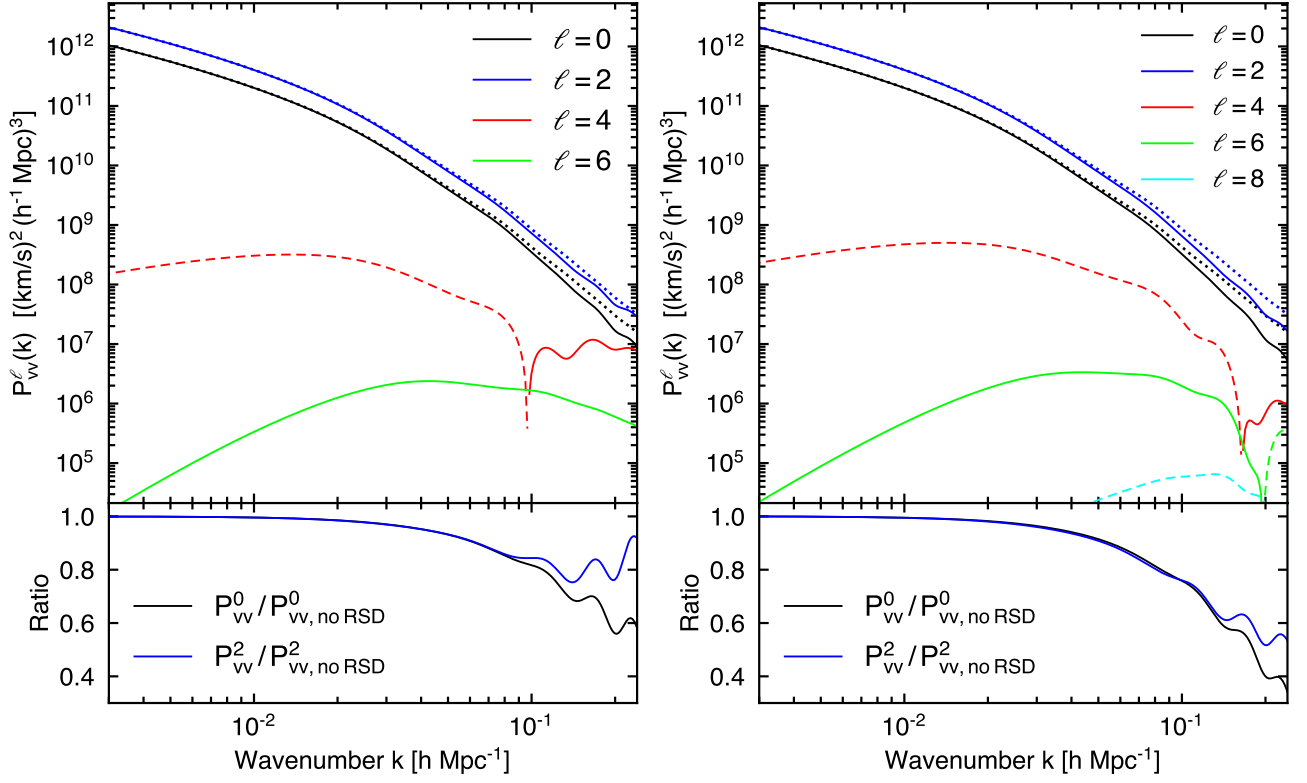


FIG. 6: Power spectrum multipoles without dispersion damping (left panel) and with dispersion damping (right panel). Note that the full power spectrum model, with exponential dispersion damping, generates higher-multipole orders ($\ell = 10, 12, \dots$) but are too small to be seen in frame. Here, as in figure 4, we use $\sigma_v = 350$ km/s for the Gaussian damping model, $D_{1\text{pt}}^2(x) = \exp(-x^2)$.

Comparing $\mathcal{K}_S^{(A)}$ with $K_S^{(2)}$ (42) shows they differ by a geometric factor $(k_z/k^2)^2$, which appears when converting between the velocity field and its divergence, cf. eq. (39). In any case, whatever the details of the kernel, $A(\mathbf{k})$ has the same form as eq. (60a) and can thus be reduced to [cf. eq. (60b)]

$$A(\mathbf{k}) = 2f\left(\frac{k_z}{k^2}\right)^2 \left[4P_L(k) \int_{\mathbf{q}} K_S^{(2)}(\mathbf{q}, \mathbf{k} - \mathbf{q}) G_S^{(2)}(\mathbf{k}, -\mathbf{q}) P_L(q) \right. \\ \left. + 2 \int_{\mathbf{q}} K_S^{(2)}(\mathbf{q}, \mathbf{k} - \mathbf{q}) G_S^{(2)}(\mathbf{q}, \mathbf{k} - \mathbf{q}) P_L(q) P_L(|\mathbf{k} - \mathbf{q}|) \right], \quad (84)$$

where we have taken out the geometric factor in order to express in terms of $K_S^{(2)}$. This term corresponds to $2\langle\theta(\mathbf{k})\theta_S^s(\mathbf{k}^*)\rangle$ in eq. (57) and is in fact equal after converting to the velocity divergence, as mentioned. However, the $B(\mathbf{k})$ term is different to any contribution we have considered so far. Figure 5 shows the multipole contributions of A and B ; in particular, we see that B is generally subdominant to A .

Finally, in order to fully specify the model a particular form for $D_{1\text{pt}}^2$ needs to be given. There are a few possibilities. Here, as we are patterning our model after the TNS model for the density power spectrum, we will simply take $D_{1\text{pt}}^2(x) = \exp(-x^2)$, with $x \equiv fk_z\sigma_u$, i.e. the Gaussian damping model.¹⁸ The complete model is shown in the right panel of figure 6 (the left panel shows the model before damping). In contrast to the moment-expansion model of Section V, this damping does not need to be put in by hand; it can be fashioned entirely from $\exp\langle e^{j^1 A_1} \rangle_c$ in eq. (77) by discarding all but the first and second one-point cumulants. Doing so amounts to considering a scale-independent Gaussian probability density function for the pairwise velocities.

¹⁸ For numerical work, we will depart from the TNS model and use the linear-theory prediction for σ_u (where in the TNS model it is treated as a free parameter).

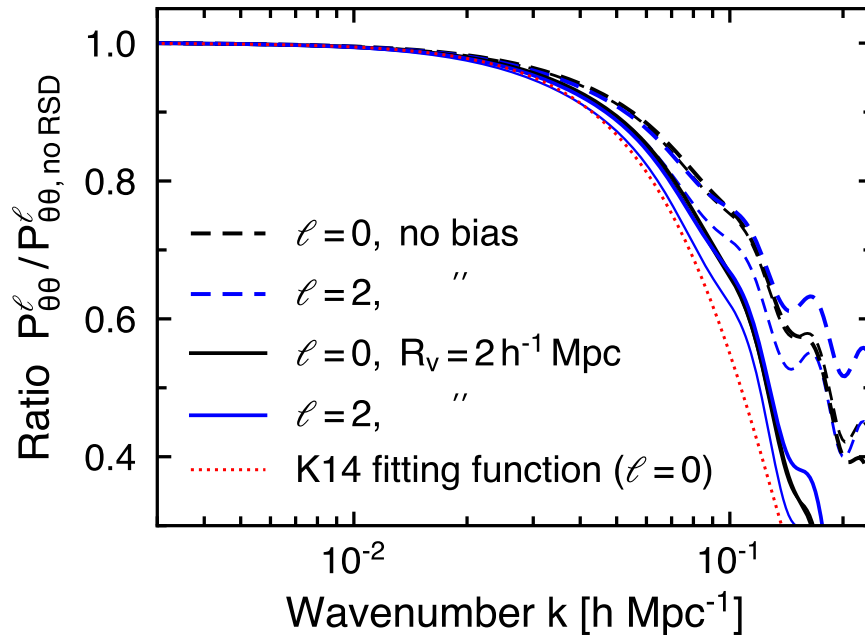


FIG. 7: Comparison between the cumulant-expansion model (thick lines) and the moment-expansion model (thin lines). As in figure 6, black lines indicate the monopole power, while blue lines indicate the quadrupole power. We also plot for the monopole power the fitting function (dotted red line) given in ref. [24]; here the shape of the suppression is described using a sinc function $D(k\sigma_u) = \sin(k\sigma_u)/(k\sigma_u)$, with the parameter σ_u calibrated on simulations. Note that the velocities measured in these simulations correspond to subhalos, not dark matter, and because of this we need to allow an additional higher-derivative velocity bias term [59] in the expansion of \mathbf{v}^s . At lowest order in derivatives, this term must be of the form $R_v^2 \nabla^2 \mathbf{v}$ [59], where R_v is of the order of the Lagrangian radius for halos. Here we use $\sigma_u = 13 h^{-1} \text{ Mpc}$, which corresponds to that found by ref. [24] for subhalos with mass $M \simeq 10^{12} h^{-1} \text{ Mpc}$ and Lagrangian radius $R_L = (3M/(4\pi\bar{\rho}))^{1/3} \simeq 1.5 h^{-1} \text{ Mpc}$. For this R_L the simulations of ref. [89] indicate $R_v = 2 h^{-1} \text{ Mpc}$. The solid lines include the velocity bias, whereas the dashed lines do not include velocity bias.

As the model stands, it should be noted that it does not yet capture any multi-streaming effects. Taking into account such effects is of course important for realistic modelling of the usual FoG effect due to galaxy virial motions. We thus emphasize that the exact model (76) assumes the single-streaming approximation for the mapping (1) (and in spite of the appearance of $D_{1\text{pt}}^2$, this is the case even if the dynamics could be evaluated exactly). As such, the usual shortcomings of models of redshift-space clustering can also be found in our model. For instance, the velocity dispersion σ_u should be treated as an empirical parameter.

VII. CONFIGURATION SPACE

We now pass from Fourier space to configuration space where the object of study is the anisotropic correlation function. Of course, the correlation function is just the Fourier transform of the power spectrum. But the presence of a LOS and the fact that we are dealing with a vector field are complicating factors. Without specifying the particular form of the power spectrum, this section derives exact expressions for the correlation functions, working again in the plane-parallel limit. We begin with a brief review of the well-known real-space theory to help us illustrate later on the differences arising in redshift space.

A. Real space

The velocity divergence correlation function for any two points separated by \mathbf{r} is $\xi_{\theta\theta}(r) \equiv \langle \theta(\mathbf{x})\theta(\mathbf{x} + \mathbf{r}) \rangle$, and reads in terms of its power spectrum $P_{\theta\theta}(k)$,

$$\xi_{\theta\theta}(r) = \int \frac{d^3\mathbf{k}}{(2\pi)^3} P_{\theta\theta}(k) e^{-i\mathbf{k}\cdot\mathbf{r}}. \quad (85)$$

Notice that by statistical isotropy and homogeneity $\xi_{\theta\theta}$ can only depend on the separation distance $r = |\mathbf{r}|$ (and likewise for the power spectrum, but for wavenumber).

Recalling eq. (39), the velocity correlation tensor $\Psi_{ij}(\mathbf{r}) \equiv \langle v_i(\mathbf{x})v_j(\mathbf{x} + \mathbf{r}) \rangle$ is given in terms of $P_{\theta\theta}$ by

$$\Psi_{ij}(\mathbf{r}) = \int \frac{d^3\mathbf{k}}{(2\pi)^3} \frac{k_i}{k} \frac{k_j}{k} \left(\frac{\mathcal{H}f}{k} \right)^2 P_{\theta\theta}(k) e^{-i\mathbf{k}\cdot\mathbf{r}}. \quad (86)$$

This symmetric tensor when decomposed into perpendicular and parallel parts (relative to the separation \mathbf{r}) reads in general

$$\Psi_{ij}(\mathbf{r}) = \Psi_{\perp}(r) (\delta_{ij}^K - \hat{r}_i \hat{r}_j) + \Psi_{\parallel}(r) \hat{r}_i \hat{r}_j, \quad (87)$$

for some radial functions $\Psi_{\perp}(r)$ and $\Psi_{\parallel}(r)$. (Alternatively, this form can be deduced from symmetry considerations, reasoning that any homogeneous and isotropic rank-2 tensor takes the form given by eq. (87) [90].) As indicated by the subscripts these correlation functions can be interpreted as those of the perpendicular and parallel components of \mathbf{v} relative to the pairwise separation \mathbf{r} .¹⁹ Note that the dependence of Ψ_{ij} is on \mathbf{r} and not r , as eq. (87) makes clear; intrinsic correlations only depend on r through Ψ_{\perp} and Ψ_{\parallel} . Integrating over directions $\hat{\mathbf{k}}$ in eq. (86) the correlation functions are given by [91]

$$\Psi_{\perp}(r) = \int_0^{\infty} \frac{k^2 dk}{2\pi^2} K_{\perp}(kr) \left[\left(\frac{\mathcal{H}f}{k} \right)^2 P_{\theta\theta}(k) \right], \quad (89a)$$

$$\Psi_{\parallel}(r) = \int_0^{\infty} \frac{k^2 dk}{2\pi^2} K_{\parallel}(kr) \left[\left(\frac{\mathcal{H}f}{k} \right)^2 P_{\theta\theta}(k) \right], \quad (89b)$$

where we have the kernels $K_{\perp}(x) \equiv j_1(x)/x$ and $K_{\parallel}(x) \equiv j_0(x) - 2j_1(x)/x$. Note that $\Psi_{\parallel} = d(r\Psi_{\perp})/dr$ since \mathbf{v} is solely determined by its velocity divergence θ (so there can only be one independent correlation function). Observations of the velocity field are limited to the LOS component $\mathbf{v} \cdot \hat{\mathbf{n}}$. For the purpose of comparison with our redshift-space results we assume $\mathbf{x}/|\mathbf{x}| \approx (\mathbf{x} + \mathbf{r})/|\mathbf{x} + \mathbf{r}| \approx \hat{\mathbf{z}}$, i.e. the plane-parallel limit. The LOS correlation function is then

$$\xi_{vv}(r, \mu) \equiv \langle v_z(\mathbf{x}) v_z(\mathbf{x} + \mathbf{r}) \rangle = (1 - \mu^2) \Psi_{\perp}(r) + \mu^2 \Psi_{\parallel}(r), \quad (90)$$

where $\mu = \hat{\mathbf{r}} \cdot \hat{\mathbf{z}}$. We see that ξ_{vv} interpolates between Ψ_{\perp} (when $\mu = 0$) and Ψ_{\parallel} (when $\mu = 1$). However, in general, for two distinct lines-of-sight, the correlation function depends on three variables, not just two.

Evidently, the LOS identifies the observer's position as a preferred location. Thus the orientation of the pairwise vector relative to the observer is now relevant to the computation of the two-point correlations. That is, we need both the separation and orientation of the pair relative to the LOS; the correlation function is no longer statistically isotropic. As with before, we separate out the angular dependence by yet another multipole decomposition:

$$\xi_{vv}(r, \mu) = \sum_{\ell} \xi_{vv}^{\ell}(r) \mathcal{L}_{\ell}(\mu). \quad (91)$$

The multipoles are given by

$$\xi_{vv}^0(r) = +\frac{1}{3} \int_0^{\infty} \frac{k^2 dk}{2\pi^2} j_0(kr) \left[\left(\frac{\mathcal{H}f}{k} \right)^2 P_{\theta\theta}(k) \right] \quad (92a)$$

$$\xi_{vv}^2(r) = -\frac{2}{3} \int_0^{\infty} \frac{k^2 dk}{2\pi^2} j_2(kr) \left[\left(\frac{\mathcal{H}f}{k} \right)^2 P_{\theta\theta}(k) \right] \quad (92b)$$

¹⁹ The parallel component of the velocity relative to the separation is $\hat{r}_i v^i$ so $\Psi_{\parallel}(r) = \hat{r}^i \hat{r}^j \langle v_i(\mathbf{x}) v_j(\mathbf{x}') \rangle$. The perpendicular component $\mathcal{P}_{ij} v^j$ lies in a plane orthogonal to \mathbf{r} . With $\mathcal{P}_{ij}^{\perp} \equiv \delta_{ij}^K - \hat{r}_i \hat{r}_j$, we have

$$\Psi_{\perp}(r) \mathcal{P}_{ij}^{\perp} = \mathcal{P}_{ik}^{\perp} \mathcal{P}_{jl}^{\perp} \langle v_k(\mathbf{x}) v_l(\mathbf{x}') \rangle. \quad (88)$$

or $\xi_{vv}^0 = 1/3(\Psi_{\parallel} + 2\Psi_{\perp})$ and $\xi_{vv}^2 = 2/3(\Psi_{\parallel} - \Psi_{\perp})$, using that $j_0 = K_{\parallel} + 2K_{\perp}$ and $j_2 = K_{\perp} - K_{\parallel}$. We emphasize that the correlations are anisotropic; the quadrupole moment is present ($\xi_{vv}^2 \neq 0$) even in real space. This is however nothing more than a consequence that we are computing two-point correlations of a vector field and so must depend on the orientation of the galaxy pair.

B. Redshift space

Turn now to $\xi_{\theta\theta}^s(\mathbf{s})$, the two-point function of the *redshift-space* velocity divergence field. This is related to the redshift-space power spectrum $P_{\theta\theta}^s(\mathbf{k})$ via Fourier transform:

$$\xi_{\theta\theta}^s(\mathbf{s}) = \langle \theta^s(0) \theta^s(\mathbf{s}) \rangle = \int \frac{d^3\mathbf{k}}{(2\pi)^3} P_{\theta\theta}^s(\mathbf{k}) e^{-i\mathbf{k}\cdot\mathbf{s}}. \quad (93)$$

Substituting eq. (66) into eq. (93), and using that the angular integral evaluates to eq. (D2), we can write

$$\xi_{\theta\theta}^s(s, \mu) = \sum_{\ell} \xi_{\theta\theta}^{\ell}(s) \mathcal{L}_{\ell}(\mu), \quad (94)$$

with the multipoles given by

$$\xi_{\theta\theta}^{\ell}(s) \equiv i^{\ell} \int_0^{\infty} \frac{k^2 dk}{2\pi^2} j_{\ell}(ks) P_{\theta\theta}^{\ell}(k), \quad (95)$$

which we note is the spherical Bessel transform of $P_{\theta\theta}^{\ell}$. We recall only multipoles with even ℓ can contribute to the overall anisotropy, reflecting the fact that we have symmetry under galaxy pair exchange ($\mathbf{s} \rightarrow -\mathbf{s}$). In the case of the plane-parallel limit only the $\ell = 0, 2, 4$ moments are nonvanishing (as with the multipoles of density two-point correlations).

The velocity correlation tensor in terms of $P_{\theta\theta}^s$ is

$$\Psi_{ij}^s(\mathbf{s}) = \int \frac{d^3\mathbf{k}}{(2\pi)^3} \left(\frac{\mathcal{H}f}{k} \right)^2 \frac{k_i k_j}{k} P_{\theta\theta}^s(\mathbf{k}) e^{-i\mathbf{k}\cdot\mathbf{s}}. \quad (96)$$

Notice that the difference between this expression and eq. (86) is that the power spectrum now depends on \mathbf{k} . This slight difference however means that Ψ_{ij}^s cannot be written in terms of parallel and perpendicular correlation functions, as in eq. (87). In general, we find that the parallel and perpendicular modes are not independent but become correlated. In addition, Ψ_{ij}^s possesses a more complicated multipole structure; see Appendix D for more details.

To obtain the LOS correlations from eq. (96), we can contract with $\hat{n}_i \hat{n}_j$, insert eq. (66) then perform the necessary integrations. But a simpler way is to instead begin with

$$\xi_{vv}^s(\mathbf{s}) = \langle v_z^s(0) v_z^s(\mathbf{s}) \rangle = \int \frac{d^3\mathbf{k}}{(2\pi)^3} P_{vv}^s(\mathbf{k}) e^{-i\mathbf{k}\cdot\mathbf{s}}, \quad (97)$$

where P_{vv}^s is LOS velocity power spectrum. To relate this to the velocity divergence power spectrum we recall that the velocity field is irrotational, so $v_z^s(\mathbf{k}) = -\mathcal{H}f(ik_z/k^2)\theta^s(\mathbf{k})$, which yields the exact relations (71) and (72) (i.e. independent of how θ is modelled). Since we have symmetry about the LOS we can write again as a sum of multipoles,

$$\xi_{vv}^s(s, \mu) = \sum_{\ell} \xi_{vv}^{\ell}(s) \mathcal{L}_{\ell}(\mu). \quad (98)$$

Substituting eq. (72) into eq. (97) we find that the multipoles are given by [cf. eq. (95)]

$$\xi_{vv}^{\ell}(s) = i^{\ell} \int_0^{\infty} \frac{k^2 dk}{2\pi^2} j_{\ell}(ks) \left[\left(\frac{\mathcal{H}f}{k} \right)^2 \sum_{\ell'} A_{\ell\ell'} P_{\theta\theta}^{\ell'}(k) \right], \quad (99)$$

i.e. in terms of a combination of the velocity divergence multipole moments, with $A_{\ell\ell'}$ given by eq. (72). As we have mentioned in the preceding section the μ dependence is not an indication of RSD as it is in galaxy clustering (though statistical homogeneity is still preserved in the plane-parallel limit).

We have already obtained a relation between the power spectrum multipoles of $\theta^s(\mathbf{k})$ and $v_z^s(\mathbf{k})$; see eq. (72). We now derive an analogous relation between the configuration space multipoles, i.e. between $\xi_{\theta\theta}^\ell(s)$, from $\xi_{vv}^\ell(s)$. This is perhaps most easily done if we use that spherical Bessel functions satisfy the second-order differential equation,

$$\left[\frac{\partial^2}{\partial s^2} + \frac{2}{s} \frac{\partial}{\partial s} - \frac{\ell(\ell+1)}{s^2} \right] j_\ell(ks) = -k^2 j_\ell(ks). \quad (100)$$

Substituting this into eq. (99) we obtain the following relation between multipoles:

$$\mathcal{D}_\ell \xi_{vv}^\ell + (\mathcal{H}f)^2 \sum_{\ell'} A_{\ell\ell'} \xi_{\theta\theta}^{\ell'} = 0. \quad (101)$$

[Here \mathcal{D}_ℓ is defined by the contents of the square brackets on the left-hand side of eq. (100).] Unsurprisingly, the algebraic relation in Fourier space (72) becomes a differential relation in configuration space. This expression cannot however be inverted to obtain an explicit formula for the velocity divergence multipoles since $A_{\ell\ell'}$ is overdetermined (the number of rows exceeds the number of columns). In practice, it is likely that only the monopole ξ_{vv}^0 and quadrupole ξ_{vv}^2 can be measured at a satisfactory level, given that P_{vv}^4 and P_{vv}^6 are subdominant (see figure 4). Still, this leaves $\xi_{\theta\theta}^0$ overdetermined. In any case, the practical utility of estimating $\xi_{\theta\theta}^\ell$ from eq. (101) will crucially depend on the ability to differentiate what is in practice a noisy estimate of ξ_{vv}^ℓ . Provided this can be done eq. (101) shows in principle how one can estimate the divergence field's two-point function directly from the measured LOS velocity multipoles in configuration space.

Finally, we stress that the expressions derived above are valid in the plane-parallel limit, but aside from this assumption they are exact and independent of any input cosmology or PT modelling. The $\xi_{\theta\theta}^\ell$'s can therefore be taken to be arbitrary functions (though we have assumed that the multipole moments are only nonzero for $\ell = 0, 2, 4, 6$). Alternatively, by taking the inverse Fourier transform of eq. (76), we can obtain the following exact relation for the LOS velocity two-point function:

$$\xi_{vv}^s(s_\parallel, s_\perp) = \int_{-\infty}^{\infty} dr_\parallel \int_{-\infty}^{\infty} \frac{d\kappa}{2\pi} e^{i\kappa(r_\parallel - s_\parallel)} \left(\frac{\mathcal{H}f}{\kappa} \right)^2 \left\langle e^{-if\kappa\Delta u_z} \nabla_z u_z(\mathbf{x}) \nabla_z u_z(\mathbf{x}') \right\rangle, \quad (102)$$

where $s_\parallel = s\mu$, $s_\perp = r_\perp = (s^2 - s_\parallel^2)^{1/2}$, and $\Delta u_z = u_z(\mathbf{x}) - u_z(\mathbf{x}')$.

The inner integral in eq. (102) defines a probability distribution function, expressed as the Fourier transform of the pairwise velocity generating function. Equation (102) can thus be considered the velocity analogue of the streaming model given by eq. (8). The object of interest here is the generating function and so the challenge thus lies in modelling the pairwise velocity statistics. An interesting question we can ask is whether a Gaussian distribution is valid, for then one requires only a model of the (real-space) power spectrum. We note that such an assumption has been validated in the case of clustering in the Gaussian streaming model [67, 68] (but see also ref. [71] for a non-Gaussian extension).

VIII. DISCUSSION AND CONCLUSIONS

A. RSD and the gradient expansion

Using the distribution-function approach to RSD [51], we obtained an expression, eq. (26), describing the velocity field as would be seen in redshift space. The expression is given as a series expansion and shows that at leading order the velocity field in real space and redshift space coincide. This means that distortions are a second-order effect and are therefore absent in linear theory. Whether considered in real space or redshift space, the series expansion explicitly shows that the velocity field is, as we expect, a volume-weighted quantity, despite the apparent density weighting in eq. (25) (i.e. there is no coupling to the real-space density field).

We have observed that the series expansion is organized as a hydrodynamic gradient expansion: zeroth-order terms are derivative-free and correspond to the perfect fluid that is usually considered; higher-derivative terms (which counts products of lower-order derivatives) represent short-wavelength, dissipative corrections to the perfect-fluid description (among other higher-order hydrodynamic effects). Understood in this way, distortions to the real-space motions of a perfect fluid can be likened to the dissipative effects of an *imperfect* fluid (e.g. one with heat conduction, shear viscosity, etc). However, the kind of dissipation is different to any that might be encountered in nature. This is because it depends on who is observing it. That is, the mapping (1) singles out the observer's LOS as a preferred direction; gradients appearing in the derivative expansion are really LOS derivatives ($\nabla_\parallel = \hat{\mathbf{n}} \cdot \nabla$), and it is these terms that give rise to apparent observer-dependent dynamics in the fluid.

The gradient expansion was shown to follow from a simple integral formula given by eq. (32) [see eqs. (15) and (16) for the case of the density and momentum counterparts, respectively]. This is perhaps not surprising given that the redshift-space distribution function (13) is itself given by a convolution. While formally equivalent to the gradient expansion when considered to all orders, this nonperturbative form provides heuristic way to understand how the mapping gives rise to distortions—namely, as a certain convolution which only operates on the LOS modes. Indeed, this agrees with the idea that the correlation function of galaxies in redshift space takes on characteristics of the (LOS) velocity field through the pairwise-velocity probability density function [2, 66, 86]. Technically speaking, because the shift term in the mapping—the peculiar velocity—depends on space, we have more correctly a convolution of the real-space field with a spectrum of plane waves, each with a different velocity-induced phase; in the case of the velocity field, which is not density weighted, the plane waves have an amplitude $1/(\mathbf{k} \cdot \hat{\mathbf{n}})$. (Note that despite the appearance of the Dirac delta function, the convolution cannot be carried out in general, for the shift carries \mathbf{x} dependence.)

That we have been able to write redshift-space fields as an integral transformation of their real-space counterpart is made possible by asserting the PPF assumption at the level of the (real-space) distribution function; see eq. (12). (Recall this is usually assumed after taking moments of the Boltzmann equation.) We are thus working in the regime of single-streaming in which phase-space particle trajectories do not cross in real space. However, in the more realistic case of multi-streaming the reassignment of mass tracers implied by the mapping (1) allows for multiple tracers at the same position \mathbf{x} : Even if single-streaming is valid in real space it does not preclude the possibility of multi-streaming in redshift space. The validity of our formulae should be understood with these caveats in mind.

B. Power spectrum

Two models for the redshift-space LOS velocity power spectrum have been presented. The first model we presented, eq. (61), is based on the gradient expansion, and largely follows the approach taken in refs. [51, 53–55] for the density field, and ref. [40] for the momentum field. The second model (81) is based on the integral formula, and derives from a nonperturbative expression for the power spectrum given in terms of the pairwise-velocity generating function [eq. (76)]. This model is constructed in a similar way to the well-known TNS clustering model [64]; that is, it is based on the cumulant expansion of the generating function [63], upon which the connected moments are evaluated using PT.

Both models show a damping of the power spectrum. Quantitatively, the damping begins on quasilinear scales ($k \gtrsim 0.01 h \text{ Mpc}^{-1}$), and reaches about 20% at $k \simeq 0.1 h \text{ Mpc}^{-1}$. There is also an “FoG” effect in the velocity field, much as seen in redshift-space clustering. In the first model, we have included FoG damping empirically, invoking the “dispersion models” of the galaxy power spectrum. The second model has the virtue that FoG damping naturally arises from the cumulant expansion of the generating function and appears in the exactly the same way as for clustering models [cf. eq. (77)]. The FoG effect in the velocity field—being related to virial motions of galaxies—is no less difficult to model from first principles, and we have thus adopted a Gaussian model, $D_{1\text{pt}}^2(x) = \exp(-x^2)$, $x = k\mu\sigma_u$. Using the PT prediction for the velocity dispersion at $z = 0$, $\sigma_v \equiv (H_0 f)\sigma_u \simeq 300 \text{ km s}^{-1}$, leads to an additional damping of about 10%.

The damping can be explained qualitatively in terms of the gradient expansion. Dissipation here has the effect of erasing density gradients in the fluid, and with it the correlated motions. In practice, this is the familiar FoG effect in action whereby galaxies are scattered out from clusters. As time goes on, and the velocity dispersion grows larger, galaxies are scattered further and further away from the centers of their host halos. From the dynamical point of view, there is an outflow of material (galaxies) from dense regions to less dense regions and this is akin to a heat conduction (movement from hotter to cooler regions). Of course, this is the reverse of what actually occurs when viewed in real space, though, which is that (on large scales) matter is acted on solely by gravity causing it to be drawn towards higher-density regions and away from lower-density regions.

C. Comparison with previous work

Our framework provides a physical model for the damping observed in N -body simulations by Koda et al. [24] (hereafter K14). These simulations showed two regimes of behaviour: (i) a damping in the measured monopole moment of the power spectrum beginning on scales $k \simeq 0.01 h \text{ Mpc}^{-1}$ and lasting to $k \simeq 0.1 h \text{ Mpc}^{-1}$; (ii) an enhancement in power at $k \gtrsim 0.2 h \text{ Mpc}^{-1}$ over the damping in (i) (when extrapolated to larger k). K14 explained (ii) as arising from a (largely) scale-independent random component in the velocity with assumed Gaussian statistics (zero-centered with variance σ_*^2); on the other hand, K14 explained (i) as being due entirely to the familiar FoG effect. The latter was modelled phenomenologically using an angle-independent damping function $D_{\text{K14}}^2(k\sigma_{\text{K14}}) = \sin^2(k\sigma_{\text{K14}})/(k\sigma_{\text{K14}})^2$.

Assuming (i) and (ii) arise from independent effects, K14 found that $\sigma_{\text{K14}} \simeq 13 h^{-1} \text{Mpc}$ was required for concordance with simulation. (Note that the empirical parameter σ_{K14} was found to depend somewhat on the subhalo mass bin chosen.)

A comparison between the monopole moment of our power spectrum model (81) and the K14 fitting function $D_{\text{K14}}^2 P_{vv}$ shows that our model predicts about 10% of excess power at $k = 0.1 h \text{Mpc}^{-1}$ (see dashed lines in figure 7). This is however not surprising given that the halo velocities are known to be biased tracers of the dark matter velocity field [59, 89]. As figure 7 also shows, a reasonable fit to simulations is obtained by allowing a halo velocity bias. For simplicity, we have taken into account the bias by considering only the effect at lowest order in perturbations, i.e. on the linear power spectrum. Note that the velocity bias results in a further suppression of power—e.g. at $k = 0.1 h \text{Mpc}^{-1}$ the subhalo velocity (in real space) is lower by about 4% compared to dark matter, and the velocity lower power by about 8%.

Separately, we reiterate that our model uses the linear-theory prediction for the velocity dispersion that controls the amount of FoG damping. Given the theoretical uncertainty around this parameter it is more appropriate to treat it as a nuisance parameter. Of course, this introduces an extra fitting parameter, which ensures concordance with simulation.

But it is perhaps unsurprising that we need an empirical FoG parameter. After all, the model given by eq. (81) is styled on the TNS model, which itself requires that the FoG velocity dispersion be treated as an empirical parameter. It is likely that a more careful treatment of the FoG damping model (as in refs. [87]) will be needed than the simple one we have given here. Nevertheless, our results show that the damping cannot be entirely blamed on FoG effects: about half of the observed damping should be attributed to the coherent streaming motions (i.e. not related to the internal motions of clusters).

A more comprehensive comparison of our models with simulations may also need to consider the possibility of a velocity bias. In this work we have assumed no velocity bias between galaxies and matter, $\mathbf{v}_g = \mathbf{v}$. The issue of bias is a complicated subject (see ref. [59] and references therein) and well beyond the scope of this work. However, we note that on scales $k \lesssim 0.2 h \text{Mpc}^{-1}$ halos do not appear to be biased velocity tracers [60, 61]. In the case of subhalos, considered in K14, the situation is different. On small scales a subhalo velocity bias is fairly well established from simulations [92–96]. And this bias does not necessarily need to arise from baryonic effects; owing to dynamical friction, dark-matter-only simulations have also observed such a bias [93].

In addition, while we have computed the leading-order effect on the power spectrum, a higher-order calculation may be required. Firstly, the velocity power spectrum is more sensitive to nonlinear effects than is the case for density; see figure 1. Secondly, PT breaks down on larger scales in redshift space than in real space [81], though we note that this applies more to the first model, which is based on treating both the redshift mapping and dynamics perturbatively. An obvious first step in this direction, however, is to check whether the connected four-point moment in eq. (58c) (which does not appear in our one-loop calculation) is sizable. We leave this to future work. In the end, however, such a calculation may not be necessary, given that how accurate the model needs to be specified will depend on the quality of the data at hand. Since measurement errors on the peculiar velocities directly propagate to the power spectrum’s shot noise error, any systematic bias present may not be significant enough to warrant the higher-order calculation.

Finally, we note that the second model (based on the cumulant expansion) should in principle capture more of the nonlinearity missed in the first model (based on moment expansion). This is because the second model treats the redshift mapping exactly, whereas the first model treats it perturbatively. Furthermore, while both models treat the dynamics perturbatively, the second model does not explicitly assume the smallness of the field’s amplitude. Rather, it is the correlations that are expected to be weak, and this was the logic in performing an expansion in powers of $j_1 \propto k$ in eq. (78).

IX. SUMMARY AND OUTLOOK

We have studied the effect of RSD on the motions of tracers as inferred from their redshift-space positions. Beginning with the distribution-function approach to RSD [51], we derived two expressions for the *redshift-space* velocity field—the derivative expansion (26) and the convolution formula (32). These expressions are formally equivalent at all orders, but permit different perturbative treatments. Using one-loop PT, we computed the leading-order effect of RSD on the velocity power. Working in the plane-parallel limit, two models for the redshift-space velocity power spectrum were presented, each based on a different perturbative approach:

- I. Power spectrum model (61) is obtained from the derivative expansion (26). The effect of RSD is captured in a set of LOS-dependent mode-coupling kernels (63); these kernels are modified from the standard one-loop kernels, and are akin to the redshift-space density kernels given in ref. [81]. This model is closely related to those [40, 51] derived from the (density-weighted) velocity-moment expansion.

II. Power spectrum model (81) is obtained from the convolution formula (32). It follows from using the cumulant-expansion theorem on the pairwise-velocity generating function appearing in the exact expression (76). This model may be considered the velocity analogue of the TNS model [64] for the galaxy power spectrum.

Our main findings are as follows. Both models I and II predict a damping of the power spectrum beginning on quasilinear scales $k \gtrsim 0.01 h \text{Mpc}^{-1}$; at large-scales $k \rightarrow 0$ the effect is suppressed by higher-derivative terms. Heuristically, the damping may be understood as a RSD-induced dissipation: in redshift space, we have an apparent outflow of galaxies directed along the LOS towards lower-density regions, behaviour which is not described by a purely gravitating perfect fluid. From the gradient-expansion perspective of hydrodynamics this implies an apparent nonvanishing heat conductivity. The overall effect is to suppress the tendency for galaxies moving under gravity to fall towards regions of higher density. This is a long-range FoG effect; it is present in addition to the usual FoG effect due to the virial motions of galaxies, which also exists for the velocity field. (There is no analogous Kaiser effect, however). In the case of model I an FoG-type damping is entirely absent from the model and needs to be put in by hand; in the case of model II the damping arises from one-point moments within the pairwise velocity generating function. The damping is qualitatively consistent with behaviour observed in N -body simulations [24], and a quantitative fit to simulations thus requires treating the velocity dispersion parameter empirically (as with galaxy clustering models).

Our broader motivation for this study has been to supply in part the theoretical predictions needed for an eventual multi-tracer analysis of galaxy density and peculiar velocities [24]. In the past, a proper comparison between data and theory has not been possible, with workers (e.g. [26, 31, 32]) having relied on a phenomenological model. In this regard the framework we have presented provides much of the needed analytic modelling (and numerical implementation). While it is clear that more detailed modelling is needed before confronting with data (e.g. of the dynamics, in relaxing the plane-parallel assumption, etc), we hope that the framework we have developed can nevertheless provide a template for future efforts on this front. Suffice to say this first study has largely been devoted to theory. In future work we will investigate the advantages of performing analysis in redshift space using mock data. Questions of particular interest include: quantifying the information gain in constraining the growth rate and breaking of parameter degeneracies in redshift space; the extent to which systematic biases arise from using the phenomenological damping model; and assessing the trade-off between smaller errors in galaxy redshift-space positions versus the loss of cosmological signal from the power suppression.

ACKNOWLEDGEMENTS

We thank Chris Blake for helpful comments and suggestions, and for his comments on this manuscript. We also thank Jun Koda for making us aware of the heat-conduction analogy and bringing to our attention ref. [39]. LD is supported by the Australian government Research Training Program. The code used to obtain the numerical results in this work is publicly available and can be found at <https://github.com/lhd23/RSDPT-FFTLLog/>. We acknowledge use of the software libraries NumPy [97], SciPy [98], and Matplotlib [99].

Appendix A: Power-law FFTLog numerical method

In this appendix we give details on the numerical evaluation method for the power spectrum model. In this model, and in PT more generally, we frequently encounter convolutions, such as

$$P_{22}(k) = 2 \int \frac{d^3\mathbf{q}}{(2\pi)^3} [G_S^{(2)}(\mathbf{q}, \mathbf{k} - \mathbf{q})]^2 P_L(q) P_L(|\mathbf{k} - \mathbf{q}|). \quad (\text{A1})$$

These loop integrals are generally unpleasant to evaluate efficiently and precisely. Firstly, the mode coupling is over a large dynamic range of the power spectrum; secondly, many such integrals need to be performed if $P_{22}(k)$ is to be returned at all wavenumbers k of interest—as well as with different values of the cosmological parameters (e.g. for Markov chain Monte Carlo sampling).

To evaluate these integrals (and others) we use a recent method [56] based on the FFTLog algorithm [82] (see also ref. [83]). The key idea is to exploit the fact that by representing the power spectrum as a discrete Fourier Transform in $\ln k$, rather than k , we can express the linear power spectrum $P_L(k)$ over some finite range of scales of interest as

$$P_L(k) = \sum_{m=-N/2}^{N/2} c_m k^{\nu+i\eta_m}; \quad (\text{A2})$$

i.e. as the sum of (complex) power laws [the symbols are defined below]. This last fact is important as many integrals, including those of the form (A1), are analytic in the case of a power-law power spectrum. Because no numerical integration is involved this method is significantly faster than standard quadrature or Monte Carlo integration. In particular, the FFTLog approach requires $\mathcal{O}(N \log N)$ steps, outputting all k at once. (This is in contrast to the $\mathcal{O}(N^3)$ steps needed for quadrature integration.)

Strictly speaking, the equality in eq. (A2) is only approximate for finite N , and the periodicity of the right-hand side of eq. (A2) means we need to restrict attention to some finite range. The chosen N will depend on how featureful the function to be approximated is; in the case of the standard Λ CDM power spectrum an N of only about 200 is sufficient to accurately represent the linear power spectrum down to the BAO wiggles. In this method the coefficients of the discrete Fourier transform encode the cosmological information, allowing the cosmology to be separated out from the integrals. These integrals can then be performed analytically (and only once), then stored in look-up tables. Below we discuss in more detail the FFTLog approach to convolution integrals. Other difficult integrals, many involving spherical Bessel functions, can also be evaluated using another variant of the FFTLog method.

For a logarithmic sampling of points in k -space, the Fourier coefficients in eq. (A2) are given by

$$c_m = \frac{1}{N} \sum_{j=0}^{N-1} P_L(k_j) k_j^{-\nu} k_{\min}^{-i\eta_m} e^{-i2\pi m j/N}, \quad \eta_m = \frac{2\pi m}{\ln(k_{\max}/k_{\min})}, \quad (\text{A3})$$

with the understanding that $c_{\pm N/2}$ is multiplied by a factor of 1/2 to get the correct endpoint weighting. Here $c_m^* = c_{-m}$ by the reality of the power spectrum; ν is a real number called the *bias*, which is to be chosen to avoid spurious divergences (see below); and $k_j = k_{\min} (k_{\max}/k_{\min})^{j/N}$, since the points are uniformly spaced in $\ln k$. In practice, when we compute the FFT, the input signal is the “biased” power spectrum $P(k)k^{-\nu}$.

Now, convolutions of the form (A1) reduce to a linear combination of irreducible integrals, which can be carried out analytically [100]:

$$\int \frac{d^3\mathbf{q}}{(2\pi)^3} \frac{1}{q^{2\nu_1} |\mathbf{k} - \mathbf{q}|^{2\nu_2}} = k^{3-2(\nu_1+\nu_2)} l(\nu_1, \nu_2), \quad (\text{A4})$$

where

$$l(\nu_1, \nu_2) \equiv \frac{1}{8\pi^{3/2}} \frac{\Gamma(\frac{3}{2} - \nu_1)\Gamma(\frac{3}{2} - \nu_2)\Gamma(\nu_1 + \nu_2 - \frac{3}{2})}{\Gamma(\nu_1)\Gamma(\nu_2)\Gamma(3 - \nu_1 - \nu_2)}. \quad (\text{A5})$$

Implementation. The discrete Fourier transform suffers two edge effects—ringing and aliasing. *Aliasing*, in which small-scale features leak into large scales, can be mitigated by padding the input signal array with zeros on both ends. Rapid oscillations at the ends of the input signal, or *ringing*, can be suppressed by passing the signal through a low-pass filter to the Fourier coefficients.

1. Integrals of type 22

Terms of the type P_{22} are convolutions and may be written in the FFTLog approach as

$$\begin{aligned} \int_{\mathbf{q}} I_{\ell}(\mathbf{q}, \mathbf{k} - \mathbf{q}) P_L(q) P_L(|\mathbf{k} - \mathbf{q}|) &= \sum_{m_1, m_2} c_{m_1} c_{m_2} \sum_{n_1, n_2} f_{n_1 n_2}^{\ell} k^{-2(n_1 + n_2)} \int_{\mathbf{q}} \frac{1}{q^{2(\nu_{m_1} - n_1)} |\mathbf{k} - \mathbf{q}|^{2(\nu_{m_2} - n_2)}} \\ &= k^3 \sum_{m_1, m_2} \left[\sum_{n_1, n_2} f_{n_1 n_2}^{\ell} l(\nu_{m_1} - n_1, \nu_{m_2} - n_2) \right] c_{m_1} k^{-2\nu_{m_1}} c_{m_2} k^{-2\nu_{m_2}}, \end{aligned} \quad (\text{A6})$$

with $\nu_{m_1} \equiv -\frac{1}{2}(\nu + i\eta_{m_1})$ and $\nu_{m_2} \equiv -\frac{1}{2}(\nu + i\eta_{m_2})$. We thus see that for a given k the convolution reduces to matrix multiplication involving two copies of the vector $(c_{-N/2} k^{-2\nu_{-N/2}}, \dots, c_{N/2} k^{-2\nu_{N/2}})$, and a matrix with components given by the contents of the square brackets above.²⁰ As mentioned above, the matrix is independent of the wavenumbers and cosmology, and can be precomputed for a given N , k_{\min} , k_{\max} , and ν .

Kernel expansion

To take advantage of the FFTLog method we first need to put the $I_{\ell}(r, \mu')$ kernels (70) in the form (A4). This is done by replacing r with q/k , and rewriting $\mu' \equiv \hat{\mathbf{k}} \cdot \hat{\mathbf{q}}$ in terms of k , q , and $|\mathbf{k} - \mathbf{q}|$, with the help of the identity $|\mathbf{k} - \mathbf{q}|^2 = k^2 + q^2 - 2kq\mu'$. All resulting terms contain integer powers of k^2 , q^2 , and $|\mathbf{k} - \mathbf{q}|^2$ and thus have the general form $k^{-2(n_1 + n_2)} q^{2n_1} |\mathbf{k} - \mathbf{q}|^{2n_2}$. The kernels can then be encoded in a set of indices (n_1, n_2) and coefficients $f_{n_1 n_2}^{\ell}$. A summary of all kernels using the FFTLog expansion is given in table I.

For example, consider the kernel $2[K_S^{(2)}(\mathbf{q}, \mathbf{k} - \mathbf{q})]^2$. This depends on $\hat{\mathbf{n}}$ but does not pose a real problem, as we can simply factor out its dependence by expanding into multipoles as

$$2[K_S^{(2)}(\mathbf{q}, \mathbf{k} - \mathbf{q})]^2 = \sum_{\ell} I_{\ell}(\mathbf{q}, \mathbf{k} - \mathbf{q}) \mathcal{L}_{\ell}(\hat{\mathbf{k}} \cdot \hat{\mathbf{n}}), \quad (\text{A7})$$

$$I_{\ell}(\mathbf{q}, \mathbf{k} - \mathbf{q}) \equiv (2\ell + 1) \int_{-1}^1 \frac{d\mu}{2} \mathcal{L}_{\ell}(\mu) \int_0^{2\pi} \frac{d\phi}{2\pi} 2[K_S^{(2)}(\mathbf{q}, \mathbf{k} - \mathbf{q})]^2. \quad (\text{A8})$$

(In the case of the SPT kernels only the $\ell = 0$ multipole is nonzero since there is no explicit μ dependence.) We can then apply the method for each ℓ ; e.g. for $\ell = 0$, we can write in FFTLog form

$$\begin{aligned} I_0(\mathbf{q}, \mathbf{k} - \mathbf{q}) &= \sum_{n_1, n_2} f_{n_1 n_2}^0 \frac{k^{-2(n_1 + n_2)}}{q^{-2n_1} |\mathbf{k} - \mathbf{q}|^{-2n_2}} \\ &= \frac{k^8}{60|\mathbf{k} - \mathbf{q}|^4 q^4} - \frac{k^6}{30|\mathbf{k} - \mathbf{q}|^4 q^2} - \frac{k^6}{30|\mathbf{k} - \mathbf{q}|^2 q^4} \\ &\quad + \frac{k^4}{60|\mathbf{k} - \mathbf{q}|^4} + \frac{k^4}{15|\mathbf{k} - \mathbf{q}|^2 q^2} + \frac{k^4}{60q^4}. \end{aligned} \quad (\text{A9})$$

From here it is straightforward to read off the coefficients and indices of each term, then input them into eq. (A6).

The bias parameter ν is the one tuning parameter in the FFTLog approach. This parameter is needed to ensure the convergence of each integral (A5) corresponding to $l(\nu_{m_1} - n_1, \nu_{m_2} - n_2)$, which is not guaranteed if we naively set $\nu = 0$. Though (A5) will always give a finite answer [56], even for values of ν_1 and ν_2 that would yield a divergent integral, we nevertheless need to choose the bias so that the integral is free of divergences. The range of ν for which the integral is convergent can be determined by inspecting the asymptotic behaviour of the kernels. For each ℓ we have

$$I_{\ell}(\mathbf{q}, \mathbf{k} - \mathbf{q}) \rightarrow \frac{k^2}{q^2}, \quad q \rightarrow 0, \quad (\text{A10a})$$

$$I_{\ell}(\mathbf{q}, \mathbf{k} - \mathbf{q}) \rightarrow \frac{k^4}{q^4}, \quad q \rightarrow \infty, \quad (\text{A10b})$$

²⁰ The functions $l(\cdot, \cdot)$ have several useful properties and satisfy a set of recursion relations that allow the linear combination in the square brackets of eq. (A6) to be rewritten in terms of a single l [56]. As these functions are undemanding to evaluate we will not simplify further.

where we have ignored $\mathcal{O}(1)$ multiplicative factors. In the asymptotic limit the integrands of type P_{22} read

$$(IR) \quad q^2 I_\ell(\mathbf{q}, \mathbf{k} - \mathbf{q}) P_L(q) P_L(|\mathbf{k} - \mathbf{q}|) \rightarrow q^2 q^{-2} q^\nu = q^\nu, \quad q \rightarrow 0, \quad (A11a)$$

$$(UV) \quad q^2 I_\ell(\mathbf{q}, \mathbf{k} - \mathbf{q}) P_L(q) P_L(|\mathbf{k} - \mathbf{q}|) \rightarrow q^2 q^{-4} q^{2\nu} = q^{-2+2\nu}, \quad q \rightarrow \infty, \quad (A11b)$$

where the factor of q^2 comes from using volume element in spherical coordinates. From this we see that to avoid divergences for any ℓ we require a bias in the range of $-1 < \nu < 1/2$. In practice we find $\nu = -0.6$ gives good results.

2. Integrals of type 13

Terms of the type P_{13} can also be evaluated using the FFTLog approach. For example

$$\begin{aligned} 2P_{\theta\theta,13}(k) &= 6P_L(k) \int_{\mathbf{q}} G_S^{(3)}(\mathbf{k}, \mathbf{q}, -\mathbf{q}) P_L(q) \\ &= 6P_L(k) \sum_{m_1} c_{m_1} \sum_{n_1, n_2} f_{n_1 n_2}^\ell k^{-2(n_1+n_2)} \int_{\mathbf{q}} \frac{1}{q^{2(\nu_{m_1}-n_1)} |\mathbf{k} - \mathbf{q}|^{-2n_2}} \\ &= 6P_L(k) k^3 \sum_{m_1} c_{m_1} k^{-2\nu_{m_1}} \left[\sum_{n_1, n_2} f_{n_1 n_2}^\ell l(\nu_{m_1} - n_1, -n_2) \right] \end{aligned} \quad (A12)$$

These integrals are in fact more straightforward to evaluate than the convolutions above, since the angular dependence only enters through the kernel and thus allowing us integrate out μ analytically [102, 103]:

$$2P_{\theta\theta,13}(k) = \frac{1}{84} \frac{k^3}{4\pi^2} P_L(k) \int_0^\infty dr P_L(kr) \left[\frac{12}{r^2} - 82 + 4r^2 - 6r^4 + \frac{3}{r^3} (r^2 - 1)^3 (r^2 + 2) \ln \left| \frac{r+1}{r-1} \right| \right], \quad (A13)$$

where $r = q/k$.

Asymptotic limits in the IR and UV

In the large- k asymptotic limit (or IR limit) we find

$$2P_{\theta\theta,13}(k) = -\frac{1}{3} k^2 P_L(k) \int \frac{q^2 dq}{2\pi^2} \frac{P_L(q)}{q^2} \left(1 + \frac{4q^2}{35k^2} + \frac{12q^4}{49k^4} + \dots \right) \quad (A14)$$

where σ_u^2 is given by eq. (65). In the $k \rightarrow 0$ asymptotic limit (UV limit) we find

$$2P_{\theta\theta,13}(k) = -\frac{1}{3} k^2 P_L(k) \int \frac{q^2 dq}{2\pi^2} \frac{P_L(q)}{q^2} \left(\frac{9}{5} - \frac{156k^2}{245q^2} + \frac{76k^4}{735q^4} + \dots \right) \quad (A15)$$

It is easy now to read off the limits in the IR and UV:

$$P_{\theta\theta,13}^{\text{IR}}(k) = -\frac{1}{2} k^2 P_L(k) \sigma_u^2, \quad P_{\theta\theta,13}^{\text{UV}}(k) = -\frac{9}{10} k^2 P_L(k) \sigma_u^2. \quad (A16)$$

Either $P_{\theta\theta,13}^{\text{IR}}(k)$ or $P_{\theta\theta,13}^{\text{UV}}(k)$ needs to be added on to eq. (A12), depending on the choice of bias parameter. For example choosing $\nu = -0.6$ we add $P_{\theta\theta,13}^{\text{UV}}(k)$.

For $K_S^{(2)}(\mathbf{q}, \mathbf{k} - \mathbf{q}) G_S^{(2)}(\mathbf{k}, -\mathbf{q})$ we have

$$P_{\theta\theta,13}^{0,\text{IR}}(k) = -\frac{1}{12} k^2 P_L(k) \sigma_u^2, \quad P_{\theta\theta,13}^{0,\text{UV}}(k) = -\frac{19}{84} k^2 P_L(k) \sigma_u^2, \quad (A17)$$

$$P_{\theta\theta,13}^{2,\text{IR}}(k) = -\frac{1}{6} k^2 P_L(k) \sigma_u^2, \quad P_{\theta\theta,13}^{2,\text{UV}}(k) = -\frac{23}{210} k^2 P_L(k) \sigma_u^2. \quad (A18)$$

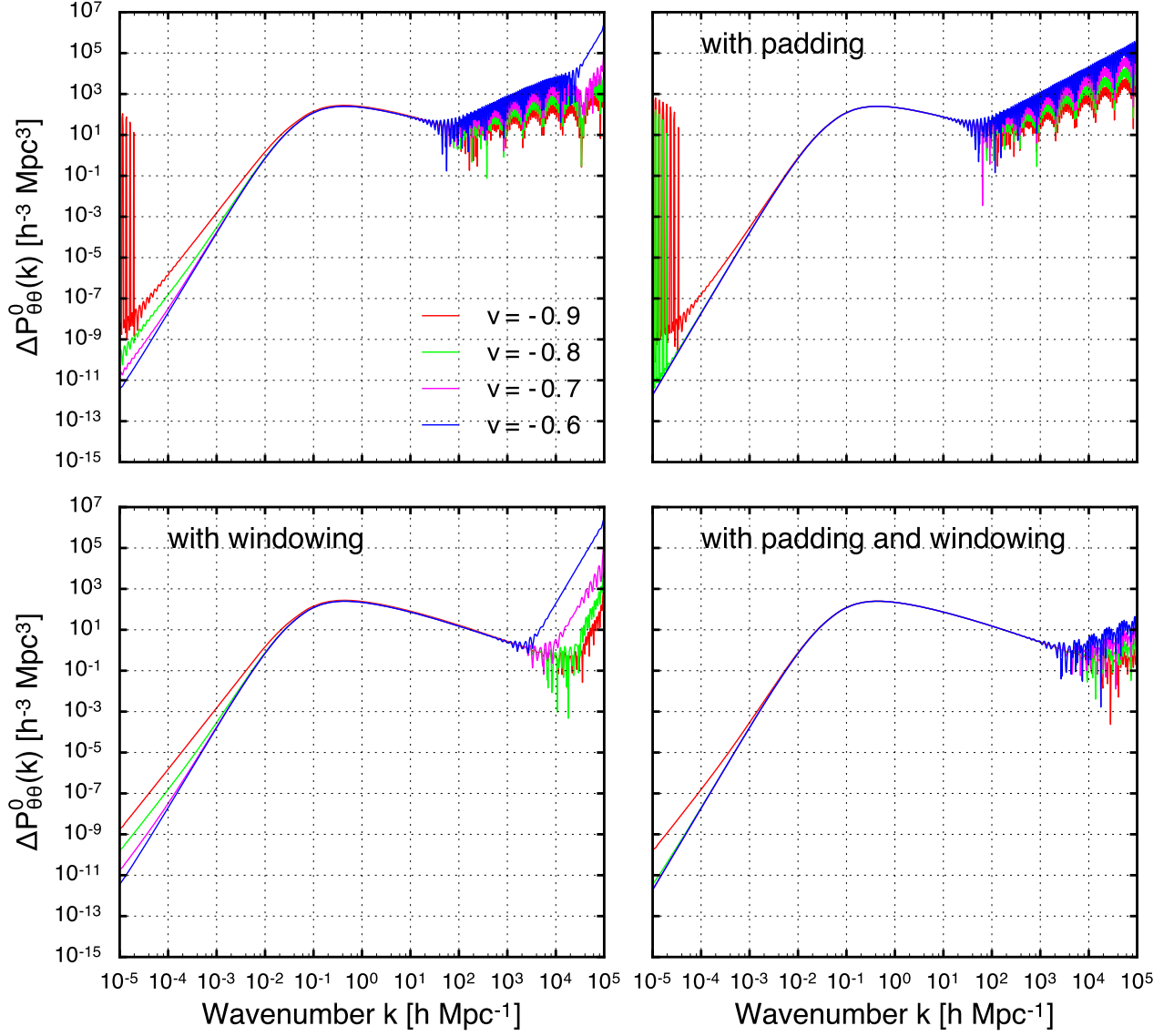


FIG. 8: Edge effects of power spectra when represented using the FFTLog approach (upper left panel). The signal shown is for $\Delta P_{\theta\theta}^0 \equiv P_{\theta\theta}^0 - P_L$, where $P_{\theta\theta}^0$ is given by eq. (69) and P_L is the linear power spectrum. The rest of the panels show how edge effects can be mitigated with the use of padding and windowing (where we use the window function given by equation (C1) in ref. [101]).

3. Configuration-space multipoles

We have noted in Section VIII B that eq. (99) is a spherical Bessel (or Hankel) transform. Given the highly oscillatory nature of the spherical Bessel functions, evaluating such transforms efficiently and precisely requires special integration methods. There is however an efficient way to evaluate $\xi_{vv}^\ell(s)$ using a slightly different FFTLog implementation [82, 83]. Here the FFTLog algorithm is based on the idea that the one-dimensional radial integral can be recast as a convolution under the transformation $k \rightarrow \ln k$ and $s \rightarrow \ln s$. In the (one-dimensional) Fourier dual space this is the product of the Fourier transforms of the power spectrum and the spherical Bessel function. The calculation of ξ_{vv}^ℓ is then equivalent to taking the inverse Fourier transform of this product. In practice, in the discrete case, one takes fast Fourier transforms, with the Fourier transform of the spherical Bessel function computed exactly using the known analytic form. In the case of the matter power spectrum only about 200 logarithmically-spaced points in the

n_1	n_2	$[2K_S^{(2)} K_S^{(2)}]_{22}$			$[4K_S^{(2)} G_S^{(2)}]_{22}$		$[K_S^{(2)} G_S^{(2)}]_{13}$		$[2G_S^{(2)} G_S^{(2)}]_{22}$	$[G_S^{(3)}]_{13}$	$k^2 \times [K_S^{(B)}]_{22}$			
		$\ell = 0$	$\ell = 2$	$\ell = 4$	$\ell = 0$	$\ell = 2$	$\ell = 0$	$\ell = 2$	$\ell = 0$	$\ell = 0$	$\ell = 0$	$\ell = 2$	$\ell = 4$	$\ell = 6$
-2	-2	1/60	1/84	3/1120	1/21	1/42	0	0	2/49	0	1/140	1/168	27/12320	5/14784
-1	-2	-1/30	5/168	1/280	-5/84	1/24	0	0	-1/49	0	-3/140	1/56	39/12320	1/2464
-2	-1	-1/30	5/168	1/280	-5/84	1/24	-1/112	-1/224	-1/49	-1/84	-3/140	1/56	39/12320	1/2464
0	-2	1/60	-2/21	9/560	-1/42	-17/168	0	0	-23/392	0	3/140	-5/56	123/6160	5/4928
-1	-1	1/15	1/21	3/280	2/21	13/84	3/112	0	25/196	5/168	3/35	0	3/440	3/2464
-2	0	1/60	-2/21	9/560	-1/42	-17/168	1/168	-1/96	-23/392	-1/168	3/140	-5/56	123/6160	5/4928
1	-2	0	3/56	-3/56	1/28	-1/56	0	0	3/196	0	-1/140	17/168	-621/6160	25/3696
-2	1	0	3/56	-3/56	1/28	-1/56	5/336	11/672	3/196	1/21	-1/140	17/168	-621/6160	25/3696
0	-1	0	-3/56	3/56	-1/28	1/56	-3/112	3/112	-3/196	-1/56	-9/140	1/56	261/6160	5/1232
-1	0	0	-3/56	3/56	-1/28	1/56	-1/56	-3/224	-3/196	-37/504	-9/140	1/56	261/6160	5/1232
2	-2	0	0	1/32	0	3/56	0	0	9/392	0	0	-1/28	291/2464	-25/704
-2	2	0	0	1/32	0	3/56	-1/84	11/672	9/392	-5/168	0	-1/28	291/2464	-25/704
1	-1	0	0	-1/8	0	-3/14	1/112	-1/28	-9/98	-1/168	0	-1/28	-111/616	5/176
-1	1	0	0	-1/8	0	-3/14	-1/112	-3/112	-9/98	25/504	0	-1/28	-111/616	5/176
0	0	0	0	3/16	0	9/28	1/84	31/672	27/196	-1/72	0	1/7	153/1232	5/352
-2	3	0	0	0	0	0	0	-1/56	0	0	0	0	-15/352	15/352
3	-2	0	0	0	0	0	0	0	0	0	0	0	-15/352	15/352
-1	2	0	0	0	0	0	0	9/224	0	-1/168	0	0	45/352	-45/352
2	-1	0	0	0	0	0	0	3/224	0	1/168	0	0	45/352	-45/352
0	1	0	0	0	0	0	0	-3/224	0	1/56	0	0	-15/176	15/176
1	0	0	0	0	0	0	0	-5/224	0	-1/56	0	0	-15/176	15/176
1	1	0	0	0	0	0	0	0	0	0	0	0	0	5/16
0	2	0	0	0	0	0	0	0	0	0	0	0	0	-15/64
2	0	0	0	0	0	0	0	0	0	0	0	0	0	-15/64
-1	3	0	0	0	0	0	0	0	0	0	0	0	0	3/32
3	-1	0	0	0	0	0	0	0	0	0	0	0	0	3/32
-2	4	0	0	0	0	0	0	0	0	0	0	0	0	-1/64
4	-2	0	0	0	0	0	0	0	0	0	0	0	0	-1/64

TABLE I: Summary of FFTLog expansion indices (n_1, n_2) and coefficients $f_{n_1 n_2}^\ell$ characterizing each kernel (top row). Note that the kernels of type P_{13} generally contain terms with $|\mathbf{k} + \mathbf{q}|$ but can be replaced (as we have done here) with $|\mathbf{k} - \mathbf{q}|$, since the integration is over all \mathbf{q} . Also note that for kernels of type P_{22} the coefficients are symmetric in n_1 and n_2 , i.e. $f_{n_1 n_2}^\ell = f_{n_2 n_1}^\ell$. The last four columns give the coefficients for the LOS velocity power spectrum model described in Section VI. (Here $\mathcal{K}_S^{(B)}$ has been multiplied by k^2 to obtain a dimensionless kernel.)

range of $k_{\min} = 10^{-4} h \text{ Mpc}^{-1}$ and $k_{\max} = 10^2 h \text{ Mpc}^{-1}$ of $P_L(k)$ are required to capture all features.²¹ In fact given the convolution contained in eq. (99), ξ_{vv}^ℓ can be further developed into another one-dimensional spherical Bessel transform [104] involving the generalized correlation function

$$\zeta_n^\ell(r) \equiv \int \frac{k^2 dk}{2\pi^2} k^n j_\ell(kr) P_L(k), \quad (\text{A19})$$

which forms a transform pair with $k^n P_L(k)$. Note $\zeta_0^0(r) = \xi(r)$, the autocorrelation function of δ . Because the RSD enters at nonlinear order this means that $\xi_{vv}^\ell(s)$ can be expressed as integrals over the products of different ζ_n^ℓ .

²¹ We use the `mcfits` implementation available at <https://github.com/eelregit/mcfits>.

Appendix B: Consistency check of derivative expansion

In the main text we gave an expression (26) for the redshift-space velocity field v_{\parallel}^s , which we obtained by formally expanding in the real-space fields. Since the apparent dependence on δ vanishes, this expression depends on terms involving only v_{\parallel} . In this appendix we will verify this result by checking that when we multiply v_{\parallel}^s by the overdensity $1 + \delta^s$ we indeed get the momentum π_{\parallel}^s . Precisely, we will show that the product of the series expansions, eqs. (19) and (26), is equal to that of eq. (23) at all orders. We specialize to the LOS component but note that the expressions given here do not assume the plane-parallel limit.

First, it will be convenient to reorganize each expansion so that the summands gather all terms consisting of a given number n of the real-space fields (loosely the ‘‘perturbation’’ order, though note that there is no requirement for the fields to be small fluctuations). Under this rearrangement the product to be shown reads [$\rho^s \equiv 1 + \delta^s$, $u^s \equiv v_{\parallel}^s/(-\mathcal{H})$, etc]

$$\sum_{n=0}^{\infty} \rho_{(n)}^s \sum_{m=0}^{\infty} u_{(m)}^s = \sum_{m=0}^{\infty} \pi_{(N)}^s, \quad \text{where} \quad \pi_{(N)}^s = \sum_{n+m=N} \rho_{(n)}^s u_{(m)}^s, \quad (\text{B1})$$

where the constrained sum is over all non-negative integers n and m with $n + m = N$; the subscripts denote the field order, so $\rho_{(0)}^s = 1$, $u_{(0)}^s = 0$, $\pi_{(0)}^s = 0$, $\pi_{(1)}^s = u$, and

$$\rho_{(n)}^s \equiv \frac{1}{(n-1)!} \partial^{n-1}(u^{n-1}\delta) + \frac{1}{n!} \partial^n u^n, \quad n \geq 1, \quad (\text{B2})$$

$$u_{(m)}^s \equiv \frac{1}{m!} \partial^{m-1} u^m, \quad m \geq 1, \quad (\text{B3})$$

$$\pi_{(N)}^s \equiv \frac{1}{(N-2)!} \partial^{N-2}(u^{N-1}\delta) + \frac{1}{(N-1)!} \partial^{N-1} u^N, \quad N \geq 2, \quad (\text{B4})$$

where ∂ is a shorthand for $\nabla_{\parallel} \equiv \hat{\mathbf{n}} \cdot \nabla = \partial/\partial r$. Since eq. (B1) defines a *Cauchy product* [105], showing that eq. (23) for π^s is the product of eqs. (19) and (26), is equivalent to showing that, order-by-order, $\pi_{(N)}^s$ is of the form given in eq. (B1). The first two cases, $N = 0, 1$, are easily checked. For $N \geq 2$, substituting eqs. (B2), (B3), and (B4), into eq. (B1), we have

$$\begin{aligned} & \frac{1}{(N-2)!} \partial^{N-2}(u^{N-1}\delta) + \frac{1}{(N-1)!} \partial^{N-1} u^N \\ &= \rho_{(0)}^s u_{(N)}^s + \rho_{(N)}^s u_{(0)}^s + \sum_{n=1}^{\infty} \sum_{m=1}^{\infty} \delta_{n+m,N}^K \left[\left(\frac{1}{(n-1)!} \partial^{n-1}(u^{n-1}\delta) + \frac{1}{n!} \partial^n u^n \right) \frac{1}{m!} \partial^{m-1} u^m \right] \\ &= \frac{1}{N!} \partial^{N-1} u^N + \sum_{n+m=N-2} \left[\frac{1}{n!(m+1)!} \partial^n (u^n \delta) \partial^m u^{m+1} + \frac{1}{(n+1)!(m+1)!} \partial^{n+1} u^{n+1} \partial^m u^{m+1} \right], \quad (\text{B5}) \end{aligned}$$

where in the second equality we have redefined the labels such that $n \rightarrow n + 1$ and $m \rightarrow m + 1$. Notice that there are terms that depend on δ , and terms that do not depend on δ . Identifying on the left- and right-hand sides the δ -dependent terms, taking $N \rightarrow N + 2$, and rearranging slightly, we then have

$$\partial^N (u^{N+1}\delta) = \sum_{n+m=N} \frac{N!}{n!(m+1)!} \partial^n (u^n \delta) \partial^m u^{m+1}. \quad (\text{B6})$$

For the δ -independent terms, by similar steps, we have

$$\frac{1}{N+2} \partial^{N+1} u^{N+2} = \sum_{n+m=N} \frac{N!}{(n+1)!(m+1)!} \partial^{n+1} u^{n+1} \partial^m u^{m+1}. \quad (\text{B7})$$

Note that these two relations are general; they hold for arbitrary functions. This implies that eqs. (B7) and (B6) are not independent relations but that the latter follows from the former. To see this take $\delta = u$, symmetrize over n and m the summand in eq. (B6), then differentiate; the end result is equivalent to eq. (B7), upon symmetrizing, then writing $\partial^{n+1} u^{n+1} \partial^m u^{m+1} + \partial^n u^{n+1} \partial^{m+1} u^{m+1} = \partial(\partial^n u^{n+1} \partial^m u^{m+1})$. Thus we need only show that eq. (B6) holds.

To show that the right-hand side of eq. (B6) simplifies to the left-hand side, we find it convenient to use the Fourier representation, in which differentiation becomes algebra:

$$\partial^n (u^n \delta) \partial^m u^{m+1} = \int d\mathbf{r} e^{-i\mathbf{k}\mathbf{r}} \int_{q_1, \dots, q_{N+2}} \delta_D(\mathbf{k} - \mathbf{k}_1 - \mathbf{k}_2) (ik_1)^n (ik_2)^m \tilde{u}(q_1) \cdots \tilde{\delta}(q_{n+1}) \tilde{u}(q_{n+2}) \cdots \tilde{u}(q_{N+2}), \quad (\text{B8})$$

where k_1 and k_2 are shorthands for $q_1 + q_2 + \cdots + q_{n+1}$ and $q_{n+2} + q_{n+3} + \cdots + q_{N+2}$, respectively. Inserting back into eq. (B6) and symmetrizing, using the multinomial identity [105]

$$(x_1 + \cdots + x_{N+2})^N = \sum_{n+m=N} \frac{N!}{n!(m+1)!} \text{Sym} \left[(x_1 + \cdots + x_{n+1})^n (x_{n+2} + \cdots + x_{N+2})^m \right], \quad (\text{B9})$$

where Sym is an instruction to symmetrize over $\{x_1, x_2, \dots, x_{N+2}\}$, we obtain the left-hand side of eq. (B6).

Appendix C: Explicit expressions for redshift-space kernels

In this appendix we present closed-form expressions for the multipole moments of the power spectrum kernels $2[Z_2(\mathbf{q}, \mathbf{k} - \mathbf{q})]^2$ and $3Z_3(\mathbf{k}, \mathbf{q}, -\mathbf{q})$ appearing in eq. (62). In the parametrization of eq. (69) the multipole moments read

$$I_{22}^\ell(r, \mu') \equiv (2\ell + 1) \int_{-1}^1 \frac{d\mu}{2} \mathcal{L}_\ell(\mu) \int_0^{2\pi} \frac{d\phi}{2\pi} 2[Z_2(r, \mu, \mu', \phi)]^2, \quad (\text{C1a})$$

$$I_{13}^\ell(r, \mu') \equiv (2\ell + 1) \int_{-1}^1 \frac{d\mu}{2} \mathcal{L}_\ell(\mu) \int_0^{2\pi} \frac{d\phi}{2\pi} 3Z_3(r, \mu, \mu', \phi), \quad (\text{C1b})$$

where $r = q/k$, $\mu = \hat{\mathbf{k}} \cdot \hat{\mathbf{n}}$, and $\mu' = \hat{\mathbf{k}} \cdot \hat{\mathbf{q}}$. The only non-zero kernels are for $\ell = 0, 2, 4$, giving a total of six kernels. The first three are found to be

$$\begin{aligned} I_{22}^0(r, \mu') &= f^2 \frac{3r^2 - 6r\mu' + 2\mu'^2 + 1}{30r^2(1 + r^2 - 2r\mu')^2} \\ &+ f \frac{6r^2\mu'^2 + r^2 - 6r\mu'^3 - 8r\mu' + 7\mu'^2}{21r^2(1 + r^2 - 2r\mu')^2} \\ &+ \frac{36r^2\mu'^4 + 12r^2\mu'^2 + r^2 - 84r\mu'^3 - 14r\mu' + 49\mu'^2}{98r^2(1 + r^2 - 2r\mu')^2}, \end{aligned} \quad (\text{C2})$$

$$\begin{aligned} I_{22}^2(r, \mu') &= f^2 \frac{18r^2\mu'^2 - 6r^2 - 18r\mu'^3 - 6r\mu' + 11\mu'^2 + 1}{42r^2(1 + r^2 - 2r\mu')^2} \\ &+ f \frac{18r^2\mu'^4 - 3r^2\mu'^2 - r^2 - 33r\mu'^3 + 5r\mu' + 14\mu'^2}{21r^2(1 + r^2 - 2r\mu')^2}, \end{aligned} \quad (\text{C3})$$

$$I_{22}^4(r, \mu') = f^2 \frac{35r^2\mu'^4 - 30r^2\mu'^2 + 3r^2 - 40r\mu'^3 + 24r\mu' + 12\mu'^2 - 4}{70r^2(1 + r^2 - 2r\mu')^2}. \quad (\text{C4})$$

Note terms with the prefactor f arise from the part in Z_2 linear in $K_S^{(2)}$, while those with a f^2 prefactor arise from the part quadratic in $K_S^{(2)}$, namely $2[K_S^{(2)}(\mathbf{q}, \mathbf{k} - \mathbf{q})]^2$; the monopole term ($\ell = 0$) without a prefactor is a mixture of all kernels comprising eq. (63b). The real-space kernel $G_S^{(2)}(\mathbf{q}, \mathbf{k} - \mathbf{q})$ of course only contributes to the monopole.

We also have

$$\begin{aligned}
I_{13}^0(r, \mu') &= -f^2 \frac{2r^2 \mu'^2 + r^2 - 4r\mu'^3 - 2r\mu' + 2\mu'^2 + 1}{30r^2(1 + r^2 - 2r\mu')} \\
&\quad - f \frac{7r^3 \mu' - 15r^2 \mu'^2 - 6r^2 + 8r\mu'^3 + 13r\mu' - 7\mu'^2}{21r^2(1 + r^2 - 2r\mu')} \\
&\quad + \frac{6r^3 \mu'^3 + r^3 \mu' - 29r^2 \mu'^2 - 6r^2 + 30r\mu'^3 + 19r\mu' - 21\mu'^2}{42r^2(1 + r^2 - 2r\mu')}, \tag{C5}
\end{aligned}$$

$$\begin{aligned}
I_{13}^2(r, \mu') &= -f^2 \frac{11r^2 \mu'^2 + r^2 - 22r\mu'^3 - 2r\mu' + 11\mu'^2 + 1}{42r^2(1 + r^2 - 2r\mu')} \\
&\quad - f \frac{21r^3 \mu'^3 - 7r^3 \mu' - 24r^2 \mu'^4 - 24r^2 \mu'^2 + 6r^2 + 37r\mu'^3 + 5r\mu' - 14\mu'^2}{21r^2(1 + r^2 - 2r\mu')}, \tag{C6}
\end{aligned}$$

$$I_{13}^4(r, \mu') = -f^2 \frac{2(3\mu'^2 - 1)}{35r^2}. \tag{C7}$$

(Note that in the last term in eq. (C5) we have taken $\mathbf{q} \rightarrow -\mathbf{q}$; these terms correspond to the second group of terms in eq. (51), which are integrated over the space of all \mathbf{q} .)

Finally, let us also note here the angular integrals in the “13” loop integrals yield

$$\begin{aligned}
\int \frac{d\mu'}{2} I_{13}^0(r, \mu') &= -\frac{f^2}{18r^2} - \frac{f}{504r^2} \left[\frac{18}{r^2} - 104 - 18r^2 + \frac{9}{r^3}(r^2 - 1)^3 \ln \left| \frac{r+1}{r-1} \right| \right] \\
&\quad + \frac{1}{336r^2} \left[\frac{12}{r^2} - 82 + 4r^2 - 6r^4 + \frac{3}{r^3}(r^2 - 1)^3(r^2 + 2) \ln \left| \frac{r+1}{r-1} \right| \right], \tag{C8}
\end{aligned}$$

$$\int \frac{d\mu'}{2} I_{13}^2(r, \mu') = -\frac{f^2}{9r^2} - \frac{f}{1008r^2} \left[\frac{18}{r^2} - 218 + 126r^2 - 54r^4 + \frac{9}{r^3}(r^2 - 1)^3(3r^2 + 1) \ln \left| \frac{r+1}{r-1} \right| \right], \tag{C9}$$

$$\int \frac{d\mu'}{2} I_{13}^4(r, \mu') = 0. \tag{C10}$$

Appendix D: Redshift-space correlation tensor

In this appendix we give details on the velocity correlation tensor $\Psi_{ij}^s(\mathbf{s}) \equiv \langle v_i^s(0) v_j^s(\mathbf{s}) \rangle$, the redshift space version of eq. (86).

As in real space, the redshift-space velocity field is sourced by scalar perturbations, and reads in terms of the velocity divergence power spectrum,

$$\Psi_{ij}^s(\mathbf{s}) = \int \frac{d^3\mathbf{k}}{(2\pi)^3} \left(\frac{\mathcal{H}f}{k} \right)^2 \frac{k_i}{k} \frac{k_j}{k} P_{\theta\theta}^s(\mathbf{k}) e^{-i\mathbf{k}\cdot\mathbf{s}}. \tag{D1}$$

Inserting the multipole expansion $P_{\theta\theta}^s(\mathbf{k}) = \sum_{\ell} P_{\theta\theta}^{\ell}(k) \mathcal{L}_{\ell}(\hat{\mathbf{k}} \cdot \hat{\mathbf{n}})$, and using the identity

$$\int \frac{d^2\hat{\mathbf{k}}}{4\pi} \mathcal{L}_{\ell}(\hat{\mathbf{k}} \cdot \hat{\mathbf{n}}) e^{-i\mathbf{k}\cdot\mathbf{s}} = (-i)^{\ell} j_{\ell}(ks) \mathcal{L}_{\ell}(\hat{\mathbf{s}} \cdot \hat{\mathbf{n}}), \tag{D2}$$

we have

$$\begin{aligned}
\Psi_{ij}^s(\mathbf{s}) &= \int \frac{k^2 dk}{2\pi^2} \sum_{\ell} \left(\frac{\mathcal{H}f}{k} \right)^2 P_{\theta\theta}^{\ell}(k) \frac{1}{(-i)^2 k^2} \frac{\partial}{\partial s^i} \frac{\partial}{\partial s^j} \int \frac{d^2\hat{\mathbf{k}}}{4\pi} \mathcal{L}_{\ell}(\hat{\mathbf{k}} \cdot \hat{\mathbf{n}}) e^{-i\mathbf{k}\cdot\mathbf{s}} \\
&= \sum_{\ell} (-i)^{\ell-2} \int \frac{k^2 dk}{2\pi^2} \left(\frac{\mathcal{H}f}{k} \right)^2 P_{\theta\theta}^{\ell}(k) \mathcal{T}_{ij}^{\ell}, \tag{D3}
\end{aligned}$$

where we have replaced k_i with $\partial/\partial s^i$ (acting on the plane waves), and in the second line we have the Hessian,

$$\mathcal{T}_{ij}^\ell \equiv \partial_i \partial_j \left[j_\ell(ks) \mathcal{L}_\ell(\mu) \right], \quad (\text{D4})$$

with $\mu \equiv \hat{\mathbf{s}} \cdot \hat{\mathbf{n}}$ and $\partial_i \equiv k^{-1} \partial/\partial s^i$. To compute the Hessian note that $\partial_i(ks) = \hat{s}_i$, $\partial_i \hat{s}_j = (\delta_{ij}^K - \hat{s}_i \hat{s}_j)/(ks)$, and $\partial_i \mu = (\hat{n}_i - \mu \hat{s}_i)/(ks)$. If we then write \mathcal{T}_{ij}^ℓ as a decomposition with respect to \mathbf{s} as

$$\mathcal{T}_{ij}^\ell = \mathcal{T}_{ij}^{\ell, \parallel} + 2\mathcal{T}_{ij}^{\ell, \times} + \mathcal{T}_{ij}^{\ell, \perp}, \quad (\text{D5})$$

we have for each term,

$$\mathcal{T}_{ij}^{\ell, \parallel} \equiv \mathcal{P}_{ik}^\parallel \mathcal{P}_{jl}^\parallel \mathcal{T}_{kl}^\ell = \mathcal{P}_{ij}^\parallel j_\ell''(y) \mathcal{L}_\ell(\mu), \quad (\text{D6a})$$

$$\mathcal{T}_{ij}^{\ell, \times} \equiv \mathcal{P}_{k(i}^\perp \mathcal{P}_{j)l}^\parallel \mathcal{T}_{kl}^\ell = \hat{s}_{(i} \hat{n}_{j)}^\perp \left[\frac{j_\ell'(y)}{y} - \frac{j_\ell(y)}{y^2} \right] \frac{d\mathcal{L}_\ell}{d\mu}, \quad (\text{D6b})$$

$$\mathcal{T}_{ij}^{\ell, \perp} \equiv \mathcal{P}_{ik}^\perp \mathcal{P}_{jl}^\perp \mathcal{T}_{kl}^\ell = \mathcal{P}_{ij}^\perp \frac{j_\ell'(y)}{y} \mathcal{L}_\ell(\mu) - \mathcal{P}_{ij}^\perp \frac{j_\ell(y)}{y^2} \frac{d\mathcal{L}_\ell}{d\mu} \mu + \hat{n}_i^\perp \hat{n}_j^\perp \frac{j_\ell(y)}{y^2} \frac{d^2 \mathcal{L}_\ell}{d\mu^2}, \quad (\text{D6c})$$

where a prime denotes differentiation with respect to the function argument y , and indices enclosed in parentheses denotes the symmetric part, e.g. $\hat{s}_{(i} \hat{n}_{j)}^\perp = (\hat{s}_i \hat{n}_j^\perp + \hat{s}_j \hat{n}_i^\perp)/2$; also we have defined $y \equiv ks$, $\hat{n}_i^\perp \equiv \mathcal{P}_{ij}^\perp \hat{n}^j$, and projection tensors, $\mathcal{P}_{ij}^\parallel(\hat{\mathbf{s}}) \equiv \hat{s}_i \hat{s}_j$ and $\mathcal{P}_{ij}^\perp(\hat{\mathbf{s}}) \equiv \delta_{ij}^K - \hat{s}_i \hat{s}_j$. Note that the first term in eqs. (D6a) and (D6c) together generalizes the usual isotropic correlation functions. In particular, if we neglect RSD then we need only consider $\ell = 0$ and we may write $\mathcal{T}_{ij}^\ell = \mathcal{T}_{ij}^0 \delta_{\ell 0}^K$,

$$\mathcal{T}_{ij}^0 = -\mathcal{P}_{ij}^\parallel(\hat{\mathbf{s}}) K_\parallel(y) - \mathcal{P}_{ij}^\perp(\hat{\mathbf{s}}) K_\perp(y) \quad (\text{D7})$$

[recall $\mathcal{L}_0(\mu) = 1$]. Substituting the foregoing expression into eq. (D3) [eq. (87)] we recover the usual (real-space) Ψ_{ij} in terms of Ψ_\perp [eq. (89a)], and Ψ_\parallel [eq. (89b)].

It is easy to obtain the LOS part of eq. (D5),

$$\hat{n}^i \hat{n}^j \mathcal{T}_{ij}^\ell = \left[\mu^2 j_\ell'' + (1 - \mu^2) \frac{j_\ell'}{y} \right] \mathcal{L}_\ell + \mu(1 - \mu^2) \left[2 \frac{j_\ell'}{y} - 3 \frac{j_\ell}{y^2} \right] \frac{d\mathcal{L}_\ell}{d\mu} + (1 - \mu^2)^2 \frac{j_\ell}{y^2} \frac{d^2 \mathcal{L}_\ell}{d\mu^2}. \quad (\text{D8})$$

When the foregoing expression is substituted back into eq. (D3), the resulting expression should be consistent with eqs. (98) and (99). Indeed this can be shown by making use of the recursion relations for the Legendre polynomials.

-
- [1] N. Kaiser, *Clustering in real space and in redshift space*, *Mon. Not. Roy. Astron. Soc.* **227** (1987) 1.
 - [2] P. J. E. Peebles, *The Large-Scale Structure of the Universe*, (Princeton University Press, Princeton, NJ, 1980).
 - [3] J. C. Jackson, *A critique of Rees's theory of primordial gravitational radiation*, *Mon. Not. Roy. Astron. Soc.* **156** (1972) 1P [[arXiv:0810.3908](#)].
 - [4] W. L.W. Sargent and E. L. Turner, *A statistical method for determining the cosmological density parameter from the redshifts of a complete sample of galaxies*, *Astrophys. J.* **212** (1977) L3.
 - [5] M. Davis and P. J. E. Peebles, *A Survey of Galaxy Redshifts. V. The Two-point Position and Velocity Correlations*, *Astrophys. J.* **267** (1983) 465.
 - [6] A. J. S. Hamilton, *Omega from the Anisotropy of the Redshift Correlation Function in the IRAS 2 Jansky Survey*, *Astrophys. J.* **406** (1993) L47.
 - [7] K. B. Fisher, M. Davis, M. A. Strauss, A. Yahil and J. P. Huchra, *Clustering in the 1.2-Jy IRAS Galaxy Redshift Survey. II. Redshift Distortions and $\xi(r_p, \pi)$* , *Mon. Not. Roy. Astron. Soc.* **267** (1994) 927 [[astro-ph/9308013](#)].
 - [8] J. A. Peacock *et al.*, *A measurement of the cosmological mass density from clustering in the 2dF Galaxy Redshift Survey*, *Nature* **410** (2001) 169 [[astro-ph/0103143](#)].
 - [9] C. Blake *et al.*, *The WiggleZ Dark Energy Survey: the growth rate of cosmic structure since redshift $z = 0.9$* , *Mon. Not. Roy. Astron. Soc.* **415** (2011) 2876 [[arXiv:1104.2948](#)].
 - [10] F. Beutler *et al.*, *The 6dF Galaxy Survey: $z \approx 0$ measurement of the growth rate and σ_8* , *Mon. Not. Roy. Astron. Soc.* **423** (2012) 3430 [[arXiv:1204.4725](#)].
 - [11] S. de la Torre *et al.*, *The VIMOS Public Extragalactic Redshift Survey (VIPERS). Galaxy clustering and redshift-space distortions at $z = 0.8$ in the first data release*, *Astron. Astrophys.* **557** (2013) A54 [[arXiv:1303.2622](#)].

- [12] S. Alam *et al.* [BOSS Collaboration], *The clustering of galaxies in the completed SDSS-III Baryon Oscillation Spectroscopic Survey: cosmological analysis of the DR12 galaxy sample*, *Mon. Not. Roy. Astron. Soc.* **470** (2017) 2617 [[arXiv:1607.03155](#)].
- [13] H. Gil-Marín *et al.*, *The Completed SDSS-IV extended Baryon Oscillation Spectroscopic Survey: measurement of the BAO and growth rate of structure of the luminous red galaxy sample from the anisotropic power spectrum between redshifts 0.6 and 1.0*, *Mon. Not. Roy. Astron. Soc.* **498** (2020) 2492 [[arXiv:2007.08994](#)].
- [14] A. J. S. Hamilton, *Measuring Omega and the real correlation function from the redshift correlation function*, *Astrophys. J. Lett.* **385** (1992) L5.
- [15] E. V. Linder, *Cosmic growth history and expansion history*, *Phys. Rev. D* **72** (2005) 043529 [[astro-ph/0507263](#)].
- [16] M. Ishak, A. Upadhye and D. N. Spergel, *Probing cosmic acceleration beyond the equation of state: Distinguishing between dark energy and modified gravity models*, *Phys. Rev. D* **74** (2006) 043513 [[astro-ph/0507184](#)].
- [17] Y. S. Song and W. J. Percival, *Reconstructing the History of Structure Formation using Redshift Distortions*, *JCAP* **0910** (2009) 004 [[arXiv:0807.0810](#)].
- [18] M. Ishak, *Testing General Relativity in Cosmology*, *Living Rev. Rel.* **22** (2019) 1 [[arXiv:1806.10122](#)].
- [19] T. Baker *et al.*, *Novel Probes Project: Tests of gravity on astrophysical scales*, *Rev. Mod. Phys.* **93** (2021) 015003 [[arXiv:1908.03430](#)].
- [20] S. Alam *et al.*, *Testing the theory of gravity with DESI: estimators, predictions and simulation requirements*, [[arXiv:2011.05771](#)].
- [21] A. Aghamousa *et al.* [DESI Collaboration], *The DESI Experiment Part I: Science, Targeting, and Survey Design* [[arXiv:1611.00036](#)].
- [22] L. Amendola *et al.*, *Cosmology and fundamental physics with the Euclid satellite*, *Living Rev. Rel.* **21** (2018) 2 [[arXiv:1606.00180](#)].
- [23] O. Doré *et al.*, *Cosmology with the SPHEREX All-Sky Spectral Survey*, [[arXiv:1412.4872](#)].
- [24] J. Koda *et al.*, *Are peculiar velocity surveys competitive as a cosmological probe?*, *Mon. Not. Roy. Astron. Soc.* **445** (2014) 4267 [[arXiv:1312.1022](#)].
- [25] P. McDonald and U. Seljak, *How to measure redshift-space distortions without sample variance*, *JCAP* **0910** (2009) 007 [[arXiv:0810.0323](#)].
- [26] D. Burkey and A. N. Taylor, *Prospects for galaxy-mass relations from the 6dF Galaxy Survey*, *Mon. Not. Roy. Astron. Soc.* **347** (2004) 255 [[astro-ph/0310912](#)].
- [27] A. G. Kim and E. V. Linder, *Complementarity of peculiar velocity surveys and redshift space distortions for testing gravity*, *Phys. Rev. D* **101** (2020) 023516 [[arXiv:1911.09121](#)].
- [28] G. B. Poole *et al.*, *The Gigaparsec WiggleZ simulations: characterizing scale-dependant bias and associated systematics in growth of structure measurements*, *Mon. Not. Roy. Astron. Soc.* **449** (2015) 1454 [[arXiv:1407.0390](#)].
- [29] C. Howlett, L. Staveley-Smith and C. Blake, *Cosmological Forecasts for Combined and Next Generation Peculiar Velocity Surveys*, *Mon. Not. Roy. Astron. Soc.* **464** (2017) 2517 [[arXiv:1609.08247](#)].
- [30] C. Howlett, A. S. G. Robotham, C. D. P. Lagos and A. G. Kim, *Measuring the growth rate of structure with Type Ia Supernovae from LSST*, *Astrophys. J.* **847** (2017) 128 [[arXiv:1708.08236](#)].
- [31] C. Adams and C. Blake, *Joint growth rate measurements from redshift-space distortions and peculiar velocities in the 6dF Galaxy Survey*, *Mon. Not. Roy. Astron. Soc.* **494** (2020) 3275 [[arXiv:2004.06399](#)].
- [32] L. Amendola and M. Quartin, *Measuring the Hubble function with standard candle clustering*, *Mon. Not. Roy. Astron. Soc.* **504** (2021) 3884 [[arXiv:1912.10255](#)].
- [33] E. da Cunha *et al.*, *The Taipan Galaxy Survey: Scientific Goals and Observing Strategy*, *Publ. Astron. Soc. Austral.* **34** (2017) 47 [[arXiv:1706.01246](#)].
- [34] B. S. Koribalski *et al.*, *WALLABY – An SKA Pathfinder H I Survey*, *Astrophys. Space Sci.* **365** (2020) 118 [[arXiv:2002.07311](#)].
- [35] C. Gordon, K. Land and A. Slosar, *Cosmological Constraints from Type Ia Supernovae Peculiar Velocity Measurements*, *Phys. Rev. Lett.* **99** (2007) 081301 [[arXiv:0705.1718](#)].
- [36] S. Mukherjee and B. D. Wandelt, *Beyond the classical distance-redshift test: cross-correlating redshift-free standard candles and sirens with redshift surveys*, [[arXiv:1808.06615](#)].
- [37] A. G. Kim *et al.*, *Testing Gravity Using Type Ia Supernovae Discovered by Next-Generation Wide-Field Imaging Surveys*, [[arXiv:1903.07652](#)].
- [38] P. A. Abell *et al.* [LSST Science and LSST Project Collaborations], *LSST Science Book, Version 2.0*, [[arXiv:0912.0201](#)].
- [39] N. Kaiser and M. J. Hudson, *On the perturbation of the luminosity distance by peculiar motions*, *Mon. Not. Roy. Astron. Soc.* **450** (2015) 883 [[arXiv:1411.6339](#)].
- [40] T. Okumura, U. Seljak, Z. Vlah and V. Desjacques, *Peculiar velocities in redshift space: formalism, N-body simulations and perturbation theory*, *JCAP* **1405** (2014) 003 [[arXiv:1312.4214](#)].
- [41] N. S. Sugiyama, T. Okumura and D. N. Spergel, *Understanding redshift space distortions in density-weighted peculiar velocity*, *JCAP* **1607** (2016) 001 [[arXiv:1509.08232](#)].
- [42] R. A. Sunyaev and Y. B. Zeldovich, *The velocity of clusters of galaxies relative to the microwave background. The possibility of its measurement*, *Mon. Not. Roy. Astron. Soc.* **190** (1980) 413.
- [43] C. Howlett, *The redshift-space momentum power spectrum – I. Optimal estimation from peculiar velocity surveys*, *Mon. Not. Roy. Astron. Soc.* **487** (2019) 5209 [[arXiv:1906.02875](#)].
- [44] P. Zhang, Y. Zheng and Y. Jing, *Sampling artifact in volume weighted velocity measurement. I. Theoretical modeling*, *Phys. Rev. D* **91** (2015) 043522 [[arXiv:1405.7125](#)].

- [45] A. H. Jaffe and N. Kaiser, *Likelihood analysis of large-scale flows*, *Astrophys. J.* **455** (1995) 26 [[astro-ph/9408046](#)].
- [46] A. Abate and O. Lahav, *The Three Faces of Ω_m : Testing Gravity with Low and High Redshift SN Ia Surveys*, *Mon. Not. Roy. Astron. Soc.* **389** (2008) 47 [[arXiv:0805.3160](#)].
- [47] A. Johnson *et al.*, *The 6dF Galaxy Survey: cosmological constraints from the velocity power spectrum*, *Mon. Not. Roy. Astron. Soc.* **444**, 3926 (2014) [[arXiv:1404.3799](#)].
- [48] C. Howlett *et al.*, *2MTF – VI. Measuring the velocity power spectrum*, *Mon. Not. Roy. Astron. Soc.* **471** (2017) 3135 [[arXiv:1706.05130](#)].
- [49] C. Adams and C. Blake, *Improving constraints on the growth rate of structure by modelling the density–velocity cross-correlation in the 6dF Galaxy Survey*, *Mon. Not. Roy. Astron. Soc.* **471** (2017) 839 [[arXiv:1706.05205](#)].
- [50] R. J. Turner, C. Blake and R. Ruggeri, *Improving estimates of the growth rate using galaxy–velocity correlations: a simulation study*, *Mon. Not. Roy. Astron. Soc.* **502** (2021) 2087 [[arXiv:2101.09026](#)].
- [51] U. Seljak and P. McDonald, *Distribution function approach to redshift space distortions*, *JCAP* **11** (2011) 039 [[arXiv:1109.1888](#)].
- [52] P. McDonald, *How to generate a significant effective temperature for cold dark matter, from first principles*, *JCAP* **04** (2011) 032 [[arXiv:0910.1002](#)].
- [53] T. Okumura, U. Seljak, P. McDonald and V. Desjacques, *Distribution function approach to redshift space distortions. Part II: N-body simulations*, *JCAP* **1202** (2012) 010 [[arXiv:1109.1609](#)].
- [54] T. Okumura, U. Seljak and V. Desjacques, *Distribution function approach to redshift space distortions, Part III: halos and galaxies*, *JCAP* **1211** (2012) 014 [[arXiv:1206.4070](#)].
- [55] Z. Vlah, U. Seljak, P. McDonald, T. Okumura and T. Baldauf, *Distribution function approach to redshift space distortions. Part IV: perturbation theory applied to dark matter*, *JCAP* **1211** (2012) 009 [[arXiv:1207.0839](#)].
- [56] M. Simonovic, T. Baldauf, M. Zaldarriaga, J. J. Carrasco and J. A. Kollmeier, *Cosmological perturbation theory using the FFTLog: formalism and connection to QFT loop integrals*, *JCAP* **04** (2018) 030 [[arXiv:1708.08130](#)].
- [57] L. M. Wang and P. J. Steinhardt, *Cluster Abundance Constraints for Cosmological Models with a Time-varying, Spatially Inhomogeneous Energy Component with Negative Pressure*, *Astrophys. J.* **508** (1998) 483 [[astro-ph/9804015](#)].
- [58] A. J. S. Hamilton, *Linear redshift distortions: A Review*, in *The Evolving Universe*, edited by D. Hamilton (1998), vol. 231 of *Astrophysics and Space Science Library*, p. 185 [[astro-ph/9708102](#)].
- [59] V. Desjacques, D. Jeong and F. Schmidt, *Large-Scale Galaxy Bias*, *Phys. Rept.* **733** (2018) 1 [[arXiv:1611.09787](#)].
- [60] J. Chen, P. Zhang, Y. Zheng, Y. Yu and Y. Jing, *Accurate determination of halo velocity bias in simulations and its cosmological implications*, *Astrophys. J.* **861** (2018) 58 [[arXiv:1803.00728](#)].
- [61] Y. Zheng, P. Zhang and Y. Jing, *Determination of the large scale volume weighted halo velocity bias in simulations*, *Phys. Rev. D* **91** (2015) 123512 [[arXiv:1410.1256](#)].
- [62] W. E. Ballinger, J. A. Peacock and A. F. Heavens, *Measuring the cosmological constant with redshift surveys*, *Mon. Not. Roy. Astron. Soc.* **282** (1996) 877 [[astro-ph/9605017](#)].
- [63] R. Scoccimarro, *Redshift-space distortions, pairwise velocities and nonlinearities*, *Phys. Rev. D* **70** (2004) 083007 [[astro-ph/0407214](#)].
- [64] A. Taruya, T. Nishimichi and S. Saito, *Baryon acoustic oscillations in 2D: Modeling redshift-space power spectrum from perturbation theory*, *Phys. Rev. D* **82** (2010) 063522 [[arXiv:1006.0699](#)].
- [65] Z. Vlah and M. White, *Exploring redshift-space distortions in large-scale structure*, *JCAP* **1903** (2019) 007 [[arXiv:1812.02775](#)].
- [66] K. B. Fisher, *On the validity of the streaming model for the redshift-space correlation function in the linear regime*, *Astrophys. J.* **448** (1995) 494 [[astro-ph/9412081](#)].
- [67] B. A. Reid and M. White, *Towards an accurate model of the redshift space clustering of halos in the quasilinear regime*, *Mon. Not. Roy. Astron. Soc.* **417** (2011) 1913 [[arXiv:1105.4165](#)].
- [68] L. Wang, B. Reid and M. White, *An analytic model for redshift-space distortions*, *Mon. Not. Roy. Astron. Soc.* **437** (2014) 588 [[arXiv:1306.1804](#)].
- [69] B. A. Reid *et al.*, *The clustering of galaxies in the SDSS-III Baryon Oscillation Spectroscopic Survey: measurements of the growth of structure and expansion rate at $z = 0.57$ from anisotropic clustering*, *Mon. Not. Roy. Astron. Soc.* **426** (2012) 2719 [[arXiv:1203.6641](#)].
- [70] J. E. Bautista *et al.*, *The Completed SDSS-IV extended Baryon Oscillation Spectroscopic Survey: measurement of the BAO and growth rate of structure of the luminous red galaxy sample from the anisotropic correlation function between redshifts 0.6 and 1*, *Mon. Not. Roy. Astron. Soc.* **500** (2020) 736 [[arXiv:2007.08993](#)].
- [71] C. Cuesta-Lazaro, *et al.*, *Towards a non-Gaussian model of redshift space distortions*, *Mon. Not. Roy. Astron. Soc.* **498** (2020) 1175 [[arXiv:2002.02683](#)].
- [72] P. Kovtun, *Lectures on hydrodynamic fluctuations in relativistic theories*, *J. Phys. A* **45** (2012) 473001 [[arXiv:1205.5040](#)].
- [73] L. D. Landau and E. M. Lifshitz, *Fluid Mechanics*, (Pergamon Press, 1987).
- [74] F. Bernardreau, S. Colombi, E. Gaztanaga and R. Scoccimarro, *Large-Scale Structure of the Universe and Cosmological Perturbation Theory*, *Phys. Rept.* **367** (2002) 1 [[astro-ph/0112551](#)].
- [75] D. J. Eisenstein and W. Hu, *Baryonic features in the matter transfer function*, *Astrophys. J.* **496** (1998) 605 [[astro-ph/9709112](#)].
- [76] R. E. Smith *et al.*, *Stable clustering, the halo model and nonlinear cosmological power spectra*, *Mon. Not. Roy. Astron. Soc.* **341** (2003) 1311 [[astro-ph/0207664](#)].
- [77] R. Takahashi, M. Sato, T. Nishimichi, A. Taruya and M. Oguri, *Revising the Halofit Model for the Nonlinear Matter Power Spectrum*, *Astrophys. J.* **761** (2012) 152 [[arXiv:1208.2701](#)].

- [78] O. Hahn, R. E. Angulo and T. Abel, *The Properties of Cosmic Velocity Fields*, *Mon. Not. Roy. Astron. Soc.* **454** (2015) 3920 [[arXiv:1404.2280](#)].
- [79] S. Pueblas and R. Scoccimarro, *Generation of vorticity and velocity dispersion by orbit crossing*, *Phys. Rev. D* **80** (2009) 043504 [[arXiv:0809.4606](#)].
- [80] J. Carlson, M. White and N. Padmanabhan, *A critical look at cosmological perturbation theory techniques*, *Phys. Rev. D* **80** (2009) 043531 [[arXiv:0905.0479](#)].
- [81] R. Scoccimarro, H. M. P. Couchman and J. A. Frieman, *The Bispectrum as a Signature of Gravitational Instability in Redshift-Space*, *Astrophys. J.* **517** (1999) 531 [[astro-ph/9808305](#)].
- [82] J. D. Talman, *Numerical Fourier and Bessel transforms in logarithmic variables*, *J. Comp. Phys.* **29** (1978) 35
- [83] A. J. S. Hamilton, *Uncorrelated Modes of the Nonlinear Power Spectrum*, *Mon. Not. Roy. Astron. Soc.* **312** (2000) 257 [[astro-ph/9905191](#)].
- [84] D. A. Varshalovich, A. N. Moskalev and V. K. Khersonsky, *Quantum Theory of Angular Momentum: Irreducible Tensors, Spherical Harmonics, Vector Coupling Coefficients, 3nj Symbols*, (World Scientific, Singapore, 1988).
- [85] T. Matsubara, *Resumming cosmological perturbations via the Lagrangian picture: One-loop results in real space and in redshift Space*, *Phys. Rev. D* **77** (2008) 063530 [[arXiv:0711.2521](#)].
- [86] J. Carlson, B. Reid and M. White, *Convolution Lagrangian perturbation theory for biased tracers*, *Mon. Not. Roy. Astron. Soc.* **429** (2013) 1674 [[arXiv:1209.0780](#)].
- [87] Y. Zheng and Y. S. Song, *Study on the mapping of dark matter clustering from real space to redshift space*, *JCAP* **1608** (2016) 050 [[arXiv:1603.00101](#)].
- [88] J. Kwan, G. F. Lewis and E. V. Linder, *Mapping Growth and Gravity with Robust Redshift Space Distortions*, *Astrophys. J.* **748** (2012) 78 [[arXiv:1105.1194](#)].
- [89] T. Baldauf, V. Desjacques and U. Seljak, *Velocity bias in the distribution of dark matter halos*, *Phys. Rev. D* **92** (2015) 123507 [[arXiv:1405.5885](#)].
- [90] A. S. Monin and A. M. Yaglom, *Statistical Fluid Mechanics*, 1975, MIT Press, Cambridge, MA.
- [91] K. Górski, *On the pattern of perturbations of the Hubble flow*, *Astrophys. J.* **332** (1988) L7.
- [92] R. G. Carlberg and H. M. P. Couchman, *Mergers and Bias in a Cold Dark Matter Cosmology*, *Astrophys. J. Lett.* **340** (1990) 47.
- [93] R. G. Carlberg, H. M. P. Couchman and P. A. Thomas, *Cosmological velocity bias* *Astrophys. J. Lett.* **352** (1990) L29.
- [94] R. G. Carlberg, *Velocity bias in clusters*, *Astrophys. J.* **433** (1994) 468 [[astro-ph/9404005](#)].
- [95] P. Colín, A. Klypin and A. V. Kravtsov, *Velocity bias in a Λ Cold Dark Matter model*, *Astrophys. J.* **539** (2000) 561 [[astro-ph/9907337](#)].
- [96] E. Jennings, C. M. Baugh and D. Hatt, *Velocity and mass bias in the distribution of dark matter halos*, *Mon. Not. Roy. Astron. Soc.* **446** (2015) 793 [[arXiv:1407.7296](#)].
- [97] C. R. Harris *et al.*, *Array programming with NumPy*, *Nature* **585** (2020) 357 [[arXiv:2006.10256](#)].
- [98] P. Virtanen *et al.*, *SciPy 1.0: fundamental algorithms for scientific computing in Python*, *Nature Meth.* **17** (2020) 261 [[arXiv:1907.10121](#)].
- [99] J. D. Hunter, *Matplotlib: A 2D Graphics Environment*, *Comput. Sci. Eng.* **9** (2007) 90.
- [100] R. Scoccimarro and J. Frieman, *Loop corrections in nonlinear cosmological perturbation theory II. Two-point statistics and elf-similarity*, *Astrophys. J.* **473** (1996) 620 [[astro-ph/9602070](#)].
- [101] J. E. McEwen, X. Fang, C. M. Hirata and J. A. Blazek, *FAST-PT: a novel algorithm to calculate convolution integrals in cosmological perturbation theory*, *JCAP* **09** (2016) 015 [[arXiv:1603.04826](#)].
- [102] Y. Suto and M. Sasaki, *Quasi nonlinear theory of cosmological self-gravitating systems*, *Phys. Rev. Lett.* **66** (1991) 264.
- [103] N. Makino, M. Sasaki and Y. Suto, *Analytic approach to the perturbative expansion of nonlinear gravitational fluctuations in cosmological density and velocity fields*, *Phys. Rev. D* **46** (1992) 585.
- [104] M. Schmittfull, Z. Vlah and P. McDonald, *Fast large scale structure perturbation theory using one-dimensional fast Fourier transforms*, *Phys. Rev. D* **93** (2016) 103528 [[arXiv:1603.04405](#)].
- [105] J. Riordan, *Combinatorial Identities*, (John Wiley and Sons Ltd., Chichester, 1968).